Scanning Probe Lithography Using Self-Assembled Monolayers

Stephan Krämer, Ryan R. Fuierer, and Christopher B. Gorman*

Department of Chemistry, North Carolina State University, Box 8204, Raleigh, North Carolina 27695-8204

Received April 9, 2003

Contents

1. Introduction

The ability to organize matter on the nanometer scale is one of the major enabling principles in the field of nanotechnology. Scanning probe microscopy (SPM) has been a key tool in achieving this goal. SPM serves two important purposes. The probe tip can visualize surfaces at the submolecular level. The ability to "see" molecules in this relatively straightforward way undoubtedly facilitated the emergence of molecular nanotechnology. Scanning probes have been employed to visualize many molecular phenomena. A few notable examples include the direct determination of the chirality of adsorbed molecules,[1−10] observation of the conformation of polymers,[11−18] dendrimers,[19−22] adsorbed supramolecular nanostructures,[23−28] and conformational and orientational dynamics of small molecules.[29−34] In addition, probe tips can be used to manipulate atoms and molecules on surfaces.[35,36] In this mode, the technique is often referred to as scanning probe lithography (SPL). Such demonstrations as writing (of the letters "IBM")[37] with xenon atoms, moving molecules to and fro (the "molecular abacus"),[38] and organization of atoms so as to illustrate the quantum nature of electrons (the "quantum corral")[39,40] have, at a minimum, piqued our collective curiosity about how we might further expand these ideas to perform useful functions at the molecular scale. Several excellent, recent reviews have treated the basic visualization and manipulation functions of scanning probes in detail.[41−44]

As one contemplates more complex, molecular-scale operations, the need for chemically well-defined surfaces becomes apparent. The term "chemically well-defined" denotes control of the placement, patterning, orientation, and packing of chemical functional groups on a surface. These functionalities will be sites for control of the physical properties of that surface region. Several of these include control of the relative wetting behavior, adhesion, friction and chemical interaction with the environment above the surface. Moreover, these functional groups can facilitate a wide variety of chemical binding and covalent bond formation reactions.[45] The range of functional, molecular-scale elements to be attached in a well-defined way depends only on the imagination but has already been illustrated (as will be described in detail herein) with such diverse structures as metallic lines, polymers, active biomolecules, and colloids. These functionalities can also facilitate transduction of such a chemical event into an optical or electrochemical signal. Undoubtedly, other functions will be illustrated beyond these.

Self-assembled monolayers (SAMs) have emerged as a prominent, flexible, and convenient way to present functionality at a surface in a chemically well-defined way. The formation, characterization, and properties of SAMs have been described and reviewed extensively.[46−49] Several features of SAMs are attractive. First, they provide a simple way to produce relatively ordered structures at the molecular scale. Second, they provide a way of presenting a wide variety of chemically well-defined terminal functional groups to a surface. The roles of these functional groups have been suggested above. Third, variation in the length of the chain between the head

* To whom correspondence should be addressed. Telephone: (+1) 919-515-4252. Fax: (+1) 919-515-8920. E-mail: chris_gorman@ncsu.edu.

10.1021/cr020704m CCC: $44.00
Published on Web 10/01/2003

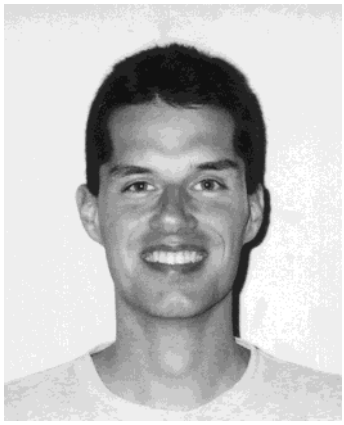

Stephan Krämer was born in Flörsheim, Germany, in 1972. He received his diploma degree in physics in 1997 from the Johannes Gutenberg University in Mainz, Germany, for his work at the Max-Planck Institute for Polymer Research, Mainz, Germany. The focus of his work was the preparation and characterization of oxidic and polymer waveguides for the development of optical sensors. In 2001 he received his Ph.D. in physical chemistry from the Johannes Gutenberg University for his research on mass spectrometry of functionalized surfaces of organic and thin metal films at the Max-Planck-Institute for Polymer Research. He is currently a postdoctoral research associate in the Department of Chemistry at the North Carolina State University. His research interests include the field of nanoelectronics and the preparation and characterization of metal nanoparticle films for biological sensor applications.

Ryan Fuierer was born in 1971. He received a B.S. degree in chemistry from St. John Fisher College in Rochester, NY. He is currently pursuing a Ph.D. in chemistry from North Carolina State University in Raleigh, NC. His research interests include the synthesis and characterization of molecular-scale electronic materials, nanoscale patterning, and the characterization of nanoparticle assemblies for use in sensor applications.

and tail groups offers some control over the interaction between the underlying substrate and the chemical environment above the SAM. Thus, in applications from sensing to building with discrete numbers of molecules, the chemical and structural control offered by SAMs seems critical.

In addition to the elements of SAMs highlighted above, the ability to pattern the chemical functionality presented by SAMs at various length scales has been important in extending their utility. A variety of "soft lithography" methods have been developed to pattern surfaces with SAM regions presenting different chemical functionalities.[50,51] The most notable of these is the technique of microcontact printing (μCP). This technique is most easily employed to pattern SAMs at the micrometer scale, although several extensions of it have been described to extend

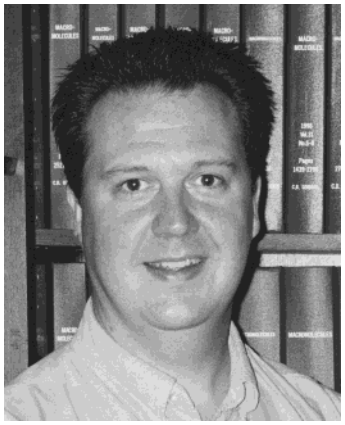

Christopher Gorman was born in Summit, NJ, in 1965. He received a B.A. in chemistry and computer science from Drew University in 1987, and a Ph.D. in chemistry from the California Institute of Technology in 1991 (with Robert H. Grubbs). He then did postdoctoral work with Dr. Seth Marder at the NASA Jet Propulsion Laboratory and with Professor George Whitesides at Harvard University. In 1994, he joined the faculty of North Carolina State University, where he is now Professor of Chemistry. His present research interests include the design and synthesis of new macromolecules with interesting and useful electronic properties at nanometer-length scales and the use of scanned probe microscopies in nanoscience to establish molecular structure–property relationships for single-molecule electronic behaviors.

its utility into the nanometer-scale regime. The use of stamps to pattern at the nanometer scale has also been exploited in the technique of nanoimprint lithography.[52,53] However, of the materials to be patterned at the nanometer scale, SAMs have the attractive feature that they present and hold chemical functionality (e.g., functional headgroups) at the surface. To exploit this chemical definition afforded by SAMs at the nanometer scale, it is attractive to take advantage of methods that probe and pattern at this length scale.

Thus, it is natural to marry the molecular-scale visualization and manipulation capabilities of SPM/SPL with the chemical definition and opportunities for creating patterns afforded by SAMs. This combination is the subject of this review. From a fundamental manufacturing standpoint, simultaneous utilization of these two elements can also be considered as a hybridization of top-down (SPL) and bottom-up (self-assembly) approaches. The importance of self-assembly in nanometer-scale construction has been highlighted.[54,55] Yet, as there are no general paradigms for the artificial construction of arbitrary objects exclusively via self-assembly, the use of SPL to direct the patterning of self-assembled structures has enabled their use in nanosynthesis.

Indeed, it is attractive (at least to chemists) to view the creation of nanometer-scale constructs as an extension of molecular-scale chemical synthesis. In this vein, we choose to categorize efforts in this area in a fashion analogous to the classification of chemical reactions. Nearly all chemical reactions can be divided into three major categories: eliminations, where a specific group is cleaved from a molecule (AB $\rightarrow$ A + B); additions, where functional groups are added to a present structure (A + B $\rightarrow$ AB); and substitutions, where one functional group is replaced by another (AB + C $\rightarrow$ AC + B). Since lithography on SAMs ultimately is about transforming chemical

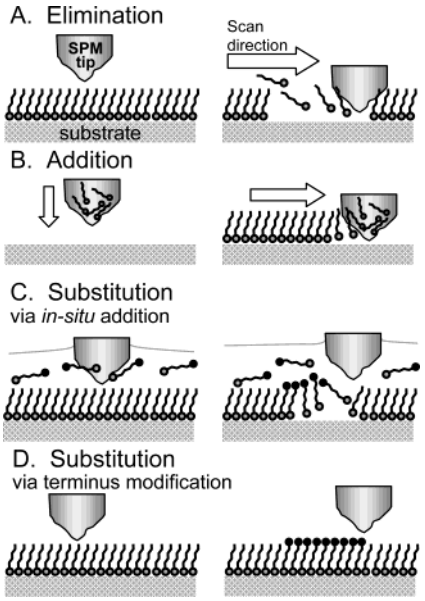

Figure 1. Schematic diagram illustrating the principles of elimination, addition, and substitution lithographies with a scanning probe. In general, the probe imaged the surface first with nondestructive imaging parameters, to find an area suitable for patterning. Elimination was achieved by the removal of the SAM in proximity of the probe by mechanical or electrical means (A). In addition lithography, a probe coated with a molecular "ink" was brought into contact with a nominally "bare" substrate. The ink transferred from the probe to the surface (B). Substitution lithography could proceed by two different pathways. In the first substitution pathway, the tip removed the SAM while scanning and an in-situ addition of a different molecule into the bare region occurred (C, substitution via elimination and in-situ addition). The alternative substitution via SAM terminus modification occurred by the probe modifying the headgroups of the SAM through electrochemical or catalytic interaction (D).

functionality presented at a surface, the lithographic approaches can also be categorized in this way. Specifically in this review, techniques grouped in "Elimination" denote SAM patterns that were created by removing the film from the substrate. Figure 1A depicts this process. The probe images the surface first in order to find an area suitable for patterning under conditions that do not perturb the SAM. Elimination involves the removal of the SAM in the proximity of the probe by mechanical or electrochemical means. Chronologically, this was the focus of much of the early SPL work done on SAMs. As will be described, material is often added in subsequent, ex-situ treatments of the patterned substrate. "Addition" of a SAM precursor to a substrate denotes delivery of molecular "inks" that formed patterns on bare surfaces (Figure 1B). A probe coated with molecular ink is brought into contact with a nominally "bare" substrate. The ink gets transferred from the probe to the surface. "Substitution" denotes in-situ mechanical or electrochemical pattern fabrication strategies. Substitution approaches are further subdivided into two categories: (1) initial elimination of the SAM film, followed by in-situ addition of a self-assembly (SA) precursor to the exposed substrate (Figure 1C), and (2) chemical change to the terminal functional group of the SAM, which can be used for further localized chemistry (Figure 1D). At the end of each section, tables listing the experimental details of the experiments are provided.

The use of scanning probes to perform lithography has been the subject of several prior reviews.[43,56−60] These include some discussion of lithography on SAMs. This review intends to provide a comprehensive description of all types of SPL on SAMs and covers the literature up to the first part of 2003.

SAMs have also been used in other types of nanometer-scale patterning efforts that do not involve scanning probes. In addition to the microcontact-printing and nanoprinting applications mentioned above, SAMs have also been employed as electron-beam and UV patterning resists,[61] including examples where the chemical functionality presented by the SAM is modified upon this type of exposure.[62] Other examples include the patterning of a substrate followed by monolayer formation[63] and bottom-up patterning by using SAM-based multilayers to bridge gaps between previously defined elements.[64] The conductivity of individual molecules has been probed by inserting them into defect sites in a SAM,[42,65−67] and polymer growth from adventitiously inserted initiator molecules into a SAM has been investigated.[68]

2. Elimination Lithography

A natural idea for the creation of structures is the removal of material from a surface in a controlled manner. The carving of symbols and letters into stone or the scratching of wax with a quill are some early examples. The basis of these techniques can be categorized as elimination. A part of a canvas is removed and results in a pattern. This type of nanometer-scale scraping or ploughing had previously been demonstrated on a variety of surfaces including polymers, liquid crystals, bilayers, and other types of resists.[69−78]

Elimination lithography on self-assembled monolayers has emerged from two different directions of research. One came from the investigation of resists for electron beam lithography. In pushing the resolution limit of electron beam lithography, thinner and thinner resist layers became important. This led to the investigation of thin polymer films and self-assembled monolayers as resist materials. The use of scanning tunneling microscopes (STM) emerged from these results, because STM produces a current of low-energy electrons, and it thus can induce processes reminiscent of those induced by the electron beam. The second direction emerged shortly after the invention of scanning probe techniques. It was quickly noted that, under certain conditions of imaging, the tip perturbed the sample. Thus, scanning probes act as some combination of probe and stylus. Determining the conditions under which the tip alternately acted as a nondestructive probe and as a stylus initiated the field of scanning probe lithography. Scanning probe lithography has been explored on virtually every class of substrate, and excellent, general reviews of these efforts have been published by Penner and Quate.[43,59] The research

reviewed here focuses specifically on the use of SAMs in scanning probe lithography (Table 1).

In this section, modification by STM under ambient conditions is described first. This is followed by a discussion of work performed in ultrahigh vacuum (UHV). Then elimination lithography using an atomic force microscope (AFM) is reviewed. A few SPL examples with scanning electrochemical probe microscopy and near-field scanning probe microscopy have also emerged and will be described. In general, the results of elimination lithography are often evaluated by some type of subsequent modification of the pattern.

2.1. STM Modification under Ambient Conditions

An early example of SPL was demonstrated by Kim and Bard who described the modification of *n*-octadecanethiolate-SAMs (C_{18}S-SAM) on Au(111) with an STM operated in ambient conditions.[79] The surface modifications were observed upon the repeated scanning of a specific area with a set-point bias voltage of 1 V and a set-point tunneling current of 1 nA. The surface pits (e.g., vacancy islands), typically observed in STM images of SAMs, were seen to expand laterally during this process.[80,81] This observation was attributed to a strong interaction between the STM tip and the surface. Purposeful modification of the SAM occurred by increasing the set-point current and lowering the bias, which effectively brought the tip closer to the surface. The removal of the SAM was termed "etching" and was presumed to be the physical removal of the thiolate molecules by the tip. This assumption was supported by STM images that revealed the formation of holes in the SAM with material accumulation at the periphery of the scan area. Control experiments described the repeated scanning of a bare (e.g., unmodified) gold substrate under etching conditions that did not change the Au(111) surface. SAM modification could also be accomplished by applying a voltage pulse of ±(3−5) V to the tip (termed "voltage excursions"). The pulses resulted in material transfer between the tip and the substrate or vice versa, depending on the polarity of the applied voltage.

Crooks and co-workers established some of the early considerations in STM-based elimination lithography of SAMs under ambient conditions.[82] Their first report demonstrated the fabrication of geometrically well-defined patterns through removal of a C_{18}S-SAM from a Au(111) surface by applying a large substrate bias (+3 to +8 V) and repeated scanning. One experiment created 60 nm × 60 nm sized squares by scanning the area four successive times under an applied substrate bias of +3 V, with 110 pA tunneling current, and at 31.25 Hz scan frequency (1.875 μm/s). To ensure complete SAM removal, the bias was lowered to +300 mV for a series of four scans, while the other parameters were held constant. The decrease of the bias voltage resulted in a smaller tip−substrate distance to remove SAM material mechanically. Scan line analysis of the preferentially removed areas showed more shallow depths (ca. 0.7 nm) than the reported ellipsometric thickness of a C_{18}S-SAM (2.2−2.8 nm). The authors attributed the finding to the fact that STM measures apparent height based on relative conductance of different regions of the surface. Thus, the apparent topography of a pattern imaged by STM differs from its real topography. The extent of SAM removal was characterized with cyclic voltammetry (CV) using the patterns as ultra-microelectrodes. Using $Ru(NH_3)_6^{3+}$ as an electrochemical probe, one 5 μm × 5 μm pattern gave a current response in CVs corresponding to a round electrode with a radius of 3.6 μm. The current response scaled linearly when the number of similarly sized patterns generated was increased. The authors concluded from these results that the removal of nearly all of the organic material in the patterned areas occurred.

Lercel and co-workers used STM as a low-energy electron source for SPL of C_{18}S-SAMs on gold and gallium−arsenide.[83] The tip was biased negative with potentials between 1 and 10 V over a range of tunneling currents of 10 nA to 110 pA. Square-shaped grating patterns (sizes between 2 and 140 μm) were formed by scanning the tip over an entire raster scan area. Noncontact mode AFM images of the resulting patterns on gold and on GaAs revealed the modifications resulted in raised features of ca. 2−4 nm in height. The mechanism for the fabrication of the raised features was not clear. The authors suggested that the electron beam was damaging the molecules and parts of the molecules were drawn toward the tip by the electric field, creating bonds in the damaged layer that could combine with oxygen. Mechanical removal of the SAM and the substrate also occurred by bringing the tip in close contact with the sample using low-bias and high-tunneling-current parameters. The smallest structures fabricated were 15 nm on GaAs and 20 nm on gold. The line widths on gold were usually larger, which the authors attributed to the higher density of states in gold dictating a larger tip−substrate gap. This resulted in a larger diameter of the electron beam from the tip. The lines on gold could be transferred into the underlying substrate with a wet etching step, while transfer results on GaAs were inconclusive.

In a similar approach, Xu and Allee used C_{18}S-SAMs on GaAs and Langmuir−Blodgett (LB) films of a polymer (PMMA) and octadecanol on various substrates for STM-based lithography.[84] A line pattern was written in the C_{18}S-SAM on GaAs with a tunneling current of 0.5 nA and a bias voltage of 10 V. AFM images after the patterning process revealed ca. 15 nm wide protruding lines, which could not be dissolved in organic solvents. The patterns could be transferred into the GaAs substrate by a wet etching step with either aqueous ammonium hydroxide or a citric acid etch. The observed line width increased to 25 nm as the result of this etching procedure. The authors observed substantial surface roughening of the SAM after etching, which was attributed to defects in the monolayer.

Lercel et al. compared the pattern transfer of various SAM systems modified with electron beams (e^--beams) of various energies (10 eV to 50 keV).[85] SAMs were prepared from octadecyltrichlorosilane

(OTS, $CH_3(CH_2)_{17}SiCl_3$) on silicon dioxide and titanium dioxide, and octadecanethiol ($C_{18}SH$) on gold and GaAs. Electron beam exposure of the SAMs was manifested with a high-energy electron beam lithography system (50 keV), scanning electron microscope e^--beams with 1 keV to 25 keV exposures, and low-energy e^--beams generated from an STM tip (up to 10 eV for the conducting substrates). The patterns were imaged by an AFM in contact and noncontact modes and were also visualized using various types of wet and dry etches. Patterns generated from high-energy e^--beams yielded resolution of ca. 25 nm, while the minimum line size achieved with an STM was ca. 15 nm.

Sugimura and Nakagiri patterned silane layers on silica substrates.[86] Trimethylsilyl (TMS) monolayers were prepared by the vapor deposition of hexamethyldisilazane (HMDS, $(CH_3)_3Si-NH-Si(CH_3)_3$) onto a thin silicon oxide layer. The authors investigated the patterning of the TMS layers under ambient conditions in air, oxygen, or nitrogen atmospheres. Patterns were achieved by scanning an area at a sample bias of +5 V and a tunneling current of 200 pA. The structures were visualized by oxidation of the underlying substrate via a H_2O_2 treatment followed by the condensation of atmospheric water. Optical microscope images showed that the patterned area was hydrophilic, while AFM images revealed slight protrusions (ca. 0.5 nm) from the surrounding areas. Further proof for the degradation of the TMS layer was obtained by wet chemical etching experiments. The samples were immersed into a NH_4F/H_2O_2 solution, and the resulting structures were investigated by optical microscopy and AFM. Both microscopy techniques revealed that the TMS-SAM effectively protected the unpatterned areas from the wet chemical etchant. AFM images of patterns after etching showed the lithographic regions appeared as depressions in the Si substrate, with the narrowest line resolution of ca. 80 nm. The chemistry of the surface reaction was concluded to be primarily an anodic oxidation of the silicon induced by the STM. An adventitiously adsorbed water layer effectively facilitated this electrochemical event. The atmosphere itself did not alter the patterning result if the humidity was kept constant. Water electrolysis and related electrochemical reactions induced beneath the tip were reckoned to be responsible for the degradation mechanism of the organosilane layer under the atmospheric conditions in the experiment.

Shortly after the first demonstrations of elimination lithography of SAMs on gold or silicon surfaces, the Crooks group described the use of these patterns in an ex-situ modification of the substrate. Schoer et al. reported the subsequent low-temperature chemical vapor deposition (CVD) of copper into patterns generated by STM.[87] The researchers removed the C_{18}S-SAM as described above, and subsequently treated the sample with a copper CVD precursor ((hexafluoroacetylacetonato)copper(I)−(1,5-cyclooctadiene), (hfac)Cu−(1,5-COD)) which decomposed at temperatures between 120 and 200 °C. This temperature range was found to be compatible with the thermal tolerances of the C_{18}S-SAM resist (ca. 140 °C). It was observed that the copper grew selectively only in the exposed (patterned) areas. XPS measurements confirmed the high purity of the deposited copper, while areas outside of the pattern gave negligible signals for copper. A second demonstration of the selective CVD connected two larger patterns with a single SPL scan line. Scanning electron micrographs after the CVD process showed a 50 nm wide copper line between the larger pads. The authors observed that even patterns with incomplete removal of the SAM were sufficient to produce nucleation sites for the copper precursor and enabled the separated copper grains to grow together.

Crooks and co-workers proposed that the patterning mechanism for the SPL induced removal (or deposition) of material from organic films in air was electrochemical in nature.[88] The inherent, thin water layer that covers film surfaces in ambient conditions was suggested to act as a thin layer electrochemical cell and that adventitious impurities served as an electrolyte for a low-current electrochemical process. By fabricating patterns in nonanethiolate- (C_9S-) and C_{18}S-SAMs at various relative humidities (RHs) and atmospheres (N_2 and air), it was reasoned that the atmosphere played little role in the desorption event but the relative humidity was a crucial factor. At RHs below ca. 25%, no thiolates were removed, while larger RHs induced desorption. At this time, Schoer et al. produced the smallest known, intentionally created features in a SAM with a diameter below 10 nm and a volume of less than 100 nm^3. The creation of the features on the surface was independent of the tunneling current, which led to the assumption that bombardment with high-energy electrons was not responsible for the patterns. The authors showed that the created patterns could be transferred into the underlying substrate by an etching step. The etched structures from patterns in a C_9S-SAM were deeper and more irregularly shaped compared to the C_{18}S-SAM, but showed dependence on the relative humidity similar to that of the longer alkanethiolates. The effect on patterning of reverse bias polarity was also addressed, indicating "mounds" of material were deposited on the SAM. Removal of this accumulated surface material could only be achieved when normal patterning conditions were applied.

Schoer and Crooks later showed that the created patterns were also dependent on the total amount of current (Coulomb dose), which again supported the hypothesis of an electrochemical process for the removal of the SAM.[89] The authors investigated the shape of the created patterns' dependence on the applied bias and the tunneling current used for the lithography. Figure 2 shows four patterns created with different biases (different Coulomb doses). The depth of the patterned squares increased with larger applied bias, depicted by incrementally darker patterned regions in the images. Studies with an increased number of scans (equal to an increase in the Coulomb dose) led to similar results. Additionally, the authors discussed the mechanical effect caused by the tip. The authors assumed that at the standard imaging conditions (SIC: $V_b = +0.3$ V; $I_t = 150$ pA; 0.4−5 μm/s) the tip was already penetrating the

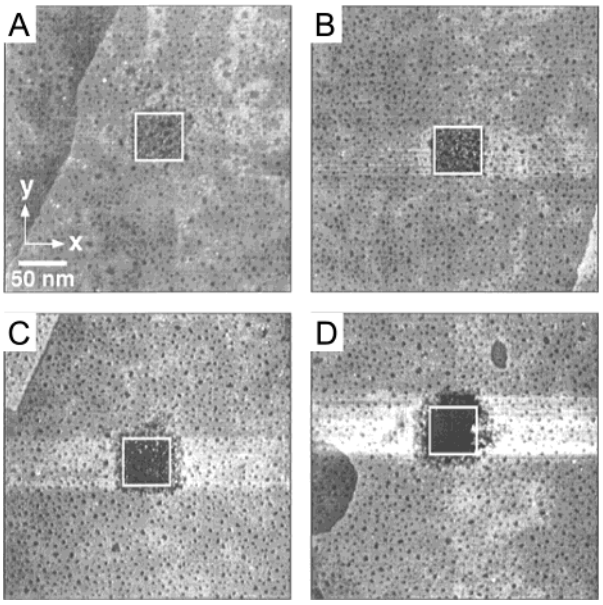

Figure 2. STM images of four nominally 50 nm × 50 nm patterns fabricated in a C_{18}S-SAM in air. The tunneling currents were (A) 0.05, (B) 0.15, (C) 1.5, and (D) 6 nA, respectively (*z*-scale: 2 nm). Reprinted with permission from ref 89. Copyright 1997 American Chemical Society.

surface of the SAM and impurities were inserted into the film. This assumption was consistent with later findings by the Weiss group on the relative height of the tip above SAMs of various thickness.[90] STM images revealed distortions in the order of the SAM and some deposited material on the periphery of the scanned region in the fast-scan direction. Patterns formed under standard patterning conditions (SPC: V_b = 3 V; I_t = 150 pA; 2.05−8.2 μm/s) created a disordered region surrounding the primary pattern. This effect resulted from long-range interactions between the tip and the surface and was believed to be due to faradaic electrochemical processes. The size of this disordered region was dependent on the relative humidity and could reach as far as hundreds of nanometers around the primary pattern. Additionally, debris from the removed monolayer was deposited onto the tip, decreasing the resolution of the images after the patterning process.

Delamarche et al. compared the results of patterning SAM resists with high- and low-energy e^--beams.[91] High-energy electrons were generated from a transmission electron microscope (TEM, 100 keV) or scanning electron microscope (SEM, 1, 10, or 35 keV) under a moderately high vacuum, while low-energy e^--beam patterns could be created with an STM. A self-assembled layer of mercaptomethylethanamide (MMEA, $HSCH_2CONHCH_2CH_3$) known to produce homogeneous, dense, and stable monolayers was formed on gold substrates. The molecule protected the gold from further thiol adsorption but did not function as a protective layer against cyanide etch (post-treatment). After patterning, the substrate was washed in different solvents (water, ethanol, heptane) and exposed to hexadecanethiol (C_{16}SH) solution to create C_{16}S-SAMs in the patterned areas. These regions were resilient to a post-treatment etch solution of aqueous KOH/HCN. Empirically, the authors determined that an electron dose from high-energy electron beams of 3 electrons/MMEA molecule was sufficient for the patterning. The MMEA-SAM could also be chemically converted to an effective etch stop without C_{16}SH treatment with larger electron doses. Two possible explanations for the phenomena were discussed. One suggestion was that, at high doses, the MMEA monolayer itself was converted into a form that was resistant to the etching solution. A second possibility suggested that "contaminants" accumulated on top of the SAM functioned as a resist layer. The authors observed the high-energy electron beam irradiated MMEA resists required much larger doses than the exposure of a 50 nm thick PMMA resist, presumably due to the thinness (transparency) of the MMEA-SAMs. Therefore, the authors changed their focus to the lower electron energy regime created by STM. The researchers determined the nonperturbative parameters for scanning the monolayer in ambient conditions to be 1 V bias and 50 pA tunneling current. The threshold voltage for patterning of the MMEA resist was determined to be 4 V, with the most reproducible structures achieved at 10 V bias, 50 pA tunneling current, and a scan speed of 15 μm/s in an argon atmosphere. Gold patterns up to 5 μm long and 40 nm wide were created over large areas. Figure 3 shows a series of SEM images of features in gold created using the lithography process described above, followed by transfer into the substrate. Figure 3A displays a square resulting from scanning 1024 lines consecutively. The line pattern seen in Figure 3B was created by scanning 25 lines, while Figure 3C resulted from only one pass of the tip. The test grid (Figure 3D) demonstrates single line patterns several micrometers in length. The exact mechanism for the patterning scheme was not known, and why 50 000 electrons/molecule were required to pattern with a STM also remained unclear. Regardless, compared to the results achieved with the high-energy e^--beam experiments, this STM-based lithography proved to be easier because it could be operated at ambient conditions. The higher energies of standard electron beam lithography, which allowed much faster movement of the probe, proved to be nonadvantageous for the use of SAM resists.

Self-assembled layers of chemically bound nanoparticles were mechanically patterned by Yang et al. via STM.[92] Hexanedithiolate-/decanethiolate-capped gold clusters were deposited onto gold on mica. Lithography was performed at greater than 2.55 V bias and 15.6 μm/s scan speed to locally remove the gold particles in squares corresponding to the scan dimensions. A complete removal of all particles within the pattern usually required four consecutive scans. No effect of humidity was reported, but the tunneling current played an important role. Tunneling currents of 0.5 nA and a 10 mV bias removed surface bound particles. The authors assumed that this was a clear indication that the removal was not due to an electrochemical effect and was based on mechanical scratching.

2.2. STM Modification in UHV

Müller et al. investigated the patterning of C_{16}S-SAMs and *n*-docosanethiolate (C_{22}S-) SAMs on gold

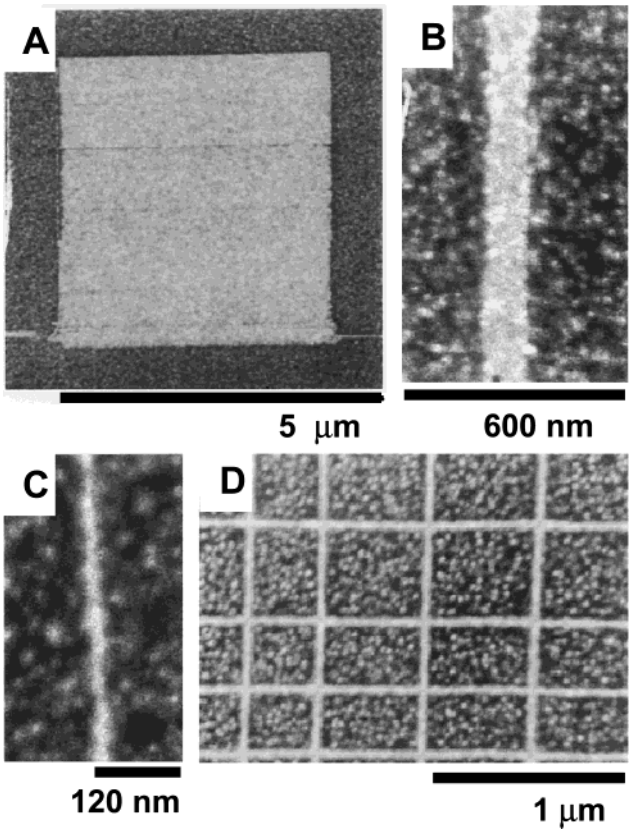

Figure 3. SEM images showing a series of features in gold created through STM-based lithography on a MMEA/Au substrate (I_t = 50 pA; V_b = 10 V; 15 μm/s), immersing the sample into a solution of $C_{16}SH$ for 30 s, and subsequent etching of the gold. A 5 μm × 5 μm square resulting from scanning 1024 consecutive lines (A). The lines seen in B and C resulted from 25 and one pass with the tip, respectively. The test grid (D) demonstrated single line patterns several micrometers in length. No proximity effect was seen at the crossing points. Reprinted with permission from ref 91. Copyright 1997 American Chemical Society.

with an STM operated in field emission mode in ultrahigh vacuum.[93] In this technique, high bias voltages (greater than 30 V) created tip−sample distances that were much larger (10−100 nm) than in normal STM imaging modes. The ultrasharp field emission tips were electrochemically etched single crystalline tungsten wires that yielded a line resolution of 20 nm at 10 μm/s scan speeds. The resulting patterns were transferred into the substrate by wet etching treatments. The researchers found no significant difference in the performance between the different chain lengths used.

Mizutani et al. investigated molecular-scale patterning and subsequent "healing" of C_9S-SAMs on gold (created by gas-phase deposition in UHV) and reported some of the smallest SPL-generated features to date.[94] The researchers worked under UHV conditions to avoid possible "uncharacterized" electrochemical processes that might occur due to the surface water layer in ambient conditions. Patterns were created when the tip was moved closer to the surface, and voltage pulses (between +2.6 and +3 V, 70−200 ms in duration) were applied. The smallest created feature of ca. 2 nm was achieved with a pulse of +2.6 V of 100 ms duration. Figure 4A shows an

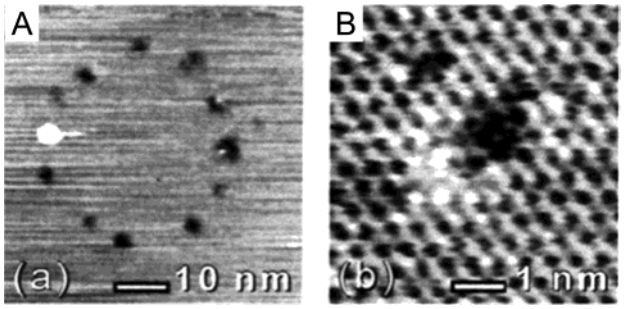

Figure 4. STM images showing (A) a circular pattern fabricated from voltage pulses of 2.7 V that created 11 holes and one protrusion and (B) one of the smallest intentionally created holes (100 ms pulse duration; V_b = 2.6 V). The SAM order in the periphery of the created pattern was disordered. Reprinted with permission from ref 94. Copyright 1998 American Chemical Society.

example of a circular pattern of these pulsed SAMs with a magnified image of one pulse region in Figure 4B. The most important observation in this paper was that the monolayer underwent changes after the applied pulse. Under continuous scanning, a self-healing process was observed in less than 5 min. The authors suggested that the molecules adsorb at the tip during the voltage pulses and were "re-supplied" during the imaging process. This assumption was supported by the fact that the self-healing process did not occur when the tip was retracted from the surface. Nevertheless, some of the created structures did not recover completely.

Hartwich et al. presented the STM-based etching of a $C_{16}S$-SAM on polycrystalline gold and Au(111) in which SAM modification occurred during one patterning scan (SPC: V_b = 1 V; I_t = 1 nA).[95,96] Surface feature sizes as small as 15 nm were created on Au(111). In a second report, the SPL patterns were transferred into the underlying substrate by a wet chemical etching process.[97] SEM images and noncontact mode AFM images showed similar results (line widths). This work was later extended to study the lithographic behavior of $C_{16}S$- and 4′-nitro-1,1′-biphenyl-4-thiolate-SAMs on gold surfaces and OTS-SAMs on silica.[98]

Keel et al. described the removal of the top gold layers from Au(111) surfaces modified with $C_{12}S$-SAMs.[99] Using an UHV-STM with tunneling parameters of 0.1 V and 1 nA (etching conditions), the surface was modified in a manner that coalesced the characteristic surface vacancy islands after one patterning scan. Irregularly shaped deposition of debris (the height of one layer of gold atoms) outside the scanned region was observed. Temperatures above 320 K showed more drastic changes in the surface morphology during the "etching" process, which were attributed to the higher mobility of the surface molecules and the surface gold atoms at elevated temperatures. Experiments performed under ambient conditions with a tunneling current of 1.2 nA required voltages between 0.1 and 0.4 V and altered the surface more than that observed under vacuum. It was concluded that the SAM played an important role. The binding of thiol molecules to the gold surface altered the bond strength between the top two gold layers significantly. No alteration in the morphology

of a bare gold surface was observed under the same etching conditions.

2.3. Modification with AFM (Mechanical and Electrical)

During an investigation of the structure and stability of decanethiolate ($C_{10}S$-) and $C_{18}S$-SAMs on gold, Liu and Salmeron observed that molecules could be displaced on the surface when the sample was scanned with an AFM tip under a high applied load (up to 100 nN).[100] After this displacement was observed, the molecules near these "defect" sites appeared to diffuse laterally back and subsequently "repaired" the initial SAM. Later, a similar study for alkylsilanes on mica was reported.[101] The force needed to displace silanes was higher than for the alkylthiolates of the same carbon chain length, but the actual value was dependent on the radius of the tip. Sharper tips decreased the required load by a factor of 10. This work illustrates the first step in the nanografting and nanoshaving processes discussed below in the section describing substitution lithography.

Kelley et al. described the mechanical removal of thiol-modified double-stranded DNA (dsDNA) by an AFM.[102] The DNA on a Au(111) substrate was imaged under a very low force (smaller than 200 pN). To remove the dsDNA, both the force applied to the AFM tip and the scan speed were increased. This resulted in the formation of squares exposing the underlying gold. The depth of these depressions was measured and taken to be the film thickness. By performing this process in an electrochemical cell and subsequently varying the potential applied to the surface, changes in thickness of the dsDNA layer were observed. These changes were attributed to the orientation of the dsDNA molecules with applied bias.

Zhou et al.[103] investigated changes in the surface morphology of thiol functionalized DNA SAMs upon exposure to complementary single-stranded DNA (ssDNA) or mercaptohexanol (HOC_6SH). The modified ssDNA was self-assembled to a flat gold surface and imaged with an AFM. By increasing the force applied to the tip (30−50 nN), the DNA was mechanically scraped away in square-shaped patterns. In this way, the researchers measured the thickness of the organic layer. When the patterned SAMs of ssDNA were immersed into complementary ssDNA, an increase in the thickness of the SAM was observed. The authors attributed this result to the formation of dsDNA, which had a more vertical conformation than the ssDNA. The same method was used to alter the height differences of patterned regions. After the writing of squares into a SAM composed of dsDNA, a second oligonucleotide with more bases (longer molecule) was assembled into the holes. Initially the AFM images showed that the height of the squares decreased but was still below the film thickness of the dsDNA background. When this sample was reacted with complementary DNA, the depressions changed to protruding squares.

Uosaki and Zhao employed a current sensing AFM (CSAFM) for localized removal of a SAM. This instrument consisted of a conductive cantilever that could collect surface information/morphology in the same way as a traditional AFM. This instrument had the added ability to monitor current in a two-electrode configuration (similar to STM). The researchers investigated the patterning dependence on applied bias, applied force, and the effect of water on patterning efficacy in an inert solvent (toluene).[104] The CSAFM enabled the authors to simultaneously compare topography and current images of the resulting pattern. The removal of SAM in patterned regions was supported by the appearance of ca. 1 nm (measured) depressions in the topography image, while the current sensing image showed high apparent height contrast between the "bare" substrate and the background SAM. This result suggested that the resist layer was no longer present, resulting in higher currents passing through the patterned regions. Figure 5 shows the topography (Figure 5A) and current images (Figure 5B) of a $C_{18}S$-SAM pattern generated by 3 nN applied force and 3 V substrate bias. Figure 5C shows $I-V$ curves during patterning (i), after patterning (ii), and outside the pattern (iii). Current voltage measurements revealed that the patterned areas gave resistance values of 1.7×10^9 Ω, much lower than an unmodified substrate (metal), but higher than a $C_{18}S$-SAM resist (insulator). From these data, the authors concluded that the desorbed material or contaminants from solution most likely re-adsorbed to the gold substrate. A series of experiments was conducted to investigate the patterning parameters for the CSAFM-based negative lithography. A systematic variation in applied bias under constant force yielded a critical threshold voltage of 2.0 V to remove the $C_{18}S$-SAMs. Application of the opposite bias (substrate negative) showed that a larger magnitude (−2.6 V) was required for the removal of the SAM. The applied force needed for elimination was observed to decrease with increasing bias. At biases larger than 2.9 V, no force dependence with applied bias was found. The authors suggested that the process was dominated by an electrochemical event at higher applied bias. Studies on the influence of water also revealed that lower bias was required to pattern under water-saturated toluene, whereas patterning performed under dry toluene required larger biases. This result supported that trace amounts of water facilitated the electrochemistry at the tip−substrate interface. The researchers concluded that the mechanism for the removal of organothiolate from the gold surface was electrochemical in nature, similar to the mechanism proposed by Crooks et al. for elimination lithography with a STM (vide supra).

A large body of work has described and exploited probe-based lithography to produce patterns involving the anodic oxidation of silicon. These experiments all employ silicon or a silica layer on silicon covered with a SAM as a resist. As will be illustrated below, the type of SAM has a large effect on the threshold bias and resolution of this process. Oxidation could be viewed as "adding" to the surface due to the silicon expansion. However, since the SAM is likely locally removed or "eliminated", these techniques are discussed in this section.

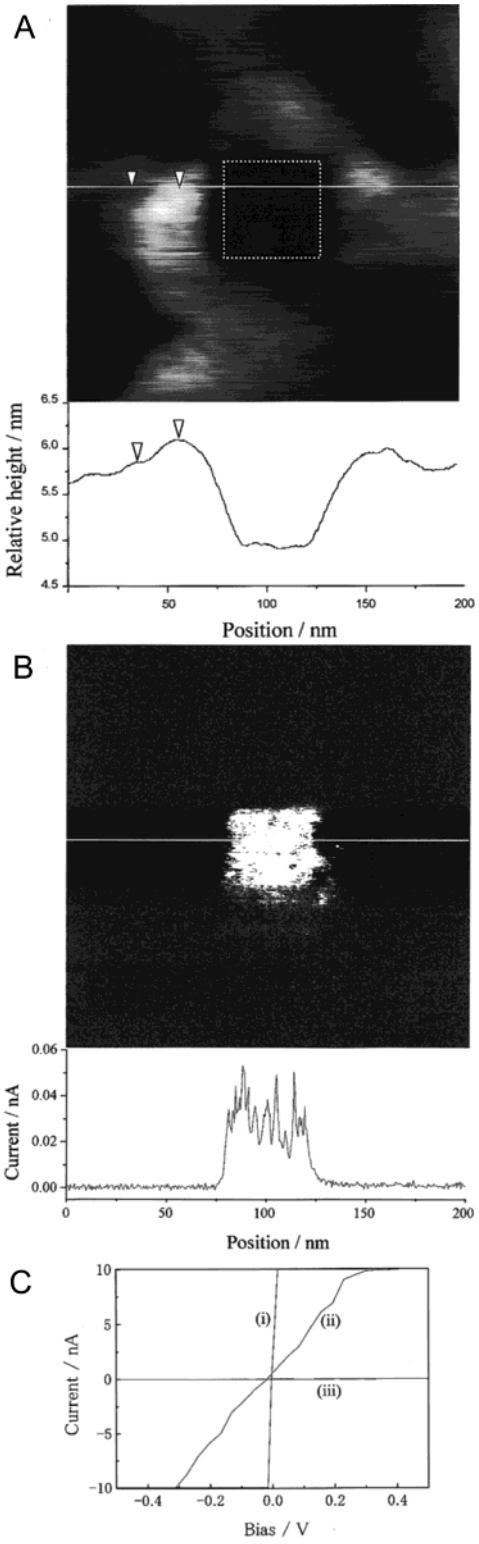

Figure 5. Topography (A) and current (B) images of a nominally 50 nm × 50 nm square in a C_{18}S-SAM on gold (under water-saturated toluene; lithographic conditions, ca. 3 nN force and 3 V bias; imaging conditions, 4 nN force and 0.05 V bias). The corresponding cross-section is shown below each image. (C) $I-V$ curves recorded (i) during the patterning inside the square, (ii) just after patterning inside the square, and (iii) outside the square (e.g., on C_{18}S-SAM). Reprinted with permission from ref 104. Copyright 2001 American Chemical Society.

Similar to previous (anodic oxidation) patterning demonstrations with an STM,[86] Sugimura et al.

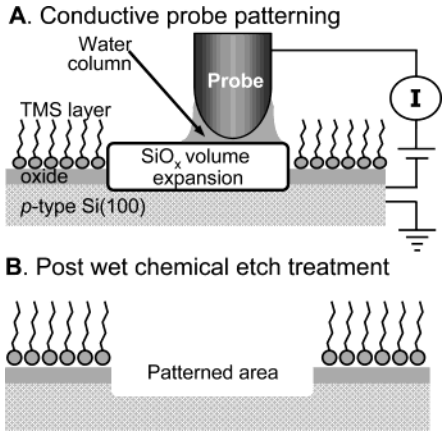

Figure 6. Schematic diagram of the anodic oxidation of a silane monolayer coated silicon oxide surface. (A) A conductive probe was scanned under an applied bias in a well-defined area on the sample surface. At ambient conditions, a water column formed between the tip and the surface and acted as an electrochemical cell. The pattern appeared as a protruded structure through the volume expansion of the SiO_x. (B) The pattern could be transferred into the silicon substrate via a wet chemical etching treatment.

employed a conducting AFM for the nanooxidative patterning of TMS-SAMs on silica that was based on tip-induced electrochemistry.[105] As illustrated in Figure 6, the conductive probe was connected to the substrate by a water meniscus (termed a "water column") that was attributed to capillary condensation in ambient conditions. The silane-based monolayer was degraded, and the native oxide silica surface once again became hydrophilic, (e.g., hydroxyl-terminated). In a similar approach, the authors showed with optical microscopy that the anodized patterns were hydrophilic from the condensation of water on chilled substrates.[106] The patterned regions protruded slightly above the surrounding SAMs. This protrusion was believed to be a volume expansion from the anodization of the (SiO_2) substrate by the incorporation of oxygen. After patterning, the structure was transferred into the substrate by a wet etching process with $NH_4F/H_2O_2/H_2O$. The narrowest line width obtained was 30 nm, but the isotropic etching process resulted in a widening of the lines. Patterning with positive biases required more than +3 V for complete patterning, while the negative voltage needed was at least −5 V. Larger biases led to more complete degradation of the TMS-SAMs and therefore, a more effective etching procedure. The researchers observed a difference in the onset of the degradation threshold voltage in the positive and negative polarities that was believed to be due to the asymmetric nature of the tip−sample junction.

The exact mechanism of the degradation of the silane-based layer was unknown, and the number of electrons needed to remove a molecule was calculated to be several hundred. The authors assumed that not all of these electrons were necessary for an electrochemical process associated with the degradation of the TMS layer. The authors speculated that these results were caused by tunneling or field emission currents passing through the molecule. Leakage current through the water column by lateral electron

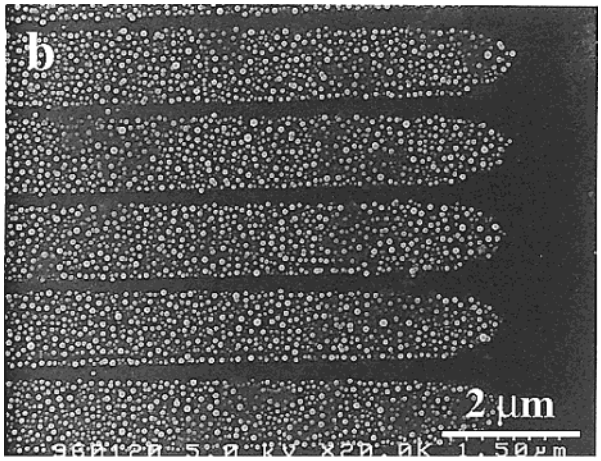

Figure 7. Scanning electron microscope image of fluorescent latex nanoparticles immobilized onto a pattern generated by STM ($V_b = +5$ V, 0.2 μm/s scan speed in N_2 with 80% RH) after APS treatment and immersion in latex particle suspension. Reprinted with permission from ref 108. Copyright 1997 American Chemical Society.

hopping or electrons contributed to/from other reactions not related to the degradation of the organic monolayer also could cause these results. The amount of current injected per unit area was also observed to decrease as the patterning scan speed increased. To further understand the role electrons played in the degradation of organic monolayers, Sugimura and Nakagiri performed AFM lithography in constant current mode and observed that an injected electron density of several pC/μm fabricated clear etched features in the SAMs.[107] When this current density was applied, scan speeds up to 5000 μm/s could be used. However, the limits of the mechanical stability of the AFM system were reached and created irregular patterns. At injections of 1000 pC/μm, the area surrounding the scanned region was altered, and LFM images suggested contaminants could be present due to different friction contrasts than previously obtained of silicon oxide. Relative humidity studies strongly suggested that the degradation rate was also accelerated with increased humidity. Scan rate studies revealed that the depth and width of the line transferred into the substrate by etching increased with decreased scan rate. The researchers explanation was that the amount of injected current per unit time was changing.

In an ex-situ approach to generate chemically heterogeneous patterns, Sugimura and Nakagiri lithographically prepared a TMS-SAM as described above but added a second silane (3-aminopropyl)-triethoxysilane (APS, $H_2N(CH_2)_3Si(OCH_2CH_3)_3$)) that reacted to the surface hydroxyl groups generated in the anodic oxidized patterns.[108] To confirm the selective growth of the APS layer, aldehyde-modified, fluorescently tagged, latex nanoparticles were reacted with amine functionalities in the patterns. Fluorescence optical micrographs (Figure 7) confirmed that the latex nanoparticles were bound only in the patterned areas. Further experiments revealed that the amine groups of the confined APS areas could be reacted with the amine groups of proteins (e.g., horseradish peroxidase) with the help of a glutaraldehyde cross linker. Tapping mode (noncontact mode AFM) and phase contrast AFM images revealed the adsorption of protein to the APS confined regions with no apparent nonspecific binding to the TMS regions of the SAM. Another ex-situ addition approach reacted heptadecafluoro-1,1,2,2-tetrahydrodecyl-1-trimethoxysilane (FAS) by CVD to the SiO_2 structures created from anodic oxidation in an OTS-SAM.[109] The samples were monitored before and after with topographic AFM images and Kelvin probe force microscopy (KFM). The large molecular dipole of FAS contributed to surface potentials that were 50 mV higher in the patterned lines than in the surrounding OTS-SAM, which showed up clearly in KFM images. Patterns generated by anodic oxidation transferred into the oxide layer by a wet chemical process served as a template for the electroless plating of Au.[110] Here, the plating proceeded selectively on the Si surface due to the galvanic displacement between Si and Au ions, while the OTS-SAM surface remained free of deposits. The line resolution of the electroless plating achieved was 200 nm, confirmed with SEM and Auger spectroscopy.

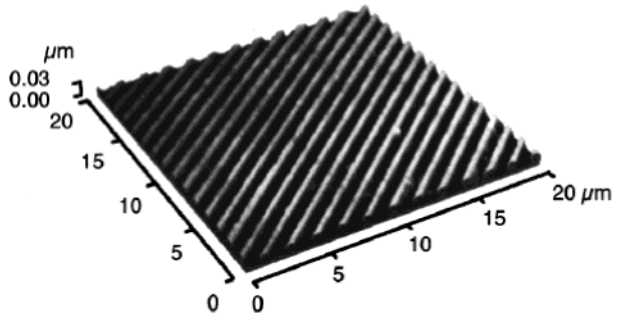

Figure 8. AFM images showing the results of AFM anodic oxidation and wet etching of a pattern in an ODS-SAM on a multilayer resist: scan speed, 10 μm/s; probe current, 5 nA; etching steps with 0.5 wt % hydrofluoric acid (0.5 min) and 25 wt % tetraammonium hydroxide (3 min). Reprinted with permission from ref 111. Copyright 1999 Society of the American Institute of Physics.

Sugimura et al. also used localized current injection (from a conducting AFM tip) to pattern insulating SiO_2 substrates by utilizing a multilayered resist containing a conductive layer.[111] An amorphous silicon resist was thermally grown on SiO_2 and cleaned by ultraviolet light-generated ozone, which created a thin silicon oxide layer. This layered structure was then coated with an octadecylsilyl SAM (ODS-SAM). The SPL patterning parameters were similar to those described previously by this group. A two-step wet chemical development process transferred the structures to the underlying thermal oxide film. First, etching in dilute hydrofluoric acid led to the removal of the exposed photochemical oxide. A second wet etch step with tetramethylammonium hydroxide (TMAH, 25 wt %) was performed, and the pattern mask for the further etching of the thermal oxide was achieved. By immersion of the substrate into hydrofluoric (HF) acid, the oxide was structured with the same patterns written with the AFM probe. An example of Si structures created with this process is shown in Figure 8.

Sugimura et al. also described the influence of SPL parameters on the patterning of organosilane SAMs

on silicon substrates.[112] The effect of the pulse duration on the size and height of patterns created in SAMs composed from ODS-SAMs was investigated by lateral force contrast. By comparing the results from the different measured parameters, the authors concluded that the surface modification was a multiple-step process and electrochemical reactions between the tip and the sample in the water column took place. The line width was dependent on the writing speed with a lower width limit of 20 nm, but the authors believed this value to be convoluted with the shape and size of the probe.

Zheng and co-workers chemically positioned Au nanoparticles on a silicon surface using a nanooxidation technique for the preparation of quasi-one-dimensional lines.[113] After SPL patterning (ca. 8 V, 4 μm/s) of a SAM prepared from octadecyltrichlorosilane on silica, amine-terminated silanes were self-assembled into the oxidized, patterned areas. Then, 12 nm diameter gold nanoparticles were electrostatically bound to these amine-terminated SAM regions. SEM images showed the particles were exclusively immobilized on the predefined patterns.

Using a methodology similar to that described above, Li et al. presented the fabrication of lithographic patterns that could trap single gold colloids.[114] The researchers investigated the role of the humidity, pulse duration, and pulse voltage on the diameter of the oxidized (patterned) spots. Prior to patterning, OTS-SAMs were incubated in the presence of small silane molecules (phenyltrichlorosilane or 3-(chloropropyl)trichlorosilane) to avoid colloidal binding in the defect sites of the SAM when exposed to the gold nanoparticle (AuNP) solution. By controlling the size of the SPL pattern, the number of particles adsorbed could be controlled. With a spot diameter of 100 nm, the efficiency for binding 15 nm particles was determined to be 100%. As the diameter was decreased to 28 nm, only 30% of the oxidized/functionalized spots on the surface were found to bind a colloid. The authors believed that the effective area where the adsorption took place was smaller than the measured diameter of the oxidized area due to an inhomogeneous degradation of the OTS layer. As the spot diameters became smaller, the number of OTS molecules remaining in the patterned region increased, effectively decreasing the number of binding possibilities for the gold nanoparticles. The nonplanar shapes of the oxidized silicon patterns were also believed to contribute to the lower efficiency for binding. Nevertheless, the authors demonstrated the ability to control the number of particles down to the binding of a single Au particle in a single oxidized dot. Figure 9A shows an AFM image of the original oxide patterns, and Figure 9B depicts 15 nm diameter AuNP absorbed onto this structure.

Nanoparticles patterned on silica surfaces have also been used by Zheng et al. as masks in the anodization of a silica substrate. This strategy facilitated the fabrication of silicon nanopillars under ambient conditions (Figure 10).[115] Gold colloids (18 nm) were initially anchored to the surface with a mercaptopropyltriethoxysilane SAM (MPTS-SAM), as illustrated schematically in Figure 10A. An area

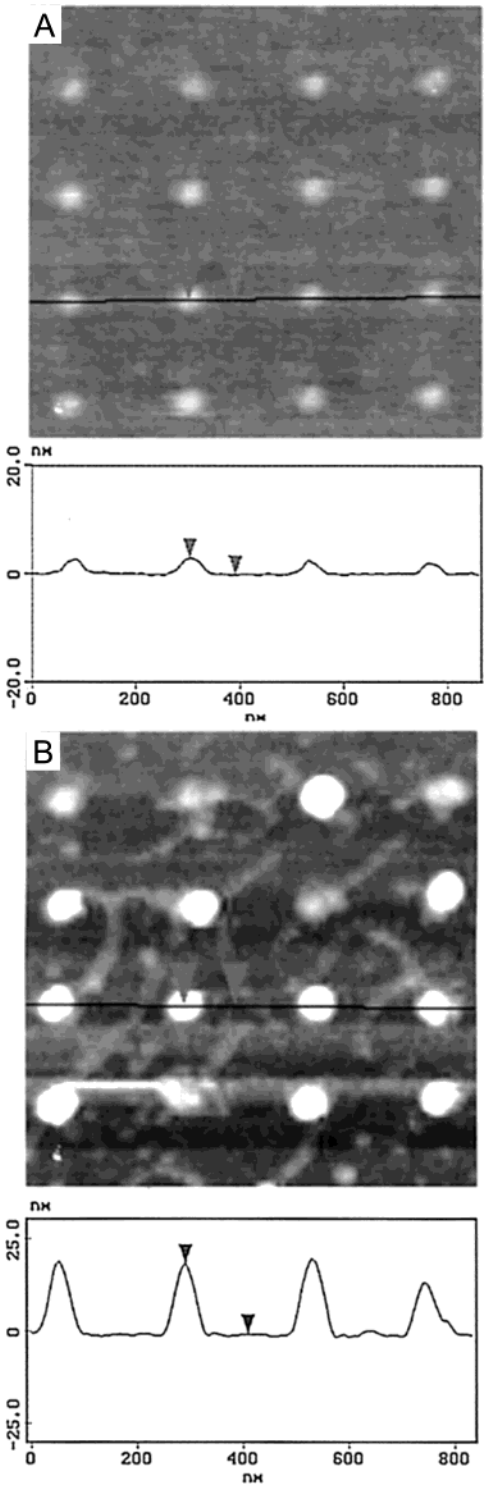

Figure 9. (A) Tapping mode AFM images of an oxide dot array fabricated by anodic oxidation of an OTS/SiO_x sample after back-filling with (aminopropyl)trimethoxysilane (dot height, ca. 2.5 nm; diameter, 70 nm). (B) The same template after the adsorption of 15 nm gold nanoparticles. Single particles were adsorbed to the oxide patterns. The section analysis data for both images are given below the corresponding image. Reprinted with permission from ref 114. Copyright 2003 American Chemical Society.

was scanned with an applied bias of +9 V to oxidize the silicon in this region (Figure 10B). By comparing the height of the nanoparticles before and after the anodization, the measured height of the nanoparticles decreased slightly from 18 to 15 nm, which

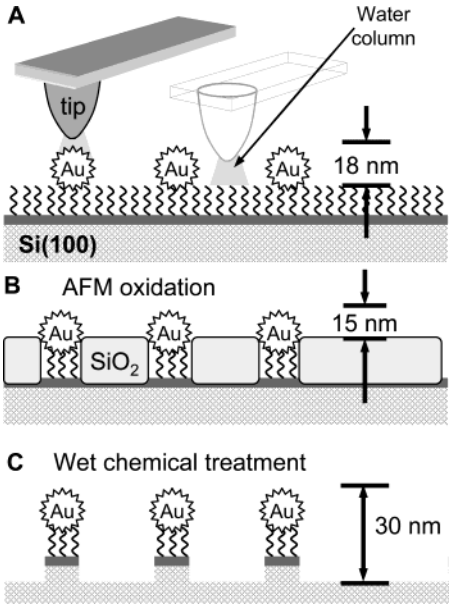

Figure 10. Schematic diagram of (A) selective anodization of the silicon regions not masked by nanoparticles. (B) The volume expansion of the silicon led to a decreased height contrast between the particles and the substrate. (C) After a wet etching step, silicon columns capped with a nanoparticle were formed.

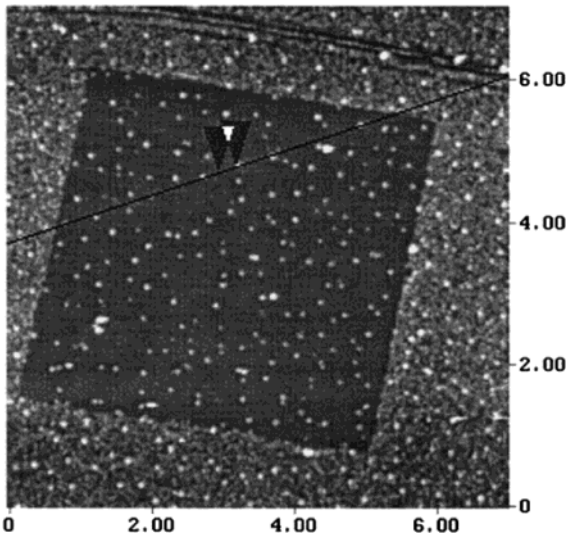

Figure 11. Noncontact mode AFM image (7 μm)^2 of a patterned square (ca. 5 μm $\times$ 5 μm) containing silicon columns. Reprinted with permission from ref 115. Copyright 2000 American Chemical Society.

supported the assumption that the silicon around the nanoparticles oxidized and slightly expanded (Figure 10B). After wet etching of the sample, columns remained under the nanoparticles (Figure 10C). The measured diameter of these columns (in the lithographically patterned area) was 71 nm with a height (including the AuNP) of 30 nm (Figure 11). The real lateral dimension of the features could be smaller due to the convolution of the tip shape and the columns. This experiment showed that nanoparticles could be used as masks for the electrochemical modification of a silicon surface.

Kim et al. followed the same silicon anodization approach as Sugimura et al., reporting the use of octadecyldimethylmethoxysilane (ODMS) as an organic resist for lithography with a conductive AFM (cAFM).[116−118] The organic monolayer was degraded under a constant force and an applied negative voltage of −10 to −30 V. The authors assumed that the voltages used resulted in field emission from the tip. This patterning resulted in protruded features caused by the volume expansion of the silicon during the anodization. It was shown that the patterns could be transferred into the substrate by a wet etching step with buffered oxide etch (BOE). This etching process was selective and the organic layer was nearly unaffected, while the oxide layer was removed. The smallest reported line width was ca. 70 nm written at a scan speed of 120 μm/s.

Several efforts studied the effect of various types of surface monolayers and multilayers with this type of patterning via anodic oxidation of silicon. Kim et al. anodized silicon terminated with multilayered structures based on zirconium phosphonate chemistry.[119] During the course of multilayer formation, it was observed that lines patterned on a Zr^{4+}-terminated surface were smaller than lines patterned on a phosphonate-terminated surface. The researchers concluded that the surface charge of the Zr^{4+} was enhancing the effect of the anodization.

The effect of surface charge on the efficacy of patterning was also investigated by Kim et al.[120] The films were fabricated by the sequential adsorption of phosphoric acid and metal ions (Zr^{4+} or Ca^{2+}). The adsorption of Zr^{4+} resulted in a net positive charge, while Ca^{2+} led to neutral surfaces. Film preparation was confirmed by ellipsometry and AFM. The authors reported the effect of systematically changing the applied bias voltages and scan speeds during patterning and compared the resulting line widths and heights of the silicon protrusions. It was observed that the positively charged film could be patterned at lower applied voltages and higher scan speeds than the neutral surface. The authors concluded that the positive charge (on Zr^{4+} films) led to an enhancement of the lithographic process by altering the electron-transfer process, causing the Zr^{4+} films to be patterned at lower voltages.

In a similar vein, Lee et al. investigated the silicon protrusions generated on charged amphiphilic layers physisorbed on silicon surfaces.[121] The bipolar amphiphiles, 1,12-diaminododecane (DAD-2HCl) and *n*-tridecylamine (TDA-HCl), were adsorbed onto a negatively charged silicon wafer creating ammonium-chloride-modified and methyl-terminated films, respectively. Various AFM anodizations were performed at a relative humidity of 50% with different scan speeds (30−480 μm/s), applied voltages (10−25 V), and currents (13−14 nA). The ammonium-chloride-modified surface led to broader and higher protruding lines than the surface terminated with methyl groups. The authors attributed this to an enhancement effect by the charged ammonium ions.

Mixed monolayers of the above-mentioned amphiphiles were used to investigate terminal surface group effects on the efficacy of anodic patterning of silicon wafers with this AFM lithography.[122] It was shown that the mixing ratio on the surface was

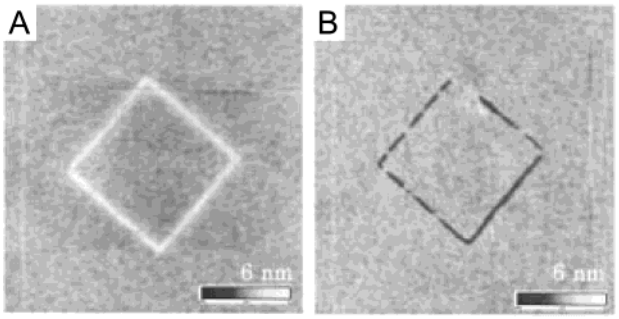

Figure 12. AFM images showing a lithographically defined pattern in a palmitic acid LB layer adsorbed to a SiO_x/Si substrate. Diamond pattern with protruding lines was written with −10 V applied tip bias (A), and that with grooves, with +10 V applied tip bias (B) (*z*-scale: 6 nm). Reprinted with permission from ref 123. Copyright 2002 American Institute of Physics.

strictly related to the ratio of the molecules in solution and played an important role for the threshold voltage necessary to produce lines of a predetermined height. Under fixed anodization parameters, as the amount of DAD-2HCl in solution was increased, the voltage for creating a line of 10 nm width decreased. However, it was observed that the current during the patterning process was nearly constant for the different mixtures, which supported a faradaic process for the anodic oxidation. Increased ratios of DAD-2HCl resulted in increased line widths. The amount of ammonium chloride groups present on the surface was believed to be responsible for this phenomenon. The authors argued that when the surface was more hydrophilic, the water meniscus present was larger, leading to wider lines.

The effect of polarity change applied to the AFM cantilever was the focus of a report by Lee et al., who patterned LB resists/films prepared from palmitic acid ($C_{15}COOH$) physisorbed on a silicon oxide surface.[123] Under positive substrate biases, protruding lines in silicon were generated. Under reverse biases, grooves with a smaller width were found. The depth of the groove correlated with the thickness of the LB layer. The authors supplied two possible explanations for the selective removal of the molecules from the surface under reverse bias. The first hypothesis was based on the dissociation reaction of the palmitic acid. The second hypothesis described the degradation of the resist under a strong electric field, which was concluded to be the dominant process based on the increase in groove depth with increasing bias. At −5 V, the negative-tone pattern was just half the depth of the film thickness and increased with increasing bias. This work was the first example for the creation of protruding lines or grooves by merely changing the polarity of the applied bias. Figure 12 shows an example of a diamond pattern generated with a −10 V bias to create a protrusion (Figure 12A), and a similar pattern created with a bias of +10 V resulted in a groove (Figure 12B).

She et al. described the effect of applied force on the groove formation in LB films of OTS on freshly cleaved mica substrates.[124] All measurements and mechanical modifications were done in 40−70% relative humidity at room temperature. The OTS monolayer was removed between applied forces of 400 and 800 nN. Forces above 800 nN formed deeper holes, which indicated that the mica substrate was affected. The narrowest lines (50 nm) could be written with a high applied force of 700 nN.

Ara and co-workers used alkyl monolayers covalently bound to silicon as resists for nanolithography.[125] Again, this process was proposed to oxidize the underlying silicon as described above. Alkyl monolayers were created by the reaction of 1-alkenes with hydrogen-terminated silicon. The authors showed that these layers could be anodized with an applied bias of +5 V. It was pointed out that the voltage necessary for pattern formation was roughly half of that needed for the patterning of alkylsiloxane (alkylsilane) monolayers on silica. The researchers showed that the anodized lines could either be etched away or modified with another alkyl silane. With this technique, letters with a line width of 40 nm were produced.

Tully et al. explored the use of dendritic monolayers on silicon as positive resists for SPL, contending that their properties make them ideal for self-assembly on a surface.[126] These properties include the globular shape, monodispersity, and the higher stability due to the dense structure. Adlayers of four different chlorosilane-terminated poly(benzyl ether) dendrons were formed and characterized by contact angle goniometry, ellipsometry, and AFM. These techniques indicated high coverage of a dendron-based film on the surface. During lithographic patterning with a conducting probe AFM, the feature size was found to depend on the applied voltage and the scan speed. Higher applied voltages at constant speeds produced wider, taller silicon protrusions, while increased scan speeds at a given voltage afforded more narrow lines. For example, a sample bias of 8−10 V and a scan speed of 500 nm/s produced lines averaging 60 nm wide and 2 nm high. The authors believed the protruding lines were because of a field-enhanced oxidation or an electrochemical anodization of the underlying silicon (which created a volume expansion of the Si by the incorporation of oxygen). Additionally, the researchers showed that the dendron layer could be used as etch resists for the transfer of the anodized Si patterns into the silicon wafer. Treatment of the patterned substrates with dilute HF created grooves of a size commensurate with the SPL-generated patterns in the organic layer.

Tully et al. then prepared thin films of poly(benzyl ether) dendrimers containing carboxylic acid moieties either at the focal point or at the dendrimer periphery and investigated their behavior as a positive resist for SPL.[127] The dendrimers were bound to a aminosilane-modified Si(100) surface. Two types of patterns were observed. Positive toned images were reportedly created by degradation of the organic film with current injection, or negative toned patterns were created by oxidation of the underlying substrate. Singly charged, ionically bound dendrons required a patterning bias larger than 20 V, which formed holes with a 35 nm diameter and a depth that correlated with the thickness of the monolayer. SPL patterning

using dendrimers that contained multiple ionic charges at the peripheries produced negative toned, protruding lines ca. 80 nm in width and 11 nm in height following application of 15 V at 500 nm/s scan speed. This pattern was then subject to an etchant, removing the dendrimer film to give rise to 28 nm high features.

2.4. Scanning Probe Lithography with SECM

Scanning electrochemical microscopy (SECM) was used for the electrochemically induced, localized desorption of dodecylthiolate ($C_{12}S$-) SAMs to create micrometer-sized patterns.[128] SECM produces much larger features than can be created with other SPL techniques. However, as shown below, it has the advantage that the probe can subsequently monitor electrochemical events in patterned regions in a well-defined fashion.

SECM-based patterning occurred by moving an auxiliary microelectrode (5 or 25 μm radius) in a predefined pattern above a conducting surface (which served as the working electrode), under either a reductive or oxidative applied potential to degrade the SAM. Subsequent imaging of the patterns produced was accomplished in the same solution with the microelectrode functioning as the working electrode. The researchers improved SAM desorption by using different polarity potential ramps that initiated reductive or oxidative desorption of the SAM. The authors used the freshly exposed gold surface for the subsequent adsorption of bis(2-aminoethyl)disulfide dihydrochloride followed by a carboxylated osmium complex which reacted with the amino groups of this adlayer. This structure was characterized by XPS imaging to map elemental distributions. The same group used this technique for the formation and imaging of enzymatically active spots on an alkanethiolate-covered electrode.[129] Desorption of the $C_{12}S$-SAM was performed in KOH (5 or 50 mM) with potential cycles between -1200 mV and $+1200$ mV. The newly formed gold areas were modified with cystaminium dihydrochloride. Subsequent immersion into periodate-oxidized glucose oxidase yielded the final structures. These patterns could be observed by monitoring the enzymatic activity of these glucose oxidase-containing spots with SECM. Most recently, Wilhelm and Wittstock used SECM to locally desorb horseradish peroxidase with the subsequent exposure of the pattern to glucose oxidase, which was imaged with generation-collection mode.[130]

Shiku et al. reported the formation of hydroxyl radicals through the degradation of self-assembled monolayers of silanes on glass with a SECM.[131] In a first step, octadecyltrichlorosilane, propyltrichlorosilane, or (3-mercaptopropyl)trimethoxysilane monolayers were prepared and subsequently immersed into a solution of 0.05 M H_2SO_4 containing $FeCl_3$ and H_2O_2. The microelectrode of the SECM was placed 5 μm above the surface. Voltage pulses were applied for predetermined times to create hydroxyl radical sites on the surface. The resulting patterned regions were then functionalized with the enzyme diaphorase. Local diaphorase activity could subsequently be monitored by SECM by detecting the diaphorase-catalyzed current of ferrocenylmethanol coupled with the oxidation of reduced nicotinamide adenine dinucleotide (NADH). The size of the hydroxyl-radical-modified area increased with the pulse period and ranged from ca. 20 μm for 20 s to more than 200 μm for 1800 s.

SECM has also been employed to locally deposit gold islands that were used as templates to tether enzymes or fluorescent dyes through cystamine linkers. One might envision this demonstration as particularly useful for the fabrication of nanoscale assemblies. In particular, this technique might be extended to the variety of systems that have been studied when tethered to gold nanoparticles.[132]

2.5. Scanning Probe Lithography with NSOM

Sun et al. employed near-field optical microscopy (NSOM) to pattern $C_{12}S$-, mercaptoundecanoic acid-(MUA-), and mercaptoundecanol-SAMs on gold substrates.[133,134] The light from a frequency-doubled argon ion laser ($\lambda = 244$ nm) was coupled into a fused silica fiber, which had an Al-coated tip with an aperture of ca. 50 nm. The fiber was scanned at a distance of 5−10 nm above the surface. The UV light photooxidized the surface bound thiolate molecules to sulfonate species, which were much more weakly bound to the substrate. The patterned surface could be either dipped into a solution with a different thiol, replacing the weakly bound sulfonate from the surface, or dipped into an etching solution for structuring the gold. In one example, the patterned substrate was immersed into mercaptoundecanioc acid. As can be observed in Figure 13, the topography image (Figure 13A) showed no difference between the two SAM regions, while the friction image (Figure 13B) clearly showed the patterned lines. The line width was 50

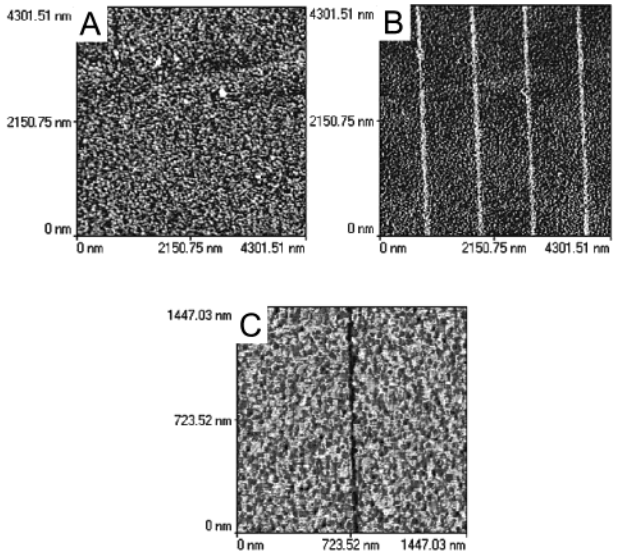

Figure 13. AFM images of parallel lines of MUA in a $C_{12}S$-SAM on gold created by NSOM lithography. (A) The topography image showed no contrast. (B) LFM image showed lines with a width of 50 ± 5 nm. (lithographic conditions: 0.2 μm/s writing speed; 60 mW laser power). (C) LFM image of a 30 nm line of $C_{12}S$- in a MUA-SAM (lithographic conditions: 1 μm/s writing speed; 20 mW laser power). Reprinted with permission from ref 134. Copyright 2002 American Chemical Society.

Table 1. Elimination Lithography

SPM and tip used	SAM type	substrate	line resolution	SIC	RC	comments	ref
STM; Pt/Ir	$C_{18}S$-	Au(111)/Ti/ mica	10 nm × 10 nm squares	3−5 V, 0.5−1 nA	10 mV, 10 nA, RT, air	early SPL example	79
STM; Pt/Ir	$C_{18}S$-	Au(111), annealed ball	25 nm × 25 nm squares	0.3 V, 0.1 nA, 0.536−0.67 μm/s	3−8 V, 0.1 nA, 0.78−6.7 μm/s, RT, air	electrochem explanation for STM, SPL μm electrode fabrication	82
STM; W	$C_{18}S$-	Au on silicon, GaAs	20 nm (Au); 15−20 nm (GaAs)	tapping mode AFM	3−10 V, 0.1−10 nA, RT, air	wet etching into Au film, raised structures	83
STM; conductive diamond	TMS	p-type Si(100)	80 nm	AFM, optical micrographs	5 V, 0.2 nA, 0.1−0.6 μm/s, RT, air	isotropic etching	86
STM; W	$C_{18}S$-	GaAs	15 nm	STM	10 V, 0.5 nA	wet etching into substrate	84
STM; Pt/Ir	$C_{18}S$-	Au(111), annealed ball	50 nm to 5 μm	SEM	4−8 V and then 0.3 V, 0.15 nA, 0.8−6.7 μm/s, multiple scans, RT, air	Cu deposition in etched SAM	87
STM; −	$C_{18}S$-	Au on silicon, GaAs	20 nm (Au); 15−20 nm (GaAs)	tapping mode AFM	3−10 V, 0.1−10 nA, RT, air	etching into substrate	85
STM; Pt/Ir	$C_{18}S$-, C_9S-	Au(111)	50 nm × 50 nm squares	0.3 V, 150 pA, 1.2 μm/s	3 V, 0.15 nA, 2.05 μm/s, multiple scans, RT, air, N_2	RH studies	88
STM; Pt/Ir	$C_{18}S$-	Au(111)		0.3 V, 150 pA, 0.4−1 μm/s	3−4 V, 0.03−6 nA, 2.05 μm/s, multiple scans, RT, air	shape dependence from Coulomb dose	89
STM; Pt/Ir	$HS\text{-}CH_2CONHCH_2CH_3$	Au	∼30 nm	0.8−1 V, 10−50 pA, 15 μm/s	4 V, 50 pA, RT, air	etching expts, high-energy e^--beam	91
STM;, Pt/Ir	monolayer-protected, Au clusters	Au on mica	200 nm × 200 nm squares	STM and AFM, 0.3 V, 0.2 nA	0.3 V (0.45 nA) to 3 V (0.2 nA), 0.9−15.6 μm/s, RT, air	mechanical removal of AuNP	92
UHV STM; W	$C_{16}S$-, $C_{22}S$-	polycrystalline Au	70 nm	SEM, AFM	−65 V, 6 nA, 10 μm/s (UHV)	etching into substrate	93
UHV STM; Pt/Ir	C_9S-	Au(111)	2−5 nm	0.8 V, 20 pA (UHV)	2.6−3.5 V pulses (UHV)	diffusion studies (healing), $I-V$ measurements	94
UHV STM; W	$C_{16}S$-	Au(111)	15 nm	0.1 V, 100 pA	1 V, 1 nA (air); 10 V, 1 nA (UHV)		96
UHV STM; W, Pt/Ir	$C_{16}S$-	Au	60 nm	0.1 V, 100 pA	1 V, 1 nA (UHV)		97
UHV STM; W, Pt/Ir	$C_{16}S$-, OTS, 4-nitro-1,1-biphenyl-4-thiolate	Au, Si	20 nm	0.1 V, 100 pA	1 V, 1 nA (air); 10 V, 1 nA (UHV)	UHV and air patterning	98
STM; 80/20 Pt/Ir	$C_{12}S$-	Au(111) on mica	10 nm × 10 nm reported; 50 nm × 50 nm shown	∼ 1 V, 50 pA	0.1 V, 1.2 nA (air); 0.1 V, 1.0 nA (UHV)	variable temps 303−363 K	99
AFM; −	$C_{10}S$-, $C_{18}S$-	Au(111)		1 nN	10−280 nN	pressure dependent on tip radius	100
AFM; −	ODS	Si(100)		1 nN	∼ 10 nN		101

Table 1. (Continued)

SPM and tip used	SAM type	substrate	line resolution	SIC	RC	comments	ref
AFM; Si_3N_4	thiolated dsDNA (15 base pairs)	Au(111) on mica	100 nm × 100 nm square	<200 pN	higher load through increased set point; 2.4−4.5 μm/s	removal of DNA for the determination of DNA orientation	102
AFM; Si_3N_4, sharpened 0.06−0.12 N/m	thiolated ssDNA (20 mer)	Au(111)	∼100 nm × 100 nm square	0.2−0.4 nN, Tris buffer, 24 ± 1 °C	30−50 nN, Tris buffer, 24 ± 1 °C	measurement of change in film thickness with hybridization	103
AFM; Si_3N_4, NiCr coated	TMS	SiO_x	30 nm	+20 to +3 V, −5 to −10 V, <500 μm/s	60% RH, RT	etching into substrate	105
STM; −	TMS	SiO_x on p-type Si (100)			±(2−20 V), 10−100 pA, 20−500 μm/s, 60% RH	bias polarity patterning studies	106
AFM; doped Si, Si_3N_4, NiCr coated	TMS	SiO_x	20 nm	scan speed up to 5000 μm/s		etching	107
AFM; −	TMS	SiO_x			5 V, 200 pA, 1.2−2 μm/s, 20−80% RH, N_2	adsorption of fluorescent -tagged particles	108
cAFM; −	ODS	thick SiO_2	50 nm	AFM, 1 nA, 20 μm/s	5 nA, 10 μm/s	multilayer resist; current injection	111
cAFM; doped Si	ODS, FAS	SiO_x	90 nm	KFM, AFM	10 V, 0.1 μm/s		109
AFM; doped Si	ODS	SiO_x on n-type Si(100)	20 nm		12−20 V, 1−5 nA; 20−50 μm/s, 45% RH	etching, electroless Au deposition	110
cAFM; doped Si	ODS		20 nm	LFM, 0.5 V, 20 μm/s, 26% RH	7−10 V, 2.8 nN, 5−500 nm/s	voltage pulse duration studies	112
CAFM; Si_3N_4, Au coated	MPTS	n-type Si	71 nm		9 V, 1 μm/s, 42% RH	AuNP mask for oxidation; Si columns	115
AFM; doped Si	OTS	n-type Si(111)/ SiO_x	39−45 nm	AFM	8 V pulses, 4 μm/s, ∼ 58% RH, air	adsorption of AuNP, MPTES ink	113
AFM; doped Si, TiN coated	OTS back-filled with short-chain silanes	p-type Si(100)	15 nm	tapping mode AFM	6−12 V pulses, 10−500 μm/s, 25−55% RH	two silanes; AuNP immobilization	114
AFM; Si	ODMS	SiO_x	70 nm		−10 to −30 V, <120 μm/s	etching	116
cAFM; Si	ODMS	SiO_x on p-type Si(100)	75 nm		-10 to -30 V, 14 nA, 120 μm/s		117
cAFM; −	ODMS and polymer	SiO_x on p-type Si(100)	75 nm		−10 to −30 V, 120 μm/s, 14 nA		118
cAFM; −	EPPI	SiO_x	54 nm	AFM	−12 V, 30 μm/s		119
AFM; −	(DAD)-2HCl; (TDA)-HCl	SiO_x	protruding lines, ∼90 nm width, 10−16 Å height		10−25 V, 13−14 nA, 30−480 μm/s, 50% RH, RT		121
AFM; B-doped Si	(DAD)-2HCl; (TDA)-HCl	SiO_x	48 nm width, 16 Å height	LFM, 0.5 V, 20 μm/s, 26% RH	10−25 V, 500 μm/s, 50% RH	optimal mixed SAMs; 4/1 DAD/TDA	122
AFM; Si, Pt	phosphorus oxychloride	SiO_x on p-type Si(100)	50 nm		7−18 V, 1−500 μm, ambient temp		120

Table 1. (Continued)

SPM and tip used	SAM type	substrate	line resolution	SIC	RC	comments	ref
coated	and Zr or Ca ions						
AFM; −	$C_{15}H_{31}COOH$	SiO_x	60−80 nm		+10 V or −10 V, 40% RH, RT	grooves and protruding lines	123
AFM; Si	OTS	mica	30 nm		>400 nN, 40−70% RH, RT	mechanical removal	124
cAFM; Si_3N_4, Pt coated	$C_{18}S$-	Au(111)	15 nm	<0.5 V, <5 nN	∼ 2−4 V, >2 nN, 4.9−9.8 Hz, water-saturated toluene, toluene vapor, RT	*I*−*V* measurements	104
cAFM; Pt coated	1-dodecene	n-type Si(111)	40 nm	AFM	5 V, 200 nm/s	addition of octadecene to patterned area	125
cAFM; −	dendrons	Si(100)	60 nm		8−10 V, 200−500 pA, 500 nm/s	holes and protruding lines in dendron layer	127
cAFM; −	-NH_3-terminated dendrons	Si(100)	80 nm		15−20 V, 500 nm/s, 200−500 pA	grooves and protruding lines in dendron layer	126
SECM; Pt disk	horseradish peroxidase	Au	∼50 μm	0.4 V; ferrocenyl-methanol, KCl, and phosphate buffer	square wave, 2 V peak to peak (5 kHz, 38 s)	adsorption of glucose oxidase	130
SECM; Pt disk	functionalized silanes	glass	20 μm	0.4 V; ferrocenyl-methanol, KCl, phosphate buffer, and NADH	0.0 V; ferrocenylmethanol, KCl, and phosphate buffer	large diaphorase pattern	131
SECM; Au disk		Si	∼25 μm	0.5 V (Pt disk), 9.8 μm/s, 4 mM hexacyanoferrate and 0.1 M KCl	∼ 1.1 V, 1−5 min, 0.01−0.05 M HCl	deposition of Au islands for binding of cystamine	132
SECM; Pt disk	$C_{12}S$-	Au	100 μm	0.4 V, 10 μm/s, phosphate buffer and $K_4[Fe(CN)_6]$	sample: counter electrode; tip: working electrode; potential cycles: +1.2 to −1.6 V; 1.5 μm/s; phosphate buffer and $K_4[Fe(CN)_6]$ or KOH	removal of SAM	128
SECM; Pt disk	$C_{12}S$-	Au/glass	100 μm	0.4 V, 10 μm/s, phosphate buffer and $[Ru(NH_3)_6]Cl_3$	sample: counter electrode; tip: working electrode; potential cycles: +1.2 to −1.2 V; KOH	immobilization of glucose oxidase; measurement of the enzyme activity	129
NSOM; fused silica, Al coated	$C_{12}S$-, MHA	Au	25 nm	LFM	UV-laser, 244 nm; RT	first NSOM pattern of SAM	133
NSOM fused silica, Al coated	$C_{12}S$-, MHA	Au	50−55 nm	AFM, LFM	5−10 nm distance above surface, 1−0.2 μm/s, 20−60 mW	etching	134

nm, corresponding to the size of the probe aperture, which seemed to be the limiting factor for scanning near-field photolithography (SNP). However, the size of the gold grains from the substrate also played an important role. Nevertheless, a feature size of 30 nm corresponded to a resolution of ca. $\lambda/9$. It was also shown that it was possible to use the patterned SAMs as an etch mask for the gold substrates. A ferri-/ferrocyanide etch solution was used to etch exclusively the part of the SAM that had previously been illuminated. The unexposed regions were resistant to the etchant. The reaction time for creating structures in the gold substrate was longer than in the case of bare gold, suggesting that the oxidized SAM was not immediately collapsing in the etch solution. This optical lithographic technique required the same time frame (scan speed of 200 nm/s) as the AFM and STM type approaches discussed previously. However, it was observed that the scan speed could be increased if an acid-terminated self-assembled monolayer was used. It was suggested that the oxidation occurred much faster with this SAM. A disadvantage of the acid-terminated SAM was that it had less resistance to etching solutions compared to the methyl-terminated SAMs. This behavior was possibly due to less order within the MUA-SAM.

3. Addition Lithography

3.1. Historical Precedent for Addition Lithography

The most natural idea about writing is the application of ink to paper. The class of lithographic methods that are termed addition lithography resembles this process. Prior to the use of SAMs in this scanning-probe-based lithography category, various other types of materials were applied to a substrate under the action of a scanning probe. An example is the deposition of copper clusters onto gold from an AFM tip.[135,136] Moreover, several efforts have focused on the patterning of SAMs via addition using techniques other than scanning probes. These approaches include μCP,[50,51,137,138] micropens and nanopipets. In an early example, Lopez et al. demonstrated the use of a micropen to create 50 μm wide lines of a C_{16}S-SAM on gold.[139] More recently, these approaches have been expanded to deposit a wider range of materials. For example, materials deposited with nanopipets include DNA, proteins, enzymes, reactive gases, etchants, and photoresists.[140−144]

The fundamental scheme behind this type of lithography is diagrammed in Figure 1B. To a (nominally) bare substrate, a reactive molecule is applied via some type of pen. In the case of SPL-based lithography, the pen is the sharp tip of an atomic force microscope cantilever. The ink is composed of molecules, and a metal or semiconductor surface is the paper. In reviewing this strategy, early papers are described first, and later the types of inks and substrates are treated in kind.

In 1995, Jaschke and Butt reported the creation of aggregates of octadecanethiol on mica by the transfer of these molecules from an AFM tip to the surface.[145] The authors noted that the deposits displayed a relatively homogeneous height of 1.2 ± 0.3 nm in ambient conditions. However, little control was illustrated in fabricating patterns—irregularly shaped islands were typically deposited. Moreover, the apparent heights measured were too short to attribute them to a well-ordered crystalline SAM. The authors rationalized this appearance by suggesting that these molecules were physisorbed to the substrate, resulting in disorder in the observed domains and/or a large molecular tilt with respect to the substrate. Nevertheless, the first lithographically defined pattern (a star-shaped structure) was formed. Notably, these patterns were only obtained on the high-energy surface of mica and the authors stated, "...we do not find any deposits on glass or gold." This early report can be seen as the first example of transfer of molecules from a tip to a substrate (Table 2).

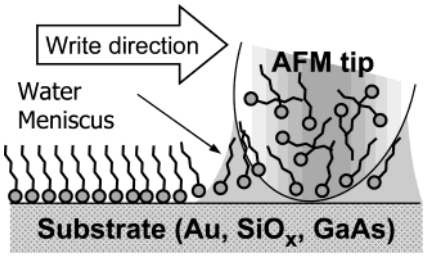

Figure 14. Schematic diagram illustrating dip-pen nanolithography (DPN). A tip coated with "ink" molecules was brought into contact with the substrate. A water meniscus formed between the tip and the substrate, which facilitated the transport of the ink to the substrate.

Two years later, Piner and Mirkin published a paper on transport of water to and from polymer and mica substrates as effected and observed by lateral force microscopy (LFM).[146] The authors concluded that this transport occurred via the meniscus formed between the AFM tip and the sample. At low humidity, water was transported from the tip to the substrate. Under high humidity (95%), water was transported from the surface to the tip. This effect was based on capillary condensation. Although the principal goal of this work was to characterize the effects of water on LFM measurements, the authors recognized that this effect could be used for lithography. Patterns of letters composed of water were written onto a mica substrate under low-humidity conditions. After a detailed discussion of the phenomena, it was concluded that the transport of water was a dynamic phenomena and was dependent on humidity, the hydrophobicity of the substrate, and the dynamics of the tip motion. This work set the stage for the subsequent development of the dip-pen nanolithography (DPN) technique.

3.2. Fundamentals of DPN

Dip-pen nanolithography is illustrated in Figure 14 and is performed as follows. AFM tips are "inked" with a material known to self-assemble on a solid substrate. The tip is then contacted to the surface. A water meniscus is formed, and the ink, which is adsorbed on the tip, is transferred to the substrate when the probe is held in contact or moved along the surface below a certain linear velocity. The material immobilizes on the surface in a subsequent chemical or electrochemical event. DPN can often use com-

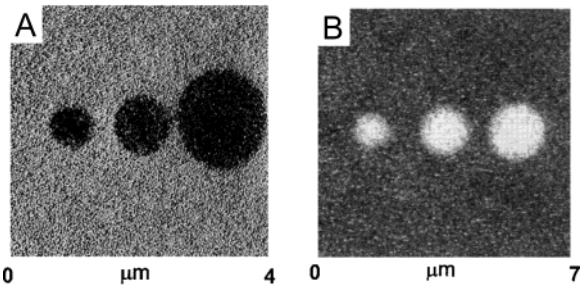

Figure 15. LFM images of dots fabricated from (A) C_{18}-SH and (B) MHA on a gold substrate by DPN. The contact times were 2, 4, and 16 min, respectively (45% RH; images recorded at 4 Hz scan rate). Reprinted with permission from *Science* (http://www.aaas.org), ref 149. Copyright 1999 American Association for the Advancement of Science.

mercially available tips, which are not modified prior to the adsorption of the ink. This technique has been highlighted in several overview articles.[147,148] Here, the different types of ink, substrate, and method are discussed in detail.

The first report of DPN demonstrated fabrication of organic patterns of dot arrays or lines with thiol-based molecular inks on polycrystalline gold and Au(111).[149] Both octadecanethiol ($CH_3(CH_2)_{17}SH$, abbreviated $C_{18}SH$) and mercaptohexadecanoic acid ($HO_2C(CH_2)_{15}SH$, abbreviated MHA) were chosen because they were known to create stable SAMs. Patterned features were routinely produced with widths that were less than 100 nm and as narrow as 30 nm. In the example shown in Figure 15, circular patterns of $C_{18}S$- and MHA-SAMs on polycrystalline gold were made by bringing the tip into contact with the substrate. The size of the dots was dependent on the contact time. Molecular resolution LFM images indicated that the $C_{18}S$-SAM on Au(111) was densely packed. The use of Au(111) deposited onto mica did suffer some disadvantage. Specifically, it was not possible to draw long (ca. micrometer-scale), continuous lines. This problem was attributed to the deep valleys surrounding the small Au(111) facets. On the much rougher polycrystalline gold, continuous lines could be written with micrometer length and 30 nm width. The line width was dependent on the average size of the grains, much as the resolution of an ink pen is dependent on the grain size of the paper.

Humidity plays an important role in DPN. Optimal results were obtained at 30−50% RH with a scan rate of 1 Hz. This rate allowed sufficient transport time for the ink to reach the surface. With increasing humidity, the feature size also increased, which was attributed to the change in the size of the water meniscus. A second important parameter was the contact time between the tip and the substrate. Longer contact times (e.g., slow scan speeds) led to larger feature sizes.

An attractive feature of DPN was that the structures could be imaged in-situ immediately after the lithography operation to assess the quality of the pattern. The same modified tip was scanned at higher rates (greater than 4 Hz) in LFM mode to provide images showing generally high contrast between the SAM and the Au substrate. Notably, neither different SAMs nor unfunctionalized gold regions can typically

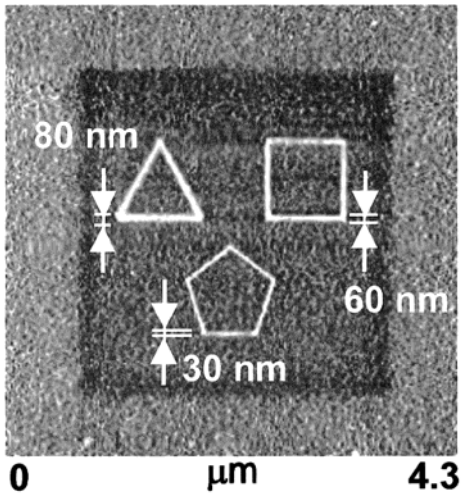

Figure 16. AFM images showing polygon shapes written with MHA on an amorphous gold substrate. The writing times per side were 30 s for the triangle, 20 s for the square, and 8 s for the pentagon (ca. 0.1 nN force; 4 Hz scan speed; 35% RH). The geometric patterns were overwritten with a $(3\ \mu m)^2$ square pattern with a $C_{18}SH$-coated tip (four scans; 0.1 nN; 4 Hz; ca. 35% RH). The polygons showed the highest lateral force contrast, while the $C_{18}S$-SAM showed the lowest. The bare gold outside had an intermediate contrast. Reprinted with permission from *Science* (http://www.aaas.org), ref 150. Copyright 1999 American Association for the Advancement of Science.

be distinguished by contact mode (e.g., normal force) AFM. Thus, friction (e.g., lateral) force is typically used to characterize DPN-fashioned patterns. It was hypothesized that imaging can be achieved without further functionalization of the surface because, during imaging, the tip moves at rates greater than the time required for ink transport from the tip to the substrate. Later, a water meniscus was argued to be responsible for ink transport. This meniscus was disrupted at a sufficiently high rate of tip travel. A more detailed discussion about this process will follow later in this section.

The second paper on DPN demonstrated the fabrication of nanostructures with multiple organothiol inks and spatial separation of 5 nm.[150] To achieve these results, registry marks were employed so that when the tip was retracted and reinked, it could be repositioned close to the previously established pattern. Thus, two molecular inks were lithographically patterned in an area that was defined within these registry marks. Specifically, a second pattern of dots was written between a pattern of dots with a spatial resolution of ca. 15 nm. Another novel demonstration in this paper was the ability to "overwrite" a nanostructure by scanning a tip modified with a second ink over the initial pattern. This procedure had the effect of creating a second SAM around the first with no apparent exchange between molecules in the respective SAMs (as detected by LFM). Figure 16 shows the result of this process. Three geometric structures were written using MHA. To backfill around this set of patterns, a tip inked with $C_{18}SH$ was raster-scanned four times at ca. 12 μm/s (4 Hz) over a scan area encompassing these three structures. The image illustrates the dependence of the writing rate upon the width of the line. By writing

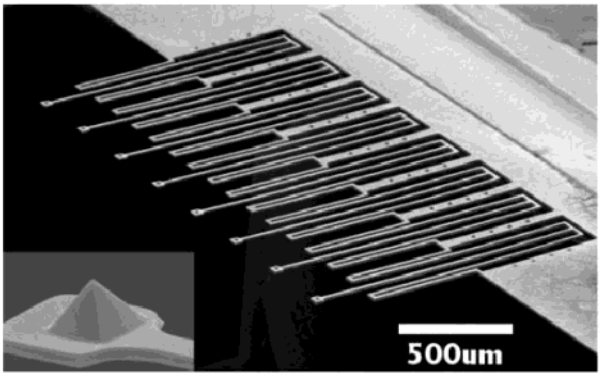

Figure 17. SEM micrograph of a linear eight-probe array for DPN. Inset shows a single tip at the end of a cantilever. Reprinted with permission from ref 152. Copyright 2002 Institute of Physics Publishing.

each side of the triangle, square, and pentagon at 30, 20, and 8 s, respectively, line widths varying from 80 to 30 nm were observed. The image in Figure 16 was collected with an unmodified tip to prevent thiol exchange. The MHA functionalized regions appeared bright (indicating higher tip friction), the ODT backfill region appeared dark (indicating lower tip friction), and the surrounding "unmodified" gold substrate appeared intermediate in friction.

It has been recognized that the inherent serial nature of SPL results in undesirably slow writing. In an effort to demonstrate a more parallel approach to DPN writing, a linear array of AFM tips (up to eight) was employed.[151] Two types of writing were demonstrated. A set of AFM tips was inked with thiol and simultaneously engaged onto the surface. Using this cantilever array, a set of patterned SAMs was drawn. Each tip drew the same pattern in a region separated, in this case, by several hundred micrometers from the others. In a second demonstration, each tip was inked with a different molecule. To produce a multiple ink pattern, each tip was used individually in series, positioning each subsequent tip in the same region as the first. In both of these demonstrations, multiple cantilevers were obtained by removing several contiguous cantilever-containing segments from a commercially available wafer block. Only the lead tip was monitored with the feedback system to position it, while the others in the array followed in a passive manner. Feedback systems were not found to be necessary for each individual tip because line width and required scan rate for patterning were found to be independent of the tip contact force.

The next advancement in the area of multiple-pen DPN was the development of a MEMS nanoplotter with a high density of probes.[152] In this work, linear arrays of tips (up to 32) were fabricated via photolithography. Figure 17 shows a linear array of 8 tips used to create 8 copies of a pattern, as shown in Figure 18. These patterns were nearly identical. The resolution achieved was not quite as high as that observed previously with commercially available single tips. Recently, Zou et al. developed a conductivity-based sensing technique to control the contact between the tips of a multiple tip array and the substrate. This method used the change in the conductivity between the sample and a metal-coated

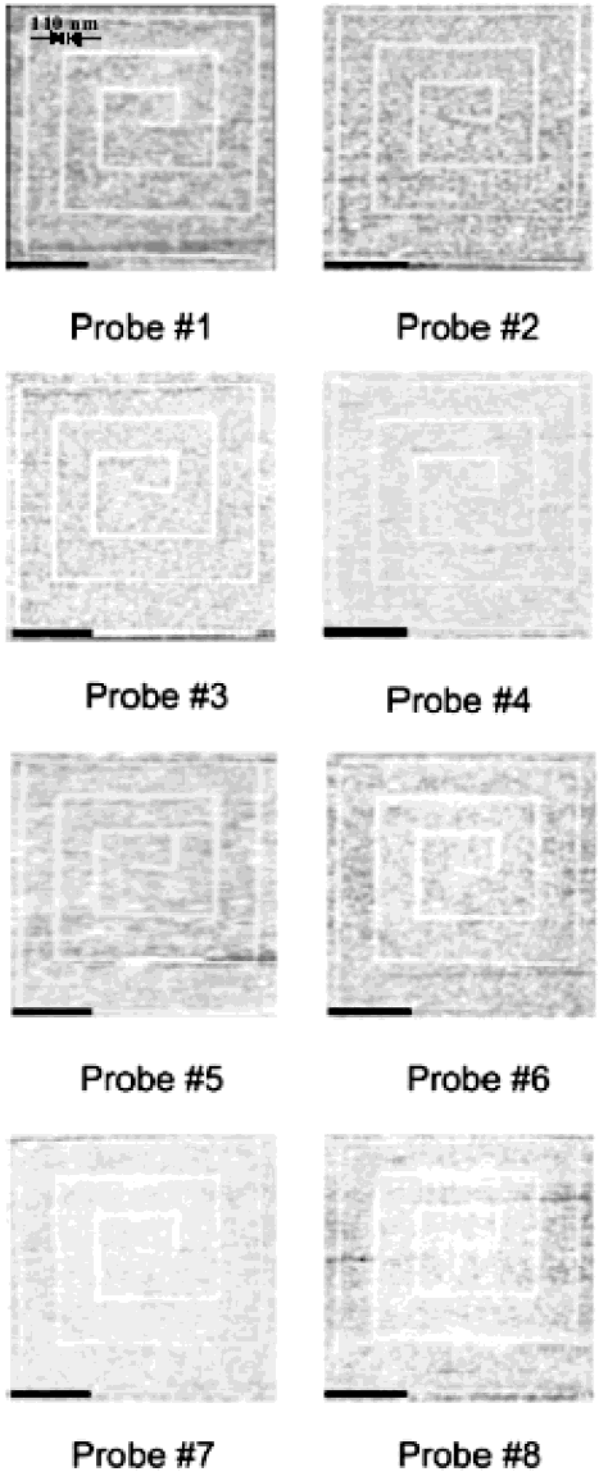

Figure 18. AFM images of eight copies of a spiral-shaped pattern generated with a probe array as shown in Figure 17. The tips were coated with $C_{18}SH$, and the written structures were transferred into the substrate by a wet etching step. The size of each scan area was 6 μm × 6 μm. Reprinted with permission from ref 152. Copyright 2002 Institute of Physics Publishing.

tip, when the tip contacted the sample surface.[153] More recently, Belaubre et al. developed a technique based on electrostatics to increase the overall ink loading of biological solutions onto arrays of passivated aluminum cantilevers. The structure sizes generated with these arrays were reported to be on the micrometer scale.[154]

DPN has also proved to be an interesting tool for the investigation of monolayer growth and interfacial diffusion.[151] In one example, the ability of a SAM to corral a second molecular ink was investigated. The fabrication and behavior of the "molecular corral" is illustrated in Figure 19. A cross structure consisting of 80 nm wide lines composed of C_{18}S-SAM was fabricated on unmodified gold, and a second tip coated with MHA was brought into contact inside the corral, allowing radial delivery of the MHA at the point of contact on the substrate. Figure 19A shows that the MHA-SAM was contained inside the barrier created by the C_{18}S-SAM. In a second experiment, a similar pattern was drawn except two inks were used. The horizontal lines of the cross were composed of MHA-SAM, while the vertical lines were composed of C_{18}S-SAM (Figure 19B). Again, a tip delivered MHA to the center of the pattern, but, in this case, the MHA could be observed to diffuse across the MHA-SAM but not across the C_{18}S-SAM (Figure 19C). This behavior could be explained in two ways. The C_{18}S-SAM could have hindered the diffusion of the ink, or it could have confined the water meniscus delivering the molecules.

In a second investigation of SAM growth using DPN,[155] a series of LFM images was obtained using an inked tip. By monitoring the change in lateral force over time, the authors were able to make statements about the growth mechanism. The growth of C_{18}S-SAM and MHA-SAM had two distinctly different characteristics. During the growth of a C_{18}S-SAM, small nucleation sites appeared first, grew larger over time, and subsequently coalesced. In contrast, during the growth of MHA-SAM, the friction of the scanned region changed nearly linearly as a function of time—no nucleation phenomenon was observed. Molecular resolution images of the resulting monolayers indicated that they were highly ordered and did not show a difference compared to SAMs prepared by solution or gas-phase deposition.

Ivanisevic et al. studied the exchange processes between four different molecules/SAMs—MHA-SAM, C_{18}S-SAM, 11-mercaptoundecylferrocenyl-SAM (FcC_{11}S-SAM), and 11-mercapto-1-oxoundecylferrocenyl-SAM ($FcCOC_{10}$S-SAM).[156] First, DPN-derived patterns of each SAM were created on polycrystalline gold and exposed to a solution of C_{18}SH. This molecule was observed to exchange both FcC_{11}S-SAM and $FcCOC_{10}$S-SAM within a matter of seconds to minutes. This result could be rationalized on the basis of the lower packing density of these two SAMs as the result of the bulky ferrocenyl headgroups.

To get a better insight, the exchange process was also performed under continous scanning with an ink-coated AFM tip. The chemical structure of the molecules influenced the rate of exchange, but the size of the structure was also found to be important. Larger regions exchanged more slowly than smaller regions. This result was interpreted to suggest that exchange took place mainly in defect sites of the SAM. A smaller region had a greater percentage of the SAM at boundary sites. Because exchange was observed mainly at the boundaries, they were presumably less ordered than the center of the region.

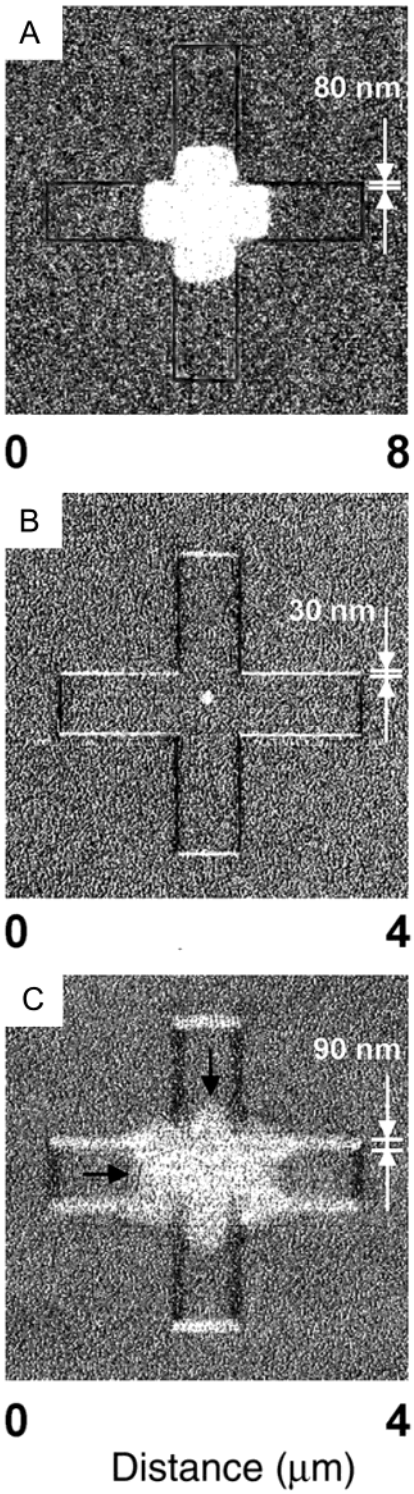

Figure 19. LFM images of "molecular corral" patterns consisting of two different inks: (A) cross-shaped structure where the horizontal and vertical lines were written with C_{18}SH (a tip inked with MHA was then brought into contact in the middle of the pattern; the MHA diffused radially, and the C_{18}S-SAM lines confined the spreading of the MHA); (B) cross-shape pattern, where the horizontal lines were written with a MHA coated tip and the vertical lines were written with C_{18}SH ink. (C) A tip inked with MHA was brought into contact with the substrate in the middle of the pattern. The MHA diffused radially and could diffuse across the horizontal lines, but not across the vertical lines (C_{18}S-SAM). Reprinted with permission from *Science* (http://www.aaas.org), ref 151. Copyright 2002 American Association for the Advancement of Science.

If the experiment was carried out with a tip coated with MHA, similar results were observed. On the basis of the relative ability to exchange one thiol for another, it was concluded that the overall relative stability of the SAMs could be ranked as MHA-SAM > C_{18}S-SAM > $FcCOC_{10}$S-SAM > FcC_{11}S-SAM. If the substrate was changed to Au(111), the exchange process was found to be much slower and could be nearly neglected. Even after 9 h of continuous scanning over a C_{18}S-SAM with a MHA-coated tip, the dot diameter was reduced only by 12%. Thus, the stability of a SAM is strongly dependent on the quality of the substrate.

Partial electrochemical desorption at the edge of DPN-generated SAM patterns was used to reduce the dimensions of these features.[157] In this case, a pattern of MHA-SAM was written, the substrate was mounted in an electrochemical cell, and the gold surface was used as the working electrode. By applying a potential of −750 mV vs Ag/AgCl, the structures decreased in size. The potential was an important factor for the control of this process. The regime between −750 and −800 mV was found to be optimal, and the rate of shrinking was very controllable as well as linear with time. With a less negative potential, no change in the size was observed. The electrochemical desorption process started on the outside of the features, considered to be defect sites (due to lower order). The smallest feature size fabricated on polycrystalline gold was 30 nm. Such feature sizes were otherwise difficult to achieve. This electrochemical shrinking method did not appear to alter the structural integrity of the SAM. Upon exposure to a gold etchant, both the shrunken and the unmodified SAM features resisted etching.

Additional papers have reported the use of DPN to create etch masks with SAMs. Weinberger et al. patterned C_{18}SH on gold evaporated onto silicon (e.g., Au/Ti/SiO_2/Si(100)).[158] The pattern was used as a resist against gold etching for a subsequent anisotropic HF etch that patterned the underlying silicon. Mirkin and co-workers showed that it is possible to create large, nearly homogeneous arrays of dots.[159] DPN patterns were written on Au/Ti/SiO_x/Si using MHA ink, and the unprotected gold was etched away using ferri-/ferrocyanide etchant. An array of 40 000 dots with a diameter of 50 nm and a spacing of 100 nm was produced. In addition, nanogaps between 12 and 100 nm wide were also fabricated. Because of diffusion of ink on the surface, these gaps were smaller than would be accounted for by the positioning of the tip.

3.3. Variation of the Ink and Substrate

The first DPN investigations employed thiol-based inks and gold substrates. However, the technique is not limited to this system. DPN has been employed with other ink and substrate combinations. Ivanisevic and Mirkin reported the use of DPN to write lines on semiconductor (silicon and gallium arsenide) substrates using disilazane molecules as inks.[160] Two potentially important features of disilazane inks were highlighted compared to trichloro- or trialkoxysilanes. First, they did not polymerize appreciably in the water meniscus. Second, the secondary amine base functionality within them catalyzed the chemisorption of the molecules to the substrate. The authors observed that patterning on these semiconductor surfaces required much longer time periods to produce similarly sized structures than the thiol/gold systems under similar conditions. However, a slight temperature increase, generated from a fiber optic light, was observed to increase the rate. The authors attributed this faster patterning rate to contributions from increased ink diffusion or the increased reaction kinetics of disilazanes at elevated temperatures. Features as small as 50 nm pattern widths were obtained. Structures on Si/SiO_x were purportedly resilient to three successive acetonitrile washes, suggesting that they were irreversibly chemisorbed to the substrate.

A number of inks that represent increasing chemical diversity have subsequently been employed with the DPN technique. The direct writing of modified oligonucleotides has been illustrated with a pattern resolution of 50 nm on Au and silicon substrates.[161] On gold, various oligonucleotides functionalized with a hexanethiol linker were employed as inks. Writing of oligonucleotides on silica was accomplished by first preparing a thiol-terminated surface by reacting the silica with mercaptopropyltrimethoxysilane. Then oligonucleotides functionalized with acrylamide moieties was applied to the surface as ink. The acrylamide underwent Michael addition with the thiol-terminated surface to covalently attach the oligonucleotides. It was noted that in order to achieve the physisorption of the oligonucleotide inks to the tip, it first had to be coated with a hydrophilic silane.

After writing patterns of oligonucleotides, the nonpatterned area of the array was passivated with C_{18}-SH (for gold) or buffered acrylic acid monomer (for silica) to hinder nonspecific binding. The biological activity was confirmed by exposure of the structures to a solution of complementary and noncomplementary fluorophore-labeled DNA. Only the fluorescent signal of the complementary DNA was observed after washing. The hybridization was also performed with complementary oligonucleotides attached to gold nanoparticles. In this way, the authors fabricated arrays of dots that were 1.6×10^5 times smaller than conventional microarrays. In an area of 100 μm × 100 μm, ca. 100 000 nucleotide spots could be formed on a time scale comparable with known microrobotic spotting procedures.

This work also demonstrated a multiple-ink experiment. Two oligonucleotide inks were patterned on silica as described above. This surface was then exposed to DNA-conjugated gold nanoparticles that contained two features that labeled them. Each type of DNA was labeled with a fluorophore. Moreover, the nanoparticles to which each type of DNA was attached were of different sizes. The particles assembled in the expected locations with little nonspecific binding outside the pattern. Fluorescence microscopy showed the expected colors of the complementary fluorophore-labeled DNA (Figure 20A). In addition, tapping mode AFM was used to image the array and displayed the two different sizes of nanoparticles in their expected positions (Figure 20B,C).

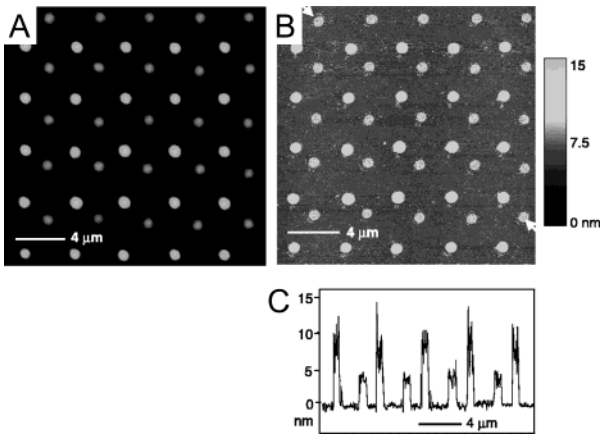

Figure 20. Direct patterning of two different acrylamide-modified oligonucleotide inks by DPN. The DNA was hybridized with their complementary ssDNA, which had different fluorescent labels (Oregon Green 488-X and Texas Red-X): (A) combined green−red epifluorescence image; (B) tapping mode images of hybridized ssDNA attached to a AuNP (5 and 13 nm diameter) to the same array structure; (C) section analysis corresponding to both nanoparticle patterns (start and finish are indicated by arrows). Reprinted with permission from *Science* (http://www.aaas.org), ref 161. Copyright 2002 American Association for the Advancement of Science.

Wilson et al. showed that collagen and a model peptide like collagen could be written on a gold surface with DPN.[162] Binding of these molecules to gold was facilitated by native cysteine (e.g., thiol-containing) units in the protein/peptide. The feature sizes observed ranged from 30 nm in width to hundreds of micrometers in length. The writing was performed in tapping mode (e.g., noncontact AFM with a resonating cantilever) and not in contact mode as in prior DPN work. This imaging mode was employed nominally because of the soft character of the biopolymer. Closer investigation with tapping mode AFM revealed a helical structure of the patterned molecules on the surface consistent with the structure of collagen. Notably, collagen deposited onto gold from solution did not show this order. The authors suggested that the tip was important in inducing order to the collagen patterns. Moreover, collagen written onto a gold surface displayed biological activity as evidenced by the binding of primary and secondary antibodies.

Stone and co-workers also reported DPN using tapping mode to write patterns of short, cysteine-containing peptides on gold.[163] The drive amplitude of the resonating cantilever played an important role and had to be increased during the course of writing. This behavior was attributed to depletion of the peptide ink at the terminus of the cantilever—presumably, the increase in drive amplitude facilitated continued transfer of the ink to the probe apex. The peptide employed contained a histidine tag on the C-terminus, and these authors originally attempted to write this peptide onto a commercially obtained nickel nitrilotriacetic acid (Ni−NTA) functionalized slide. However, despite the known propensity of binding histidine tags to Ni−NTA, no deposition was found.

The papers about DPN that have been discussed so far rely on chemical interaction for the binding of the ink to the substrate, but DPN can also be used to apply other inks that do not chemisorb to the surface. This extension has expanded the range of materials that can be patterned. Most of the efforts described below do not employ SAMs. However, as they represent evolution of the DPN technique and as they represent efforts to create chemically well-defined patterns, they are treated here. Noy et al. showed that a luminescent dye, fluorescently labeled proteins, and luminescent polymer nanowires could be written onto modified glass surfaces.[164] With a home-built instrument combining AFM and scanning confocal microscopy, the luminescence of the patterns was observed. The line width observed (600 nm) by confocal microscopy was attributed to the limit of the resolution of the instrument. It was suggested that the true line width of the patterns was smaller.

Su and Dravid followed a similar approach, employing four different organic dyes (anionic, cationic, and neutral) as DPN writing inks.[165] All the dyes (rhodamine 6G (R6G), coumarin 6 (C6), acid red 8 (AR8), and fluorescein (FITC)) adsorbed on an unmodified silica surface. This result indicated that a variety of noncovalent interactions played a role in the process. Because the resulting features could be imaged by contact mode AFM, it was concluded that the dye was bound strongly to the substrate. The neutral organic C6 dye was observed to have the highest rate of diffusion on the surface, creating the largest features in the shortest time. The topographic height of these features was larger than the size of the molecules, suggesting that aggregates had formed on the surface. The fluorescence emission was uniform over the pattern, indicating that the dye molecules were uniformly distributed.

McKendry et al. used a dendrimer ink in DPN writing on silica.[166] The influence of the molecular weight (e.g., dendrimer generation) and type of functional group within the dendrimer (which interact with the substrate) were studied. The authors showed that with increasing generation the delivery rate to the surface slowed. The number of functional headgroups did not appear to influence the results. However, if the functionality of these groups was changed from amine to hydroxyl, the delivery rate was much faster. Lines as narrow as 100 nm were written, corresponding to approximately 20 dendrimer molecules.

Lim and Mirkin also investigated fabrication of patterns of polymers by DPN.[167] Negatively charged, self-doped polyaniline and positively charged, doped polypyrrole were patterned on silica substrates that were functionalized to present a complementary charge to that of the polymer. It was shown that no writing was observed when the surface and the polymer had the same charge. Differential pulse voltammetry confirmed that the patterns imaged by LFM were electroactive polymers. The cathodic peaks matched with the values tabulated in the literature. The kinetics of the writing process for these high molecular weight polymers were found to be similar to those for small alkanethiols. The transport rate

was proportional to the square root of time, consistent with a radial diffusion process.

Proteins have also been directly written to various substrates with DPN. Utilizing electrostatic interactions between the positively charged parts of proteins and negatively charged SiO_x or through the covalent bonding between aldehyde-modified SiO_x and amine groups on proteins, Lim et al. patterned nanostructures of immunoglobulin gamma (IgG). In this approach, the cantilevers were first modified with a silane−PEG to inhibit nonspecific binding of the protein to the tip.[168] In a similar approach, Lee et al. patterned nanostructure dot arrays consisting of two different proteins (rabbit IgG and lysozyme) to gold surfaces.[169]

Most recently Manandhar et al. observed the formation of anisotropic nearly fractal patterns when a tip coated with 1-dodecylamine (DDA) was brought into contact with a mica substrate.[170] This finding was contrasted to the circular-shaped features that are observed in experiments with thiol inks on gold substrates. The authors attributed this result to anomalous diffusion and the weak binding between the DDA and the mica. The authors also described theoretical approaches to explain the nanoscale direct deposition process and concluded that the final pattern was determined by the interaction between the molecules.

The DPN technique has been further extended to involve the deposition of materials concomitant with electrochemical oxidation or reduction. The first example of electrochemical DPN (or E-DPN) was reported by Li et al. to directly fabricate several types of metal nanostructures on silicon-based surfaces.[171,172] Patterned materials included gold, germanium, silver, copper, and palladium. In this method, the tip was "inked" with a metal salt and the meniscus at the tip−substrate interface served as an electrochemical "reaction vessel" that limited the area where deposition could occur. By applying an appropriate bias to the substrate, the metal ions dissolved within the meniscus were reduced in the proximity of the tip, creating metallic structures. It was suggested that the native surface oxide present on the silicon wafers was conductive enough to facilitate the completion of the electrochemical circuit required to reduce the precursor ion ink to allow the deposition of the metal. As in all DPN experiments reported so far, the control of relative humidity was essential to maintain the meniscus and was kept between 35 and 60% in these experiments. Likewise, the lithographic dimensions were found to be dependent on scan rate and applied bias. To confirm that the lines are composed of metal, the following experiment was performed. The letter "V" was fabricated with a Pt line on the left ($V_b = 4$ V, 10 nm/s) and SiO_2 line on the right ($V_b = -10$ V, 50 nm/s), shown in Figure 21A. After elevating the substrate temperature to 500 °C in an ethylene/argon atmosphere, the Pt line showed a large amount of deposited material and the authors suggested that this material was carbon from the Pt-catalyzed thermal decomposition of ethylene. It was further observed that the metal line melted and reconstructed into metal spheres (nominally) confined along the original line, while the SiO_2 line was unaffected (Figure 21B).

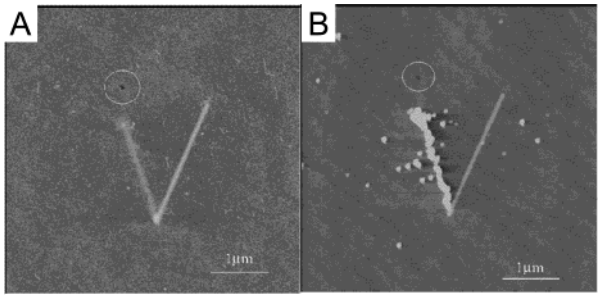

Figure 21. (A) AFM image of a "V"-shaped structure. The line on the left was drawn by E-DPN of platinum ($V_b = 4$ V; 10 nm/s), and the line on the right was created by anodic oxidation of the silicon substrate ($V_b = -10$ V; 50 nm/s; 58% RH). (B) The same structure after the heating (500 °C) under ethylene in argon for 1 h. Reprinted with permission from ref 171. Copyright 2001 American Chemical Society.

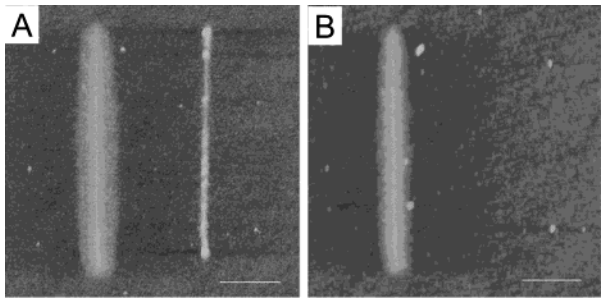

Figure 22. (A) AFM image of a SiO_x line on the left and an EDOT polymer line created via E-DPN on the right side. (B) Same patterns after the treatment with a 2:1 H_2SO_4:H_2O_2 solution. The polymer line was removed by chemical oxidation, while the SiO_x line was not altered. Reprinted with permission from ref 173. Copyright 2002 American Chemical Society.

E-DPN was also used to fabricate nanostructures composed of a conducting polymer on silicon substrates.[173] The conductive AFM tip was coated with a monomer reactant (3,4-ethylenedioxythiophene, EDOT) that was soluble in the water meniscus. By applying a cathodic voltage, patterns of conducting polymer immobilized on the substrate were created. In an experiment to confirm that the lines were composed of organic material, a SiO_2 line was drawn (left line) adjacent to a poly EDOT line ($V_b = -12$ V, 10 nm/s, 48% RH; right line), shown in Figure 22A. After the patterned lines were treated with 2:1 H_2SO_4/H_2O_2, the polymer line was removed through oxidation, but the SiO_2 line was unaffected (Figure 22B). Polymerization on thick (ca. 500 nm) thermally grown oxide on silicon was also reported by applying high negative substrate biases (e.g., −130 V). It was hypothesized that the mechanism of polymer synthesis and deposition was caused by electric-field-induced polymerization under the high electric field found at the apex of the sharp tip.

Most recently, Agarwal et al. created patterns on nickel surfaces with histidine-tagged proteins and free-base porphyrins via E-DPN in tapping mode. Under a negative tip bias, the nickel surface was ionized and the His-tagged peptide (or porphyrin) ink became bound to the surface in these regions. Opti-

mum delivery was found to occur between −2 and −3 V. The authors speculated that the surface nickel oxide was reduced to Ni^{2+}, which acted as the binding species. Interestingly, it was reported that upon static tip−substrate contact, no radial delivery (i.e., dot structures) of peptide occurred. The researchers found that only a scanning, biased tip ionized an area in order for the deposition of peptide to occur via histidine binding to ionized Ni.[174]

In another report by Liu and co-workers, it was demonstrated that the Au(III) ink could undergo a surface-induced reduction on *n*-type Si(100) without an applied potential.[175] The tips were inked from a dilute $HAuCl_4$ aqueous solution and translated along the surface in a predefined pattern. Unlike previously reported DPN of organic materials, the same tip was not used to probe the structures immediately after the lithographic operation. The nanostructures were subsequently imaged with a different tip using tapping mode AFM. A line resolution of ca. 100 nm was illustrated and found to be dependent on the geometry of the tip, the scan rate, and the relative humidity. A series of experiments were performed to explore the stability of the nanostructures written and to support that these structures were fabricated of gold. Repeated washing and heating to 300 °C did not degrade the written structures, suggesting that they were not composed of adventitious organics. Heating to 500 °C resulted in melting—the metal structures reconstructed to form spherical shapes confined to the pattern. Resistance to HF etching suggested that the structures were not composed of silicon oxide. In a similar approach by Buriak and co-workers, the same type of writing with $HAuCl_4$ solution (or a palladium containing salt) was employed to prepare patterns on a Ge(100) surface coated with native oxide.[176] Recently, Fu et al. reported patterning a barium hexaferrite precursor solution with DPN on Si/SiO_x substrates, with subsequent posttreatment at elevated temperatures, which created "hard" magnetic nanostructures consisting of barium hexaferrite ($BaFe_{12}O_{19}$). The precursor ink consisted of a mixture of iron nitrate and barium carbonate in ethylene glycol. The latter solvated and stabilized the inorganic reagents and aided wetting of the hydroxylated SiO_x substrate. The structures were characterized with AFM, magnetic force microscopy (MFM), and XPS.[177]

Another DPN patterning method relied on chemical reaction in the meniscus. Direct patterning of organic/inorganic, composite solid-state nanostructures (SiO_x, Al_2O_3, SnO_2) was achieved on silicon and silicon oxide substrates.[178] The ink consisted of a metal precursor (M = Si, Al, Sn) salt and a commercial block copolymer surfactant. The hydrolysis of metal precursors occurred in the tip−substrate interface meniscus. The amphiphilic block copolymer surfactant was employed to disperse the ink (solution) and increase its fluidity but also contributed to the mesoporosity of the final nanostructure. The latter-mentioned organic moiety could be combusted to create metal oxide mesoporous nanostructures. The metal oxide structures were stable to repeated scanning and remained intact even 1 month after fabrication. This process was different from the ones described previously because it could be employed on an insulating surface and patterned nonorganic surfaces. The speed of the deposition was comparable with the writing of alkanethiols on gold. The nanostructures created have potential applications in the field of catalysis and waveguides due to their large surface areas.

Another interesting ink used in conjunction with DPN has been nanoparticles. Liao et al. fabricated patterns of gold nanoparticles on a surface using a nanoparticle solution as the ink.[179] Specifically, DPN was performed on a silicon surface modified with (3-mercaptopropyl)triethoxysilane. The ink consisted of citrate-capped gold nanoparticles (10 nm diameter) in an aqueous solution. By scanning a predefined area, it was observed that the particles could be immobilized only in the scanned area. A high-resolution AFM image showed that the patterns were composed of loosely packed particles.

Ben Ali et al. used an AFM modified with a second independently controllable tip on a separate nanopositioning stage for the deposition of gold nanoparticles on an insulator surface.[180] One tip controlled by a nanopositioning system was used as the pen, while a second tip controlled by an AFM imaged the structures. By inking the tip with an evaporated nanoparticle solution, the authors showed that they could create small dots (diameters ranging from ca. 70 to 200 nm) on the surface with a height comparable to the diameter of the nanoparticles. TEM images were obtained that resolved individual clusters within an island. The solvent and the chain length of the capping ligand on the particles were also found to play an important role for the successful deposition.

3.4. DPN Structures as Templates

An alternative to direct deposition of a material was to employ a DPN-derived pattern as a template. Thus, the material of interest was reacted with the pattern in a second, often ex-situ step. The first reports using DPN to pattern complex structures such as those consisting of nanoparticles, DNA, or proteins often employed this strategy.

Lee et al. created protein nanoarrays by DPN.[181] Dot array patterns of -COOH-terminated thiol (MHA) were fashioned on gold. The acid sites were designed to be the connection points for protein and cellular adhesion. The area between the dots was passivated with triethyleneglycol-terminated thiol to hinder nonspecific adsorption of proteins. In a first step lysozyme, an ellipsoidal-shaped protein was assembled on the dots of the array. No binding was observed in passivated areas on the array, as evidenced in a series of AFM micrographs. In a similar fashion, rabbit IgG was attached to the array. To demonstrate the selectivity of the binding, this array was incubated in a mixture of proteins that were not expected to bind to IgG. AFM detected no changes in appearance of the array. However, when a similar rabbit IgG array was exposed to a mixture of proteins containing rabbit anti-IgG, the AFM measured a doubling in height (ca. 5.5 nm) of the dots in the array, consistent with specific antigen/antibody bind-

ing. In another experiment, the adhesion of cells patterned on features was investigated. An array contained dots of MHA with a diameter of 200 nm and spaced by 700 nm. This reduced array size was novel. Prior reports employing patterned surfaces for cell binding were limited to feature sizes larger than 1 μm. This pattern was exposed to a solution containing fibroblast cells, and the resulting slides were investigated by optical microscopy. It was observed that the cells only attached to the patterned areas and did not spread. This result showed that submicrometer surface features could promote cell adhesion.

A very similar approach was pursued by Hyun et al. who also started with patterns of mercaptohexadecanoic acid SAMs (MHA-SAMs) and back-filled them with another SAM to hinder nonspecific binding.[182] The carboxylic acid headgroups were converted into *N*-hydroxysuccinimide esters (NHS), which were active for further binding events. This group was reacted with NH_2-terminated biotin or biotin-conjugated bovine serum albumin. Fluorescently labeled streptavidin was bound to the biotin moieties. All these steps were characterized by AFM and fluorescence microscopy. The authors performed control experiments, where it was shown that the binding was specific. No nonspecific binding occurred on the NHS ester patterns or on the passivated background. The reason for choosing the biotin−streptavidin binding strategies was that this was a nearly universal, flexible method and many biotin-linked reagents were commercially available.

Recently, two groups have reported attaching cysteine-labeled cowpea mosaic virus (cys-CPMV) to surfaces using the highly selective thiol−maleimide reactions. Cheung et al. demonstrated patterning gold surfaces with an amine-terminated, PEG-containing SAM precursor employing DPN and nanografting techniques, and subsequently linking/tethering the CPMV viron with 3-maleimidopropionate *N*-hydroxysuccinimade (MPS) linker.[183] Smith et al. patterned a mixture of two dialkyl-PEG-containing disulfides inks (a symmetric 11-mercaptoundecylpenta(ethylene glycol) disulfide (98%) and mixed disulfide substituted with one maleimide group (2%)) with DPN and subsequently attached cys-CPMV.[184]

One major effort that has been demonstrated with DPN experiments has been the ability to fabricate patterns of dots or grids to serve as templates for the organization of various types of particles. DPN with functionalized thiol inks was used to generate a pattern with some "sticky ink" on a substrate, which afforded particle binding in a subsequent step. This step was typically followed by passivation of the nonpatterned areas with a "nonsticky ink" (generally C_{18}S-SAM) to inhibit nonspecific binding of nanoparticle assemblies. Subsequent incubation in a functionalized nanoparticle assembly solution resulted in chemical or physical immobilization of these assemblies on the patterned areas of interest. These architectures have potential applications in the development and study of molecular electronic devices, photonic band gap arrays, biosensors, and protein arrays for proteomics research.

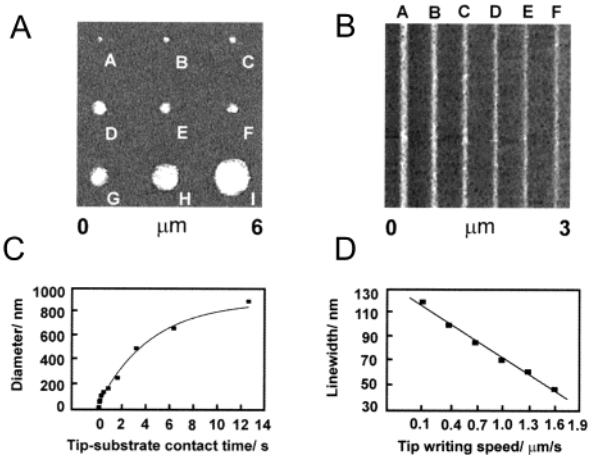

Figure 23. AFM topography images of magnetic nanoparticles adsorbed onto MHA patterns formed by DPN and back-filled with C_{18}SH: (A) dot array fabricated by varying the contact time from 0.05 s (45 nm diameter) to 12.8 s (920 nm diameter); (B) lines generated with different writing speeds [A to F: 0.1 μm/s (120 nm) to 1.6 μm/s (45 nm)]. The images were recorded with a scan rate of 1 Hz; (C) plot of the MHA dot diameter versus the tip−substrate contact time; (D) plot of the line width of MHA versus the writing speed. Reprinted with permission from ref 186. Copyright 2002 Wiley-VCH.

In one report, MHA was patterned on gold into dot arrays of varying diameters, the unpatterned areas were passivated, and the sample was exposed to charged polymer beads.[185] The polymer beads immobilized exclusively on the patterned areas of the substrate. This combinatorial approach enabled the researchers to find the optimum dot diameter that effectively immobilized the particles without significant desorption during rinsing.

In another report, magnetic nanoparticles (Fe_3O_4) were attached to templates in a similar manner.[186] In this paper, the size of the nanoparticle dots could be controlled by changing the contact time of the modified tip with the substrate or by changing the writing speed for the creation of lines. Figure 23 shows the change in dot size over the tip−substrate contact time and the decrease in the line width with increasing writing speed after the adsorption of the iron oxide nanoparticles.

Orthogonal approaches have also been studied in which multicomponent nanoparticle assemblies were guided to their intended positions with the help of DPN-patterned features.[187] The procedure (Figure 24) began with the writing of an MHA-SAM array on a gold surface. The pattern was back-filled with C_{18}S-SAM in order to prevent nonspecific binding. The carboxylic headgroup was activated with the coupling agent EDAC (1-ethyl-3-(3-dimethylaminopropyl)carbodiimide hydrochloride). A first alkylamine-modified DNA was then reacted with the surface (ink a). Taking advantage of the fact that C_{18}S-SAM regions could be replaced with MHA, a second set of dots was patterned, activated, and reacted with a different DNA-based ink (b). This process created two arrays comprising two distinct oligonucleotide sequences. The surface was then incubated with a linker (a′−b′) that was partly complementary to strands a and b. The next step was to expose the surface to a

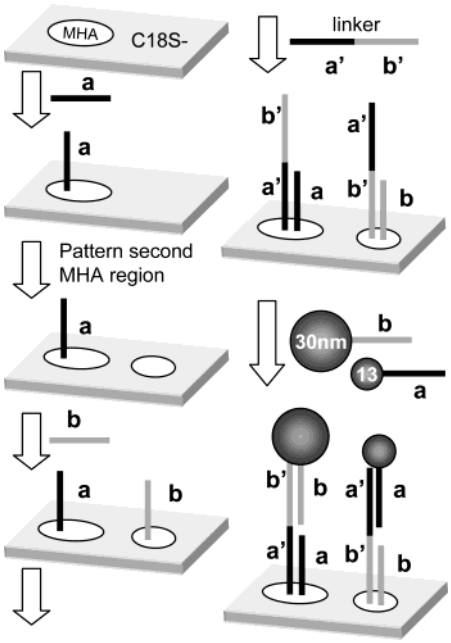

Figure 24. Schematic diagram of the orthogonal assembly of DNA nanostructures. In a first step regions containing two different types of ssDNA (strands a and b) were assembled on DPN-patterned regions created from MHA (white ellipsoid). A ssDNA (a′b′), where one side was complementary to a and the other side was complementary to b, was hybridized to the surface. Two different sized nanoparticles (either functionalized with ssDNA a or b) were bound to this pattern, resulting in regions containing nanoparticles with different sizes.

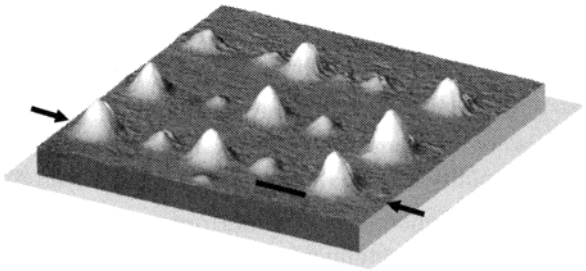

Figure 25. Noncontact AFM image of a nanoparticle array assembled by orthogonal SA as described in Figure 24 (*z*-scale: ca. 40 nm). Reprinted with permission from ref 187. Copyright 2001 Wiley-VCH.

solution containing two different sizes of particles (13 and 30 nm), each modified with ssDNA (a and b), structured to bind only to one of the two complimentary oligonucleotide patterns. The results could be visualized using AFM (Figure 25). In this way, arrays of two different particles and oligonucleotides were produced.

Another strategy for the orthogonal assembly of oligonucleotide-modified gold nanoparticles on a template surface was performed on gold substrates patterned with ω-functionalized ferrocene (Fc) tagged alkyl and acylthiol inks.[188] These electrochemically active materials had a redox potential difference of 255 mV, allowing for nonoverlapping redox processes between the two molecular inks. Appropriate changes in applied substrate potential resulted in oxidation of one or both of the patterned regions. This oxidation (to ferrocinium) made the region positively charged. Subsequent assembly of oppositely charged, polyanionic oligonucleotide coated gold colloids of two different sizes occurred onto the region of interest depending on the applied potential. Oligonucleotide-modified gold nanoparticles did not display nonspecific binding on the neutral Fc species, suggesting they did not readily adsorb to nonionic patterned regions.

Zhang et al. described a different approach for the preparation of colloid-functionalized oligonucleotide nanostructures.[189] DPN was used to generate dot arrays and lines of MHA-SAM on gold evaporated on top of the thermally grown oxide of a silicon wafer. After the patterning with DPN, the unmodified gold was etched away. The bare silica was coated afterward with *n*-octadecyltrimethoxysilane (OTS) and the MHA was removed by illumination with UV-light. The now bare gold nanostructures were reacted with disulfide-functionalized oligonucleotides. A passivation step with a $C_{18}SH$ solution enhanced the hybridization efficiency and removed nonspecifically bound DNA.

3.5. Mechanistic Aspects underlying DPN

The mechanism governing dip-pen nanolithography is still not fully understood. The importance of water (via humidity in the air) has been cited in most DPN-based demonstrations. Several mechanistic investigations are based on the presence of a water meniscus between the AFM tip and the substrate, and it has been suggested that the water mediates the transport of the ink to the substrate. Since there is no obvious way to characterize the size and shape of the water meniscus, its exact role in the mechanism is not specifically determined. The transport of the ink to the substrate is only one part of the DPN process. Assuming a water meniscus is important in the mechanism, the complete mechanistic description must involve desorption of ink molecules from the tip into the water, diffusion through the water, desolvation of the molecules onto the substrate, and their simultaneous or subsequent ordering to form a SAM. As will be discussed below, the importance of a meniscus in facilitating ink transport has been debated. In any event, the role of water is likely complex. For example, the way in which hydrophobic hydrocarbons are transferred through the water meniscus and if/how the presence of water on the surface affects the transfer and diffusion of the ink molecules are issues of current investigation.

Theoretical efforts by Ratner and co-workers modeled two important features of the DPN model. The study of the dynamics of ink self-assembly on the surface in DPN was performed through a diffusion model of the molecular ink on the surface. The role of the tip was described as an infinite source of ink, which avoided the discussion whether a water meniscus is important for the ink transport to the surface.[190] An important issue in this paper was the relative rates of "ink" diffusion from the source versus diffusion along the surface to an open binding site. Dot patterns were modeled showing that the radii grew proportionately to the square root of the tip−substrate contact time ($t^{1/2}$), in agreement with the experimental results. When the tip was moved for

Table 2. Addition Lithography

SPM and tip used	molecular "inks" employed	substrate	line resolution	SIC	RC (including RH and/or environment)	comments	ref
AFM; –	$C_{18}SH$, $C_{10}SH$	mica	400 nm dots		5−20 nN, air, ambient temp	irregular pattern	145
AFM; Si_3N_4 Au coated, 0.05 N/m	water	mica	∼800 nm	1 nN, 3−40 μm/s	1 nN, 3−40 μm/s, humidity control	transport of water to and from the tip	146
AFM; Si_3N_4	$C_{18}SH$, MHA	annealed Au (Au(111)) and nonannealed Au on mica	30−100 nm	LFM, 12 μm/s	<1 μm/s, 1 nN, ∼35% RH, air	first DPN paper	149
AFM; 0.05 N/m	$C_{18}SH$, MHA	Au(111)	15 nm	LFM, ∼ 0.1 nN, 0.9−21.5 μm/s, 23% RH	0.002 μm/s, ∼0.1 nN, 23% RH	overwriting	150
AFM; multiple tips, 0.327 or 0.03 N/m	$C_{18}SH$	Au	60 nm, 260 nm	LFM	0.1−0.5 μm/s, 1.3−2.5 nN, 35−40% RH, RT	8 and 32 tips	152
three-axis translation stage	cyanine3-labeled oligonucleotides, IgG	glass or dendrimer layer	30 μm	fluorescence microscopy	100 nN, ∼30% RH, 23 °C	applied potentials for improved loading of tips	154
AFM; 0.01 N/m	$C_{18}SH$, MHA	Au	40 nm	LFM	0.4−1.3 μm/s, −1 to +4 nN, ∼30% RH	adsorbate diffusion studies; multiple probes (up to 8 tips)	151
AFM; –	$C_{18}SH$, MHA	Au(111) on mica		LFM	10 μm/s for 2 μm, 0.1 nN, 30 ± 5% RH	study of SAM formation	155
AFM; Si_3N_4, sharpened, 0.05 N/m	$C_{18}SH$, MHA, Fc-thiols	Au, amorphous and crystalline	150 nm lines, 100 nm dots	LFM, ∼16−60 μm/s	0.5 nN, 40% RH, 24 °C	exchange studies	156
AFM; Si_3N_4, 0.05 N/m	MHA	$Au/Ti/SiO_x$	30 nm dots	LFM, 1 nN		electrochemical whittling	157
AFM; Si_3N_4, sharpened, 0.05 N/m	$C_{18}SH$	$Au/Ti/SiO_x/Si$	65 nm dots	AFM, ∼0.15−1.5 μm/s	0.2−2.8 μm/s, 0.5 nN, 30% RH, 23 °C	etching into Si	158
AFM; Si_3N_4, sharpened, 0.05 N/m	MHA	$Au/Ti/SiO_x/Si$	gaps > 12 nm	tapping mode AFM, SEM	0.01 s contact time or 0.25−0.5 μm/s, 0.5 nN, 44−49% RH, 24−26 °C	fabrication of gaps	159
AFM; Si_3N_4, sharpened, 0.05 N/m	HMDS	SiO_x, GaAs	75 nm lines and dots	LFM, 19.2−38.3 μm/s	0.02−0.4 μm/s, 0.5 nN, 30% RH, 23 °C	direct writing on SiO_x and GaAs	160
AFM; Si_3N_4	oligonucleotides	mercaptopropyl-trimethoxysilane on Si, Au	150 nm lines, 50 nm dots	LFM, tapping mode AFM	45 ± 5% RH, 23 ± 3 °C,	nanoparticles attached to DNA, hybridization to DPN DNA patterns	161
AFM; silicon probes, 1−5 or 50−200 N/m	thiolated collagen, model peptide	Au on mica	30 nm	NSOM, AFM phase and topography, 6−12 μm/s	∼0.002−0.004 μm/s, 0.5 nN	direct writing of peptide to the surface	162
AFM; 40 N/m	protein	Au on mica	70 nm	AFM phase and topography, 8−28 μm/s	tapping mode AFM, 0.45−1.5 μm/s, 10−40% RH	amine-terminated protein	163
AFM;	rhodamine G6, protein, MEH-PPV	glass	<600 nm	scanning confocal microscopy	0.2 μm/s	luminescent nanostructures	164

Table 2. (Continued)

SPM and tip used	molecular "inks" employed	substrate	line resolution	SIC	RC (including RH and/or environment)	comments	ref
AFM; Si_3N_4, sharpened, 0.05 N/m	organic dyes (R6G, C6, AR8, FITC)	SiO_x	50 nm	~32−40 μm/s, 30% RH, 23 °C	0.02−0.4 μm/s, 30% RH, 23 °C	fluorescence emission	165
AFM; Si_3N_4, 0.06 N/m	dendrimers	SiO_x, glass	100 nm	LFM, topography, >100 μm/s	20 μm/s, 52 ± 2% RH, 19.5 ± 0.5 °C	dendrimer ink	166
AFM; Si_3N_4, sharpened, 0.05 N/m	conducting polymers	charged SiO_x	130 nm	LFM, topography	0.5−0.85 μm/s, 30% RH, 23 °C	conducting polymer ink	167
AFM; Si_3N_4, 0.05 N/m	IgG	negatively charged SiO_x, aldehyde-modified SiO_x	55 nm dots	tapping mode AFM, fluorescence microscopy	0.06−0.08 μm/s, 60−90% RH, RT	modified tips	168
AFM; Si_3N_4, sharpened, 0.05 N/m	IgG	Au	45 nm dots	tapping mode AFM, 3 μm/s; contact mode AFM, 0.1 nN	20−30 s/dot, 80−90% RH, RT	arrays of different proteins	169
AFM; −	1-dodecylamine $C_{18}SH$, MHA	mica, Au		LFM	0.1 μm/s, 55% RH, 29 °C	anomalous surface diffusion, weak binding between ink and substrate	170
AFM; ultrasharp silicon cantilevers	Pt, Au, Ge, Ag, Cu, Pd	Si	30 nm	tapping mode AFM	1−4 V, ~10 GΩ, ~0.3 nA, 5−50 nm/s, 35−60% RH	E-DPN	171, 172
AFM; highly doped silicon tapping mode tip	poly-EDOT	SiO_x	50 nm	AFM	−9 to −15 V, 1−10 nm/s, 28−48% RH	E-DPN with polymer	173
AFM; tapping mode silicon cantilever, 40 N/m	histidine-tagged peptides, proteins, porphyrins	Ni	20 nm	tapping mode AFM, fluorescence microscopy	-2 to -3 V, 1 μm/s, air	E-DPN ionized Ni surface, which binds molecules	174
AFM; contact mode cantilever	$HAuCl_4$	silicon	<100 nm	tapping mode AFM	0.005−0.02 μm/s, 40−50% RH	Au ink without applied voltage	175
AFM; −	$HAuCl_4$	Ge(100) oxide coated	30 nm		0.2 μm/s, 50% RH	comparison of nanopatterning techniques	176
AFM; Si_3N_4, 0.05 N/m	mixture of iron nitrate ($Fe(NO_3)_3$) and barium carbonate ($BaCO_3$) in ethylene glycol	SiO_2/Si	90 nm	AFM, magnetic force microscopy (MFM)	0.1−0.2 μm/s, 31% RH, 24 °C	annealing of precursor leads to final material	177
AFM; Si_3N_4, 0.05 N/m	Al_2O_3, SiO_2, SnO	Si, SiO_x	140 nm	LFM, topography	0.1−0.2 μm/s, 0.5 nN, ~40% RH, ~20 °C	sol-based inks	178
AFM; Si_3N_4		mercaptosilane on SiO_x	160 nm	new tip	5 nN	AuNP ink	179
AFM; with second tip	AuNP thiol capped	Au	50 nm dots	tapping mode AFM, TEM	contact AFM	deposition of AuNP	180

Table 2. (Continued)

SPM and tip used	molecular "inks" employed	substrate	line resolution	SIC	RC (including RH and/or environment)	comments	ref
AFM; Si_3N_4, sharpened, 0.05 N/m	MHA	Au	100−350 nm	tapping mode, 40 N/m, 2−32 μm/s, ∼ 42% RH	0.5 nN, 40% RH, 24 °C	protein adsorption	181
AFM; Si_3N_4, 0.05 N/m	MHA	Au/Cr/glass	230 nm	LFM	up to 8 μm/s, 35−55% RH	protein adsorption	182
AFM; Si_3N_4, sharpened	amine-terminated thiolated PEG	Au/Cr/glass, Au/mica	30 nm	LFM	0.1−1 μm/s, 30−60% RH, 22−23 °C	patterning with nanoshaving; binding of cowpea virus	183
AFM; Si_3N_4, 0.05 N/m	MHA, 11-mercapto-undecylpenta(ethylene glycol) disulfide, disulfide substituted with one maleimide group	Au/Ti/Si	150 nm dots	tapping mode AFM	0.5 nN, 40% RH, 24 °C	binding of cowpea virus	184
AFM; silicon cantilever, 3.2 N/m	MHA	Au/Ti/glass or Si	240 nm	LFM, optical micrographs	30% RH, 23 °C	particle adsorption	185
AFM; Si_3N_4, sharpened, 0.05 N/m	MHA	Au	45 nm	LFM, topography, 3−6 μm/s	0.06−1.6 μm/s, 31% RH, 24 °C	magnetic particles	186
AFM; silicon cantilever, 3.2, 0.3, or ∼40 N/m	MHA	Au		tapping mode and contact mode AFM	1 s/(100 nm dot radius), 0.5 nN, 55% RH, 23 °C	DNA patterns	187
AFM; −	$FcC_{11}SH$, $FcCOC_{11}SH$	Au	100 nm	FE-SEM, tapping mode, LFM, ∼ 10 μm/s	0.4−1 μm/s, 38% RH	potential controlled adsorption of DNA-modified AuNp	188
AFM; Si_3N_4, 0.05 N/m	MHA	$Au/Ti/SiO_x/Si$	150 nm, 70 nm dots	tapping mode AFM	1 μm/s, 0.5 nN, 30−36% RH, 22−24 °C	etching into substrate, binding of DNA particle assemblies	189
AFM; Si_3N_4, Au coated	MHA, $C_{18}SH$	$Au/Ti/SiO_x$	∼150 nm	LFM	0.012−0.6 μm/s, 0.3−1 nN, 0−100% RH,	parameter studies	195
AFM; −	$C_{18}SH$	Au/Ti/Si	>150 nm dots	LFM	13−36 °C, N_2, air, ethanol vapor	theory of surface diffusion of ink	190
AFM; Si_3N_4, sharpened	$C_{18}SH$	Au	∼300 nm dots	LFM, >160 μm/s	N_2, controlled humidity	thiol diffusion and RH study	194
AFM; 0.05 N/m	$C_{18}SH$, MHA	Au on Si, NaCl crystal	dots	LFM	0.5 nN, 0−100% RH, 22−33 °C, N_2	ink transport study	196
AFM; sharpened cantilevers	MHA	Au	60 nm	LFM, ∼10 μm/s	0.1−1 μm/s, 15−55% RH, 22−23 °C	humidity study	

the creation of lines, the patterns were dependent on the translation speed of the tip and the deposition rate.

Ratner and co-workers subsequently described a theoretical investigation of the condensation of the water meniscus between the tip and the substrate.[191] A grand canonical Monte Carlo simulation of a two-dimensional lattice gas model described the meniscus condensation within the context of tip shape, tip−substrate distance, and tip wettability. A smaller tip radius and a larger tip−substrate distance led to a smaller meniscus diameter, and the instability of the meniscus increased. The smallest meniscus diameter found was 2.3 nm, which may suggest the limit of resolution of DPN. The real resolution limit was suggested to be larger because the effect of surface diffusion during deposition and after tip retraction was not considered. Similarly this group recently expanded their theoretical investigations of DPN to a description of the capillary force caused by the inherent water meniscus between the tip and a flat substrate.[192] The qualitative behavior was in accordance with experimental data found, but the force determined was at least 1 order of magnitude too low, which the researchers explained through the two-dimensional approach. The force was found to increase if a three-dimensional meniscus was assumed.

De Yoreo and co-workers described the effect of dissolution kinetics on feature size with DPN assuming a liquid meniscus was necessary.[193] They proposed a three-step process where thiol molecules dissolve from the tip into the meniscus, diffuse through the meniscus, and attach to the surface. Their model predicted the dependency of feature size on dwell (contact) time and tip speed, in agreement with the measured dependencies. At short contact times, the concentration of thiol in the meniscus was nearly zero and the deposition was dominated by the dissolution kinetics for the detachment of the ink from the tip. For longer contact times, the transfer process of the ink (diffusion) to the surface was the dominating factor.

In contrast, Sheehan et al. argued that a meniscus is not important in the DPN writing process by experimentally and theoretically investigating the role of humidity upon the surface diffusion of thiol. DPN was conducted at 0% RH, and the C_{18}S-SAM pattern was formed under these conditions. It was argued that, in the absence of any humidity in the environment, no meniscus was present.[194] For the theoretical description of the empirical data, a two-dimensional diffusion equation was used. This equation was solved using an analytical approach including a parameter for the kinetics of molecular transport from the tip to the surface. The surface diffusion coefficient for C_{18}SH was determined to be 8400 ± 2300 nm^2/s. This value was claimed to be independent of humidity.

In another investigation, Schwartz also concluded from successful DPN patterning experiments at 0% RH, using both C_{18}SH and MHA inks, that a meniscus was not responsible for the ink transport to the surface.[195] The modeled molecular diffusion rate was found to be independent of humidity, but the deposition depended on the write speed and the temperature. The author proposed two different diffusion models for the nonpolar C_{18}SH and polar MHA molecular inks.

Mirkin et al. most recently investigated the role of humidity in dip-pen nanolithography and presented new experimental evidence for the importance of a meniscus.[196] Two elementary processes were identified: molecular transport from the tip to the substrate via a menicus (e.g., dissolution of ink and transport through the meniscus to the substrate) and adsorption of the ink on the substrate. These processes were dependent on temperature, humidity, the physicochemical properties of ink and surface, writing speed, and the tip−substrate contact force. It was observed that the deposition was still possible if the sample and the tip where kept in 0% humidity for 24 h. To support that a meniscus was still present under these conditions, two experiments were performed. The first held a tip in contact with a sodium chloride (NaCl) crystal for a certain period of time. The images then obtained on the crystal showed wells whose size was dependent on the contact time and the humidity. Even at 0% RH, a depression was observed. The authors suggested that at 0% RH, residual water on the surface formed the meniscus. If the same experiments were performed under UHV conditions, no changes on the surface of the NaCl crystal were observed. In their discussion the authors assumed that the transport was occurring from the tip to the substrate in the presence of water. Higher temperatures raised the number of solvated molecules, and the diffusion rate in the meniscus and on the surface increased. The patterning process was described as a competition between surface diffusion and solvation of the ink in the meniscus. The adsorption of the ink onto the substrate required displacement of water. At higher humidity, more molecules were solvated because a larger meniscus was formed; however, a thicker water layer on the surface was also present that was proposed to impede ink deposition.

4. Substitution Lithography

Substitution lithography involves a process whereby a SAM covers the entire surface both before and after the patterning step. This type of approach has the advantages that all regions retain chemical definition during the entire procedure, and that the behavior of any patterned region installed can be directly compared to that of a "background" SAM that was not intended to display this behavior. From a semantic viewpoint, several of the papers already discussed could be grouped into this category. In particular, lithographic processes classified as elimination followed by ex-situ addition do result in net substitution. However, here, we restrict our discussion to processes that effect substitution in "one pot" without multiple formal steps. Two distinct types of substitution lithography processes on SAMs can be identified. In the first, localized elimination of the SAM occurs by physical or electrochemical means followed by subsequent in-situ addition of a different molecule into the exposed surface. In the second, a functional

headgroup is chemically transformed into a different functionality under the action of a probe tip. Each of these types of lithographic processes is treated below in turn (Table 3).

4.1. Substitution Initiated by Removal of SAM under Elevated Bias

In the section of this review on elimination (Section 2), work by the Crooks group was discussed in which a SAM was locally removed under the influence of a biased STM tip. These authors extended this to originate an in-situ approach for the formation of metal structures. This procedure involved initial SAM removal followed by electrochemical deposition of a metal from a Pt/Ir STM tip.[197] Prior to the patterning, the tip was coated with a thin layer of electrodeposited silver metal. The surface of a C_{16}S-SAM on gold was scanned at an applied bias of +400 mV (substrate) without apparent destruction of the monolayer. When the bias was elevated to ca. 3 V, the monolayer and some gold layers were removed in the scanned area. Subsequent scanning of a larger area around the pattern at a negative bias (−600 to −1000 mV) oxidized the silver at the tip, which was redeposited only in the exposed gold regions. No silver deposition was found outside the patterned region, and the researchers believed that the highly ordered and unperturbed SAM hindered the electrochemical (metalization) process. If the silver patterns were scanned again with a high positive bias, a partial removal of the previously deposited silver occurred. The authors suggested the lithographic scheme was electrochemical because it was dependent on relative humidity. Control experiments with bare Pt/Ir tips at high humidity or Ag-coated tips at low humidity resulted in no significant deposition of silver onto the surface.

An in-situ replacement in a SAM of one organic component by another was reported by Chen et al. who used STM to replace conjugated molecules into a C_{12}S-SAM on a gold surface.[198] Initial experiments reported creation of pits in a C_{12}S-SAM by moving the tip close to the surface ($V_b = 0.1$ V; $I_t = 0.5$ nA), and applying voltage pulses between 1.8 and 3.6 V. This experiment was performed with a coated tip and substrate immersed in 1,4-dioxane. The probability for the creation of pits was shown to depend on the amplitude of the pulse and the distance between the tip and the substrate as controlled by the set-point current. The researchers observed that positive voltage pulses had to be used; otherwise mounds of material were created on the surface. They next added a conjugated molecule (2′-ethyl-4:1′-ethylphenyl-4″:1′-ethylphenyl-1,4′-thioacetylbenzene) and deprotecting agent (NH_4OH) to the solution. STM images showed that areas originally displaying a depression in the SAM from the elimination step subsequently showed a larger apparent height than the background SAM. This result was rationalized by pointing out that, although the thickness of the SAM composed of the conjugated molecule and the C_{12}S-SAM were nearly the same, the conductivity through the SAM composed of the conjugated molecule should be higher. This two-step patterning could also be done in-situ with similar results when the replacement molecule and deprotecting agent were present in solution during the pit formation. The smallest created dots had a diameter of around 10 nm, which was equivalent to the replacement of ca. 400 molecules.

Gorman et al. reported a similar approach to a chemically well-defined, STM-based lithography.[199] SAMs composed of *n*-alkanethiol on Au(111) were locally removed under the action of a biased STM tip. The mechanism of this removal was argued to be similar to that reported by Crooks et al. (as described in the section on elimination lithography[82]). A low-current STM (ca. 10 pA set-point current) was employed to minimize the mechanical interaction between the tip and the SAM, and replacement was effected under the application of an increased set-point bias (ca. 3 V).[81] The removal was performed in a fluid solvating a second "replacement" thiol, which presumably adsorbed to the freshly exposed gold. This approach employed a low dielectric, nonpolar solvent (dodecane, mesitylene) to avoid the use of coated tips that would normally have to be employed to avoid a high leak current (greater than 1 pA) from the tip into the surrounding solution. Avoiding a coated tip eliminated concerns about the reproducibility of tip coating and potential problems with contaminations from the organic tip coating material. Figure 26 illustrates this replacement lithography approach. Under standard imaging conditions (SIC: $V_b = 1$ V, $I_t = 5$ to 10 pA), an appropriate region of the SAM on Au(111) was identified for patterning that was free of terraces or defects (Figure 26A). The replacement in the proximity of the tip was effected by elevating the applied bias (positive substrate) to the replacement conditions (RC: $V_b = 3-4$ V; $I_t = 5-10$ pA; Figure 26B). In the presence of a replacement thiol in solution, this region was observed to fill in promptly. After returning to SIC, the pattern could be subsequently imaged (Figure 26C). This technique resulted in patterns with line widths of ca. 10 nm.

In a first demonstration of thiol replacement, *n*-alkanethiolate SAM patterns were created composed of regions of different chain lengths. A C_{10}S-SAM pattern was written into a C_{12}S-SAM matrix. The apparent height of the shorter C_{10}S-SAM pattern appeared taller than the background C_{12}S-SAM matrix in the STM images. When C_{12}SH was patterned into a C_{10}S-SAM matrix, the patterned C_{12}S-SAM had a lower apparent height in the STM images. Here, the tunneling gap in fluid solution had a higher transconductance than that of the SAM itself, resulting in a reversal of the apparent heights of these regions compared to those anticipated. This reversal in apparent height contrast had been predicted previously by Weiss et al.[90] Relative humidity also was found to play a role in the relative ability to effect replacement. When the humidity of the surrounding atmosphere was below approximately 40%, the set-point voltage required for the replacement increased and the formation of pits in the gold substrate was observed. In the range of 60−80% RH,

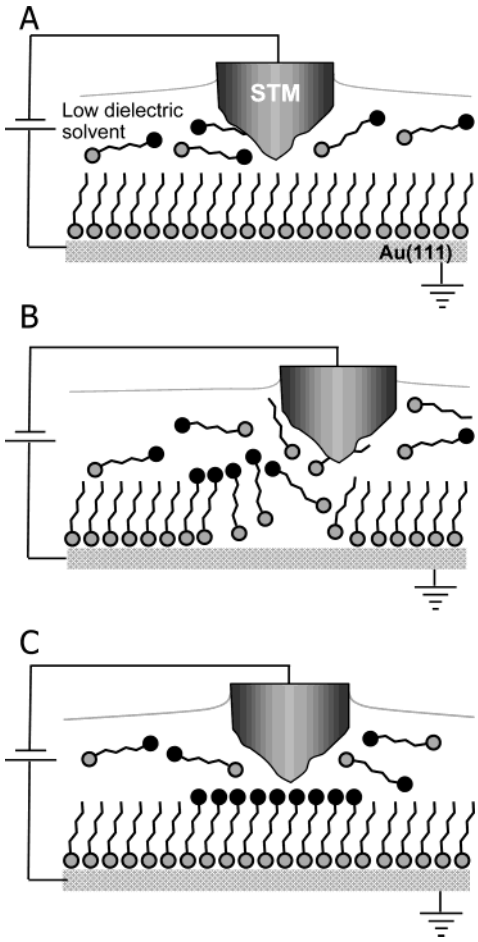

Figure 26. Schematic diagram of substitution lithography by elimination and in-situ addition. (A) The self-assembled monolayer was imaged with nonpertubative tunneling parameters to locate an area suitable for patterning. (B) Upon change of the tunneling parameters (I_t, V_b), the thiolates of the SAM desorbed in the proximity of the tip, resulting in removal of the SAM. The replacement molecules in solution assembled into the "bare" regions. (C) The patterns could be assessed by changing the tunneling parameters to their initial, nonperturbative values.

the replacement occurred at lower voltages and the pit formation was nearly completely suppressed. The effect of humidity suggested that the removal of the SAM was electrochemical in nature. A similar conclusion was drawn earlier by Crooks et al.[82] It was argued that mechanical effects in this process should be negligible because the tip was further away (e.g., higher voltage) from the SAM during replacement than under the standard imaging conditions. The line width of the replaced SAM region was ca. 7 nm at full width at half-maximum, and a spatial line resolution of ca. 15 nm was observed.

Replacement lithography was subsequently employed to create SAM regions composed of electroactive headgroups within insulating C_{12}S-SAMs. Investigation of these patterns showed bias-dependent image contrasts and allowed the current−voltage ($I-V$) behavior of electroactive tip/SAM/substrate junctions to be directly compared against an electroinactive SAM background.[200] Replacement lithography was used to create (400 nm)^2 patterns of ferrocenylundecanethiolate SAM (FcC_{11}S-SAM) and galvinolphenoxyhexanethiolate SAM ($GalC_6$S-SAM) within a C_{12}S-SAM background. Notably, the inks employed were ferrocenylundecanthioacetate (FcC_{11}-SAc) and phenoxygalvinol-substituted hexanethioacetate ($GalC_6$SAc) instead of the thiol derivatives. It has been observed that when thiols were used in replacement lithography, a larger amount of adventitious replacement (that is, replacement not stimulated by the action of the tip) occurred at defect sites in the SAM. The mechanistic differences between the use of thiols and thioacetates remain unclear. It is speculated that either a small amount of the thioacetate molecules were adventitiously deprotected, resulting in a low concentration of free thiol, or somehow the elevated bias of the STM tip promoted the deprotection reaction.

Using the STM tip, $I-V$ curves were collected over different regions (e.g., C_{12}S-SAM versus FcC_{11}S-SAM). Within the regions containing a SAM with electroactive headgroups, nonlinear $I-V$ curves displaying negative differential resistance (NDR) were measured, while in the regions of C_{12}S-SAM no NDR was observed. This experiment facilitated a direct comparison of the electronic behavior between two different types of molecules (electroactive, nonelectroactive) and was, in this regard, an ideal way to investigate molecular structure−property relationships relevant to molecular electronics. The relative transconductance of the electroactive SAM regions increased (compared to the insulating C_{12}S-SAM background) with increased imaging bias. As observed in Figure 27, at low bias ($V_b = 150$ mV), the relative transconductance between the FcC_{11}S-SAM and C_{12}S-SAM regions was similar, and the pattern of the electroactive molecules (the letters "Fc") was almost indistinguishable from the C_{12}S-SAM. At higher applied bias ($V_b = 1000$ mV), the electroactive thiolate pattern had a much higher relative transconductance compared to the C_{12}S-SAM background. It was hypothesized that both the nonlinear $I-V$ behavior and bias-dependent difference in relative transconductance occurred via resonant tunneling through the electroactive ferrocenyl moiety. This work also illustrated sequential replacement with two different thiol inks to compare simultaneously two SAM regions with different electroactive headgroups against a C_{12}S-SAM background.

SAMs constructed from these electroactive thiols provided excellent image contrast against a C_{12}S-SAM background, and this contrast was employed to correlate various experimental parameters (applied bias, scan rate, and RH) with the efficacy of replacement.[201] It was observed that there was a window of optimal replacement bias for a constant set-point current and RH. There was also a threshold bias that afforded complete replacement (3.2−3.4 V). Below that bias, incomplete or no replacement occurred, while a larger applied bias produced replacement with inconsistent line widths, damage to the surrounding C_{12}S-SAM regions, and/or etching of the Au(111) substrate beneath the tip. There also was found to be an optimal lithographic scan rate (30−50 nm/s) under constant bias (3.2 V) and constant RH (58%). Very slow scan rates (10−20 nm/s) produced incon-

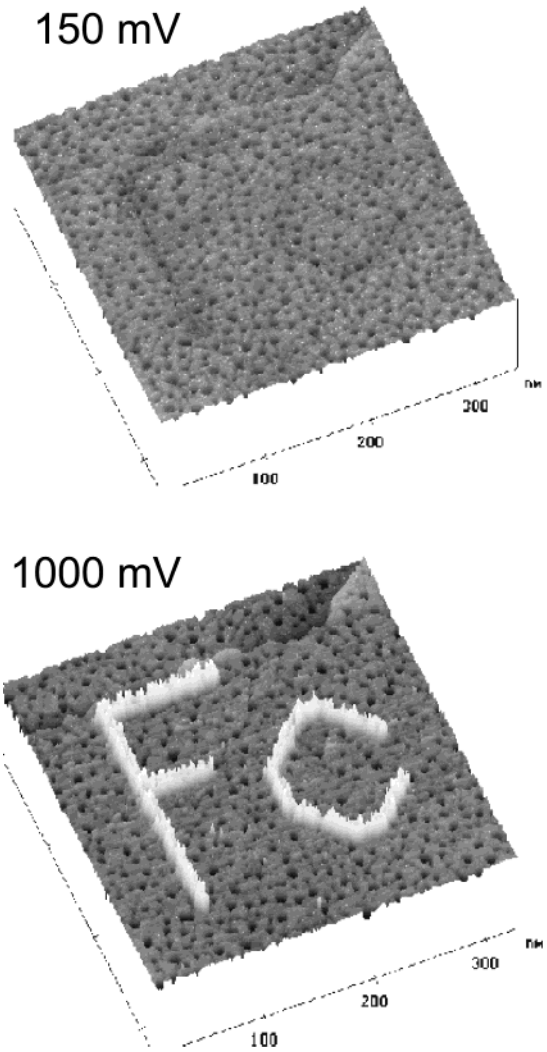

Figure 27. STM images showing the bias-dependent apparent height contrast of electroactive $FcC_{11}S$-SAM patterned into a nonelectroactive $C_{12}S$-SAM. At a low bias of 150 mV, the letters "Fc" were nearly invisible because the two molecules were similar in length. At higher imaging bias (1000 mV), the patterned $FcC_{11}S$-SAM showed a large apparent height contrast compared to the background SAM. (Imaging conditions: I_t = 10 pA; *z*-scale, 2 nm; scan speed, ca. 350 nm/s.)

sistent line widths, and very fast scan rates resulted in incomplete and diffuse replacement.

Using the findings that the manipulation of replacement parameters could affect the degree of replacement, mesoscale chemical gradient structures were fabricated. These structures were created via a systematic variation in scan rate, bias, and line spacing (Figure 28). The high replacement coverage at one end of the gradient was achieved by a close spacing (e.g., 5 nm) between the scan lines (to overlap replaced lines), a slow scan rate (broad replacement lines), and/or a higher replacement bias (broader lines). The variation in the coverage resulted from the change of one of more of these parameters. The diffuse end of the gradient was created by a combination of increased line spacing, faster scan rate, and/or lower replacement bias. The chemical gradient structures shown in Figure 29 were fabricated by systematically varying the replacement bias (from V_b = 3.1 V to V_b = 2.6 V; line spacing, 4−12 nm; Figure

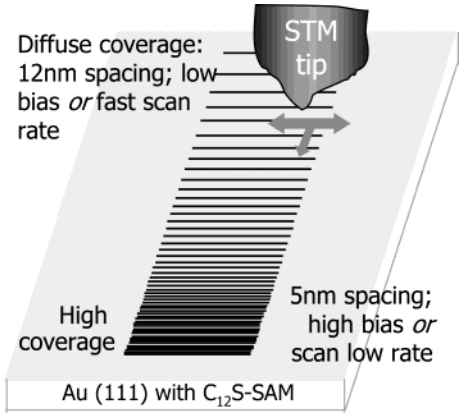

Figure 28. Schematic diagram for the fabrication of mesoscale chemical gradients. The diffuse (low) coverage end of the gradient was achieved by a non-overlapping lithographic line spacing (e.g., 12 nm) and low replacement voltage or fast lithographic scan speed. During the patterning of the gradient, the line spacing was incrementally decreased to overlap lithographic lines (e.g., 5 nm), while the replacement voltage was increased or the scan speed was decreased, resulting in high replacement coverage.

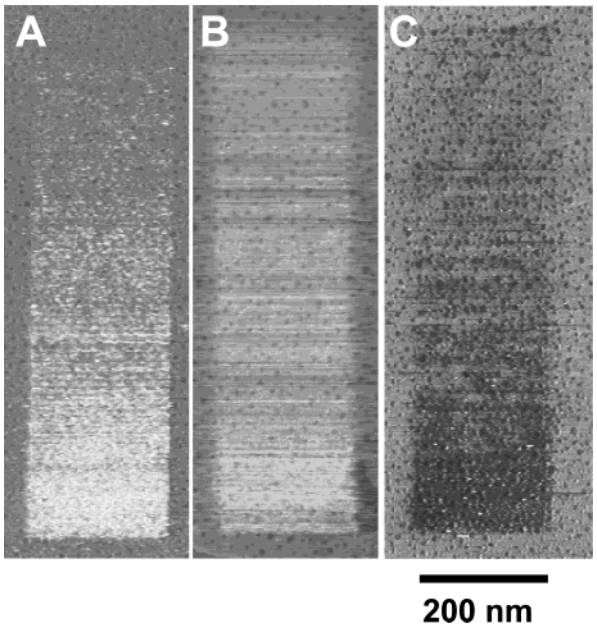

Figure 29. STM images of mesoscale chemical gradient fabricated from $FcC_{11}SH$ into a $C_{12}S$-SAM, either systematically varying the replacement voltage from 2.6 to 3.1 V (A) or the lithographic scan speed from 160 to 20 nm/s (B) (*z*-scale: 6 nm). (C) A chemical gradient of MUA in a $C_{12}S$-SAM. The replacement bias was changed from 2.5 to 3 V (*z*-scale: 2 nm). Reprinted with permission from ref 201. Copyright 2002 Wiley-VCH.

29A) or the lithographic scan rate (from 20 to 160 nm/s; line spacing, 4−12 nm; Figure 29B). Figure 29C shows a chemical gradient consisting of mercaptoundecanoic acid-SAM (from V_b = 3.0 V to V_b = 2.5 V; line spacing, 4−12 nm) and illustrates that gradients could be written with other inks than FcC_{11}-SAc. The creation of multidirectional gradients was also shown.

Another report utilizing replacement lithography demonstrated the novel use of hydrogen bonding to add and remove electroactive functionality from a mesoscale molecular assembly in a reversible fashion.[202] Multipoint, complementary hydrogen bonding

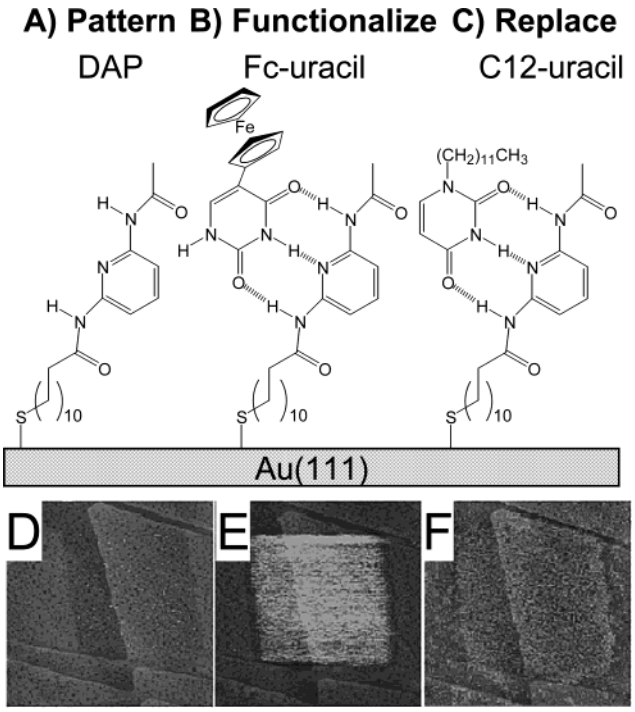

Figure 30. Schematic and STM images illustrating multipoint complementary hydrogen bonding recognition elements for the addition and removal of electroactive functionalities. (A) The host thiol molecule (DAP) was patterned via replacement lithography into a C_{12}S-SAM. An electroactive functionality was added in-situ to this structure through noncovalent binding of a ferrocene-terminated uracil (B). The electroactive functionality could be replaced with a nonelectroactive dodecyl-uracil (C). STM images after each of these steps taken at 0.5 V imaging voltage showed the change in the apparent height contrast. The replacement region of DAP had a low contrast (D). After the addition of ferrocene-terminated uracil, the apparent height contrast increased due to the electroactive moiety (E). The apparent height contrast was decreased by adding the dodecyl uracil molecule that replaced the electroactive moiety (F). (I_t = 10 pA; *z*-scale, 3 nm.) Reprinted with permission from ref 202. Copyright 2002 American Chemical Society.

recognition elements mediated the assembly steps depicted in Figure 30. The host thiol, diacyl 2,6-diaminopyridine decanethiol (DAP), was patterned via replacement lithography into a C_{12}S-SAM matrix on Au(111) from a mesitylene solution (Figure 30A). Addition of an electroactive functional moiety through a noncovalent binding event was subsequently achieved by incubation of the DAP-SAM pattern in a solution containing the complementary ferrocene-terminated uracil (Fc-uracil, Figure 30B). Subsequent replacement of the electroactive Fc-uracil by a nonelectroactive dodecyl uracil "eraser" (C_{12}-uracil) was effected by exposure of the replacement region to a solution of C_{12}-uracil (Figure 30C). STM images taken after each step are shown in Figure 30D−F, respectively. Under an imaging bias of 0.5 V, the DAP replacement region within the canvas C_{12}S-SAM had low apparent contrast (Figure 30D). When the DAP-SAM region of the surface was functionalized with the electroactive Fc-uracil, the apparent height of this region increased (Figure 30E). This contrast change was decreased with the in-situ addition of the C_{12}-uracil eraser molecule (Figure 30F). The noncovalent host−guest binding events observed in STM images were further characterized on monocomponent SAMs via cyclic voltammetry and XPS.

A replacement lithography technique employing a current sensing AFM (CSAFM) was demonstrated. The strategy of effecting local removal of a SAM under elevated tip−substrate bias followed by replacement was similar to that described above. The authors reported the replacement of a series of shorter chain alkylthiolate (C_6S-, C_8S-, and C_{10}S-) into C_{18}S-SAMs.[203] When the tip was scanned over the canvas SAM with an applied voltage of 4−5 V, the replacement occurred. The scanning parameters used were similar to those employed for the preparation of structures in which the SAM was locally removed without the addition of a second thiol.[104] Topographic images showed height changes smaller than expected theoretically, but the authors speculated this behavior was due to the applied load of the cantilever during imaging. Current images captured at 0.5 V showed the reverse contrast in fluids compared to those in air (similar to that previously observed[199]). The edge resolution of the structures was observed to be higher in current mode images than in the topography images. The authors rationalized this result by indicating that the apparent height in the current mode images arose from the exponential behavior of the tunneling current with height. In contrast, a more linear relationship between force and height would be found in topography images. The linear portion of the $I-V$ curves yielded resistance measurements of each patterned area as $(1.8 \pm 1.2) \times 10^{10}$, $(2.5 \pm 1.0) \times 10^9$, and $(2.5 \pm 1.5) \times 10^8$ Ω for C_{10}S-, C_8S-, and C_6S-SAMs, respectively. These values corresponded well with those predicted from a tunneling model (e.g., exponential increase in resistance with chain length). The exponential distance decay parameter for tunneling (β) calculated on the basis of these data agreed well with previously published values. A final experiment in which C_{18}-SH was patterned into a C_{10}S-SAM matrix was demonstrated with a reported topography height difference of ca. 1 nm between SAM regions. Current images indicated that the patterned area appeared as a depression, which was expected because the C_{18}S-SAM had a lower transconductance than the C_{10}S-SAM.

4.2. Substitution Initiated by Removal of SAM via Mechanical Desorption

The substitution lithography techniques described thus far have relied on the removal of the SAM under an applied voltage. Alternatively, SAMs can be removed by mechanical means followed by in-situ replacement with a second component. This type of mechanical displacement of a SAM with an AFM tip under a solution containing a replacement thiol was developed by Xu and Liu.[204] Typically, the SAM was first imaged with a low force (smaller than 0.5 nN) in order to find an area suitable for the surface modification, as is depicted in Figure 31. Early experiments demonstrated the localized elimination of the molecules of the SAM in solution (2-butanol). This approach was later termed "nanoshaving".

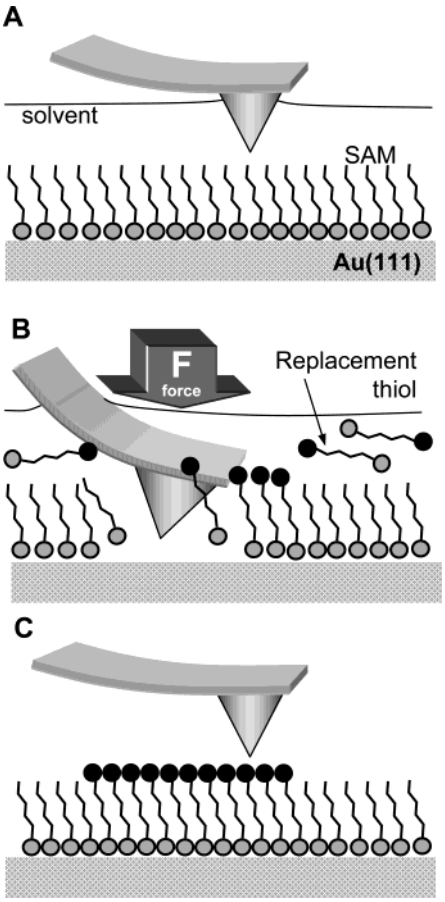

Figure 31. Schematic diagram of nanografting. A SAM was imaged with an AFM tip under a nondestructive imaging force to locate an area suitable for patterning (A). With an increased, applied force the monolayer was removed under the tip and the replacement molecules in solution assembled into the "bare" regions (B). The pattern could be imaged with a low, nondestructive force (C).

When a similar experiment was performed under a solution of a replacement thiol, the blank sites reacted with the thiol in solution and formed a region of replacement (Figure 31B). After patterning, the force was reduced to the initial imaging force, and the structure could be directly imaged with the same tip used for the surface modification (Figure 31C). The authors named this replacement procedure "nanografting".

The first nanografting experiments were performed on a C_{10}S-SAM, and patterns consisting of C_{18}S-SAMs were generated (Figure 32A and B) with corresponding section analysis (Figure 32C). High-resolution images of the canvas (Figure 32D) and the replaced region (Figure 32E) revealed a very high order with a two-dimensional close-packed structure. This structure was consistent with the well-known structure of monocomponent SAMs formed from solution self-assembly. A multiple thiol ink experiment was also demonstrated in which the solution was exchanged after each fabrication step. In this way, a C_{18}S-SAM line structure was created, subsequently erased by nanografting with the same thiol precursor as the matrix (C_{10}S-SAM), and a third line consisting of C_{18}S-SAM in close proximity to the original nanostructure was written. This experiment illustrated

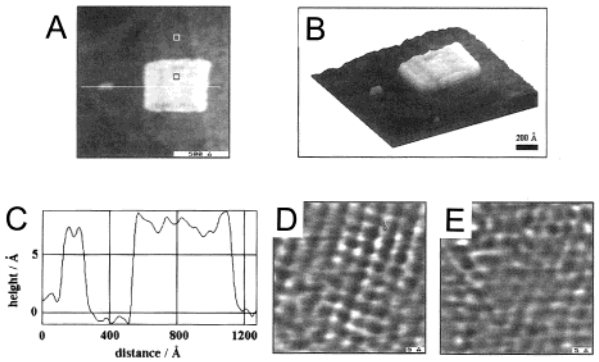

Figure 32. (A) Topographic AFM image of two squares fabricated from C_{18}SH in a background C_{10}S-SAM (replacement parameters, 5.3 nN force; imaging conditions, 0.3 nN). The cross-section showed that the C_{18}S-SAM was ca. 8 Å higher than the background. The edge resolution was 1 nm. Molecular resolution images of the C_{18}S- region (C) and the C_{10}S-SAM (D) revealed a two-dimensional close-packed structure. Reprinted with permission from ref 204. Copyright 1997 American Chemical Society.

both the fabrication and alteration of structures on the nanoscale.

The rate of replacement and degree of order in the replaced regions was, under some circumstances, observed to be different from self-assembly onto a bare surface. This point was addressed by Xu et al. in a comparison of the self-assembly process onto a bare surface with that into nanografted regions using time-resolved AFM measurements.[205] Here, it was speculated that replacement molecules were spatially confined, having limited area to insert themselves into the exposed gold surface region. The researchers found that the assembly time for the nanografted patterns was at least 1 order of magnitude faster and showed higher order and fewer defect sites than the film formation from solution. It was suggested that the more rapid assembly into nanografted regions occurred because a lying-down to standing-up transition found in the reaction on a bare gold surface was avoided. During the first step of thiol self-assembly on gold, a phase was initially observed where the molecules lie flat on the surface.[47] At a higher surface coverage (above the saturation coverage of this first phase), a solid−solid phase transition occurred, resulting in domains of molecules standing up. Consistent with this observation, nanografted structures formed slowly when their dimensions were larger than the size of the molecules and when nanografting occurred at a rate of scanning that was faster than that of assembly. Conversely, when the dimensions of the nanografted structure were smaller than the size of the molecules and when nanografting occurred at a rate of scanning that was slower than that of assembly, the rate of structure formation was much faster.

Several additional interesting demonstrations have been described to illustrate the range of possible nanostructures that can be created using nanografting. Xu et al. used a wide variety of inks with various chain lengths and functional headgroups and showed topography and LFM images of MHA grafted into a C_{18}S-SAM, C_{18}SH grafted into 2-mercaptoethanol-based SAM (HOC_2S-SAM), and HO_2CC_2SH grafted

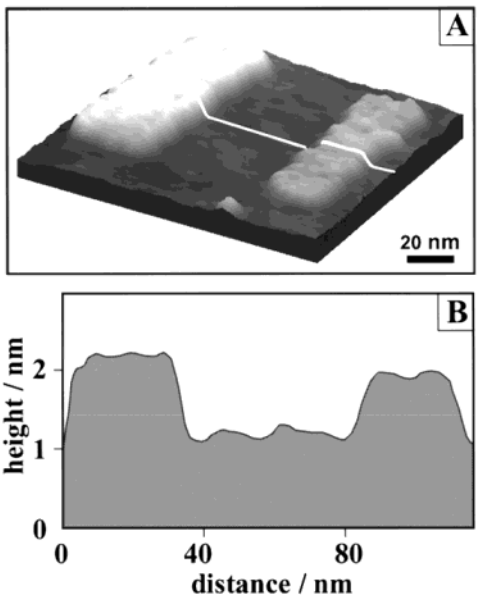

Figure 33. (A) Topographic AFM image of two rectangles fabricated from $C_{22}SH$ and $C_{18}SH$ in a $C_{10}S$-SAM matrix (replacement parameters, 15 nN force; writing speed, 50 ms/line). The corresponding cursor profile is shown (B) and revealed a height difference of ca. 1.2 and 0.85 nm for the two different replaced patterns, respectively. Reprinted with permission from ref 206. Copyright 1999 American Chemical Society.

into a $C_{10}S$-SAM.[206−209] Another example in which two different inks were sequentially employed can be observed in Figure 33. Two rectangular nanoislands patterned from $C_{22}SH$ and $C_{18}SH$, respectively, were created in a $C_{10}S$-SAM background matrix. In another report, complex patterns and complete sentences were fabricated. These structures were made possible through the combination of vector-scanning probe lithography combined with computer-assisted design.[210]

Another application of nanografting reported was the characterization of the shape of AFM tips.[211] Due to the previously mentioned spatial confinement effect of self-assembly in nanografting, the edges of patterned lines were sharp and straight. The observed line profile width was in direct correlation with the shape of the top portion of the tip, and the sides of the line profile represented the shape of the tip.

The nanografting of thiol-modified ssDNA has been illustrated by Liu et al.[212] An 18- or 12-base oligomer with hexanethiol linker was grafted into a hexanethiolate- (C_6S-) matrix under a force of 20 nN and a scan speed of 800 nm/s. The patterns showed a height that correlated with the theoretical height (84 Å for the 18-base and 59 Å for the 12-base oligomer). This observation led the authors to conclude that the DNA SAM region adopted a nearly standing-up configuration. The periodicity of SAMs routinely observed under AFM was not obtained for the ssDNA patterns, leading to the conclusion that the DNA molecules did not form an ordered and close-packed structure on the gold surface. To confirm that the structures were made out of DNA, the authors used an enzyme that cleaved the ssDNA to leave a terminal hydroxyl group. In a time-resolved AFM experiment, the change in the topographic images was easily seen as shown in Figure 34A,D,G (corresponding cursor profiles shown in Figure 34C,F,I), while friction images (Figure 34B,E,H) showed little difference in appearance (the 3′ end of the original oligomer was also terminated in a hydroxyl group). After 4 h, the initial height was decreased and the density of the ssDNA was lower, which was due to the enzyme cleaving the patterned DNA randomly. After 20 h, the pattern was nearly invisible in the topography image. The enzyme digested only the DNA but did not cleave the C−C bond of the linker. The region where the ssDNA had been was still visible in the friction mode because the surface was terminated with hydroxyl groups, compared to the methyl groups of the background SAM. These experiments showed that the structures were indeed composed of DNA and were accessible to enzymatic reactions.

Case et al. designed a protein to bind to a gold surface and employed it in nanografting experiments.[213] A tertiary parallel three-helix bundle complexed to iron (on one end) with a D-cysteine residue (on the other) provided a thiol for chemisorption on the gold substrate. By choosing the appropriate buffer, the helicity in the protein was enhanced, resulting in the average height of the protein structures that compared well with the height predicted from molecular models. The authors observed forces applied to the tip that exceeded 40 nN disrupted the grafted proteins and showed a decrease in the measured height. The grafting had to be done under a very slow scan speed, presumably due to the slow diffusion coefficient of the large protein in solution. If the scan speed was too large, bare gold areas were observed that were slowly filled by the protein, resulting in lower coverage in the nanografted regions.

Amro et al. developed an ambient condition technique that combined nanografting and DPN, termed "nanopen reader and writer" (NPRW).[214] As an AFM tip coated with a thiol ink (e.g., DPN) scanned the thiolate matrix under an elevated force, it removed the SAM molecules (e.g., nanoshaving), while the molecules from the tip were subsequently transferred into the vacant areas. The factors governing the resolution were the same as those reported for nanografting, and the patterning was independent of the humidity and the texture of the substrate. In a proof-of-concept experiment, a $C_{10}S$-SAM was used as the matrix and the tip was coated with $C_{18}SH$. The rectangular pattern of the longer alkyl chain thiolate was created and found to be ca. 8 Å higher than the background thiolates. Other thiols with different chain lengths and functional groups were also described, including $CF_3(CF_2)_{11}(CH_2)_2SH$, as well as thiols with terminal aldehyde, carboxylic acid, thiol, and hydroxyl groups.

Garno et al. presented the precise positioning of nanoparticles by nanoshaving with subsequent nanoparticle adsorption.[215] A second approach with the aforementioned NPRW technique was also employed. During nanoshaving, gold nanoclusters with mixed thiolate shells (dithiol and thiol) were present in

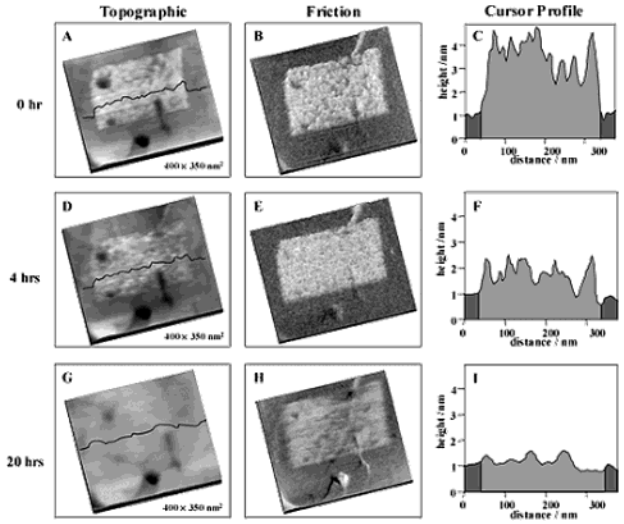

Figure 34. Time-dependent AFM images of a C_{10}S-SAM with a nanografted square of hexanethiol-modified oligonucliotide (12 base pairs). After the fabrication of the pattern, the sample was immersed in an enzyme to digest the DNA and imaged. The patterned square was clearly visible in the topography (A) and the friction image (B). The corresponding cross-section analysis (C) revealed a height difference of ca. 3 nm. After 4 h, the contrast in the topography image was decreased (D), and the friction image showed the same contrast as before (E). The cross-section (F) depicted a decreased height difference to ca. 1 nm. After 20 h, nearly no difference between the nanografted square and the background SAM was visible (G, I), while in the LFM image the square was still present (H). Reprinted with permission from ref 212. Copyright 2002 American Chemical Society.

solution to fill in the bare gold region exposed as the AFM tip locally removed a C_{10}S-SAM. In contrast to nanografting of thiolate SAMs, the adsorption process of the nanoparticles was much slower. The authors attributed the slow speed of replacement to the low concentration of the gold particles (AuNPs) in solution (10^{13}/mL AuNPs compared to ca. 10^{18}/mL for thiols) and the size of particles, which decreased the rate of colloid diffusion. An AFM image showed a 150 $\times$ 300 nm^2 area where 51 nanoparticles with an average diameter of 3.8 nm had adsorbed. In the NPRW approach, the authors physisorbed colloids to the tip prior to patterning. The high-applied force during the writing process resulted in the removal of the thiolate SAM from the substrate and the transfer of the nanoparticles to the substrate. The authors claimed that the writing process was highly selective because the transfer of the particles to the substrate required the removal of the underlying SAM and therefore, required a high-applied load. The reported coverage of nanoparticles in the patterned regions was lower than for a densely packed layer.

Schwartz reported an approach for creating structures of a thiol-modified molecule in a preformed matrix that was termed "meniscus force nanografting".[216] Thiol-modified DNA was patterned onto a gold surface that was covered with shorter, thiol-modified DNA strands. A drop of the patterning solution served to simultaneously wet the hydrophilic resist on the gold as well as the AFM tip. It was argued that the surface tension of this drop supplied enough force for the tip to locally remove the resist allowing the DNA to attach to the gold surface. Narrow line widths (ca. 15 nm) and very high linear writing speeds (ca. 320 μm/s) were featured. These DNA-based nanostructures were then hybridized to a complementary strand that had been grafted to metal nanoparticles, illustrating a complementary self-assembly process. To date, some concerns about the reproducibility of these results have been expressed.

4.3. Substitution Followed by ex-Situ Addition to Patterns

The examples discussed to this point involve substitution in which a monolayer-based pattern is the object of interest. Opportunities have been illustrated to exploit the monolayer pattern as a template for the growth or immobilization of another material. Often, this templated growth or deposition is performed in a second, ex-situ step. These types of investigations are treated in this section.

Wadu-Mesthrige et al. bound the protein lysozyme to nanografted squares of mercaptopropionic acid-based SAM ($HO_2C(CH_2)_2$S-SAM) patterns surrounded by a C_{12}S-SAM matrix.[217] This binding was via electrostatic interaction between the carboxylate headgroups of the SAM region and the protein. The authors noted that in order to prevent nonspecific binding of the protein to the C_{12}S-SAM matrix, very specific concentrations and incubation times had to be employed. More stable protein patterns could be realized if covalent binding schemes or specific chemical interactions were used. Aldehyde functional groups were suitable for binding of proteins containing amino groups through the formation of imide bonds. Patterns of aldehyde-terminated, $OHC(CH_2)_2$S-SAM were created in a C_{10}S-SAM background, and the protein IgG was adsorbed selectively in these patterned regions. The researchers showed that at least 50% of the protein remained biologically active as evidenced by their ability to bind antibodies. By using different molecules for nanografting, the creation of multi-ink patterns expanded the use of this method.

Protein patterns fabricated with various SPL strategies were reported by Kenseth et al.[218] In the first example, 5 μm MUA-SAM square patterns were nanografted into a C_8S-SAM on gold. Notably, the threshold force for nanografting of this pattern was higher than that reported by Liu and co-workers. The authors attributed this fact to the larger feature size and the faster scan speeds (greater than 20 μm/s). Rabbit IgG antibody was bound to the MUA patterns by a reaction via carbodiimide coupling. The results of this binding were observed in the topography image and cross/line section analysis (Figure 35A). Nonspecific protein binding to the C_8S-matrix was very low and was removed by scanning the surface with a force of 15 nN, which did not alter the covalently bound structures on the surface. The pattern could be further exposed to the complimentary rabbit IgG antigen (Figure 35B). In both cases, measured topography heights corresponded to the expected size of the molecules. The second technique

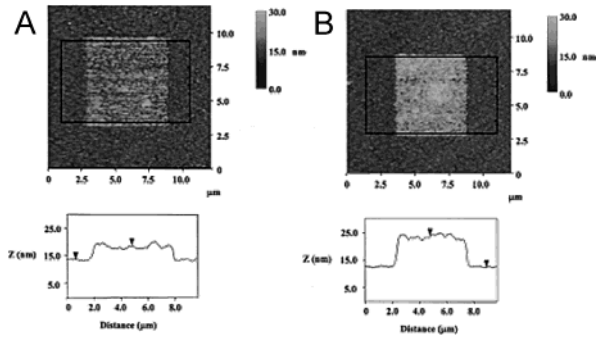

Figure 35. (A) AFM topography images (12 μm × 12 μm) of a C_8S-SAM with a square replaced with MUA after the binding of rabbit IgG through a coupling agent (EDC). (B) The same square after subsequent exposure to goat anti-rabbit IgG. The corresponding cross-section analysis was an average of the lines inside the box. (Imaging conditions: 2 nN force and 6 Hz; *z*-scale, 30 nm.) Reprinted with permission from ref 218. Copyright 2001 American Chemical Society.

demonstrated was based on nanoshaving a pattern into a (undeca-11-mercapto-1-yl) triethylene glycol methyl ether (EG3-OMe) SAM. The resist layer was scraped away from the gold surface by applying a high force, and indirect (adsorption of coupling agent and subsequent binding of a protein) and direct (adsorption of thiol modified protein) procedures for the attachment of proteins to the gold surface were demonstrated.

Liu's group fabricated three-dimensional nanostructures through nanografting, pursuing two different schemes.[219] In the first scheme, mercaptoundecanol (MUD) was patterned in a C_{18}S-SAM. The hydroxyl groups were reacted with the trichlorosilane headgroup of octadecyltrichlorosilane to form a Si−O network. This structure had a larger height than the surrounding MUD-SAM. This type of pattern transfer was termed "positive". Conversely, a negative pattern transfer was based on nanografting a C_{18}SH into a MUD monolayer. The sample was then exposed to OTS which self-assembled on the background SAM. In both experiments, the silane layer had a smaller height than would be expected from the size of the molecule. The authors concluded that the packing density was not as good as a thiolate SAM, and therefore the bilayer structure was more susceptible to compression from the tip.

Jang et al. created small patterns of enzymes by subsequent adsorption of acetylcholinesterase (AChE) to a nanografted poly(ethylene glycol)-containing SAM pattern composed from $HS(CH_2)_{11}(OCH_2CH_2)_6$-$OCH_2CO_2H$ within a $HO(OCH_2CH_2)_3(CH_2)_{11}$S-SAM background.[220] The triethylene glycol groups within each SAM region were present to resist nonspecific protein adsorption. Small, bare Au patches (termed "trapping sites") were then created by removal of the background SAM via nanoshaving. Acetylthiocholine (ATCh) was added with the intention that the trapped enzymes would cleave this molecule to form thiocholine, which contains a free thiol group. Indeed, after the addition of ATCh, bright spots on the trapping sites were apparent in AFM images consistent with the binding of the thiocholine to these bare

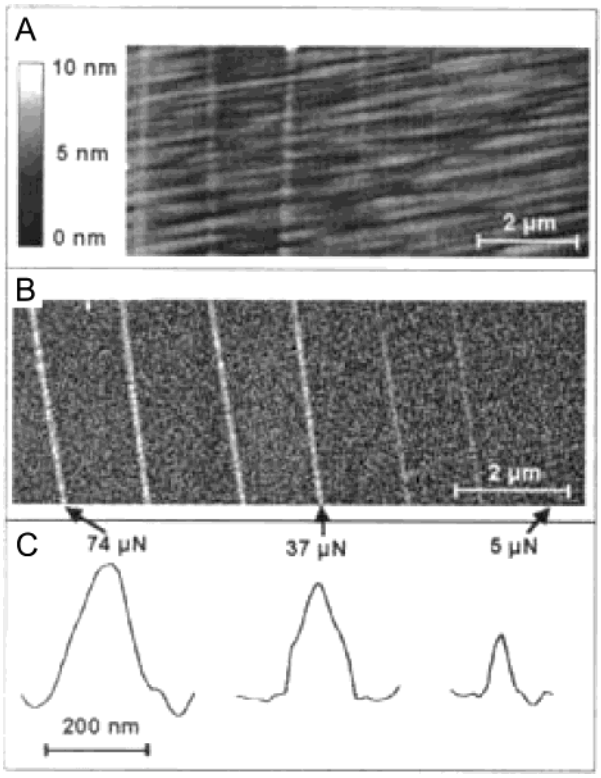

Figure 36. (A) In-situ AFM (*z*-scale: 10 nm) and (B) corresponding SEM images of lines written on silicon under the presence of $CF_3(CF_2)_7CH{=}CH_2$ with different applied forces (ranging from 74 μN (left line) to 5 μN (right line)). (C) Profiles of three different lines (vertical axis was the gray-scale value). Reprinted with permission from ref 221. Copyright 2003 American Institute of Physics.

gold regions. In a control experiment, it was shown that, if only the trap was created and the surface was brought into contact with ATCh, no change in the surface morphology occurred. These experiments led to the conclusion that the change in the pattern was due to the enzyme.

Wacaser et al. used a chemomechanical approach, similar to nanografting, to simultaneously pattern and functionalize a silicon surface.[221] A hydrogen-terminated silicon surface was immersed into one of three reactive compounds (heptadecafluoro-1-decene, 1-hexadecene, or 1-octanol). The mechanical action of the AFM tip was proposed to facilitate chemical reaction of these compounds with the surface. Figure 36 shows SEM and AFM images as well as an AFM section analysis of the same area that had been patterned with heptadecafluoro-1-decene using this technique. The line width achieved depended on the applied force (e.g., a force of 5 μN produced 30 nm wide lines). It was observed from SEM images that a force of 0.25 μN (i.e., AFM imaging force) was nondestructive to the hydrogen-termination layer. Besides lines and squares, the researchers also showed that they could write letters. Further characterization of the structures was performed with TOF-SIMS showing higher fluorine content and lower signals from $Si{-}H^+$ and Si^+ in the patterned areas. Thus, by using the AFM probe to break Si−H and Si−Si bonds in the presence of reactive molecules chemical patterns could be created.

4.4. Substitution via Tip-Induced Terminal Group Modification

A second classification of substitutive lithography involves the chemical modification of the terminal functional headgroup of the SAM. This type of modification has been stimulated by both mechanical and electrochemical means. In these approaches, it was intended to maintain the structural integrity of the SAM throughout the process. Although several papers have discussed the terminal modification of SAMs with electron beams, this type of work is not treated specifically here.[222−225] Nanopatterning with a probe tip has allowed the fabrication of multilayers through subsequent iterative addition processes, or the immobilization of functionalized particles to the locally modified SAM.

Marrian et al. employed an STM tip in UHV (10^{-7} to 10^{-8} Torr) as a low-energy e^--beam lithography source to chemically modify amine-terminated organosilane resists on silicon covered with native oxide.[226] Unlike conventional e^--beam lithography, the STM was an attractive alternative because it could generate low-energy electrons (smaller than 50 eV) with a beam diameter on the order of 10 nm. After the high-resolution e^--beam lithography (Figure 37A), the samples were treated with an aqueous Pd^{2+} catalyst solution (Figure 37B), followed by ex-situ incubation in an electroless Ni plating bath (Figure 37C). The Pd^{2+} catalyst bound only to the nonexposed areas and the Ni was selectively deposited in these regions. The authors assumed that the amino groups were locally deactivated, eliminating their affinity for the Pd^{2+} complex catalyst that promoted electroless plating of Ni films. Two different organosilane resist layers were patterned by applied tip biases of −4 to −35 V (scan rates of 0.2−2 μm/s). One resist terminated with a functional amine headgroup, (aminoethylaminomethylphenethyl)trimethoxysilane ($NH_2(CH_2)_2NHCH_2C_6H_4(CH_2)_2Si(OCH_3)_3$, PEDA), was reported to have a patterning threshold voltage of −8 V. The second resist, 4-chloromethylphenyltrichlorosilane ($ClCH_2C_6H_4SiCl_3$, CMPTS), was reported to have a threshold bias of −4 V. CMPTS contained no ligating amino group and had to be treated after patterning with a grafting agent (lithium ethylenediamine, Li-EDA) to install an amine functionality. For both silanes, larger exposure voltages were explored (more negative than −35 V), but were observed to increase feature sizes. The smallest created metal features were ca. 30 nm wide. The resolution of the metal pattern was not limited by the lithographic step itself. Electroless plating of Ni caused the growth of grains with diameters of ca. 30 nm. A later report extended the work to octadecyltrichlorosilane as a resist.[227] The patterning threshold using OTS was −10 V, and patterns could also be transferred into the underlying substrate by wet etching techniques. The PEDA resist was later used on hydrogen-passivated silicon and improved the resolution to 15 nm.[228]

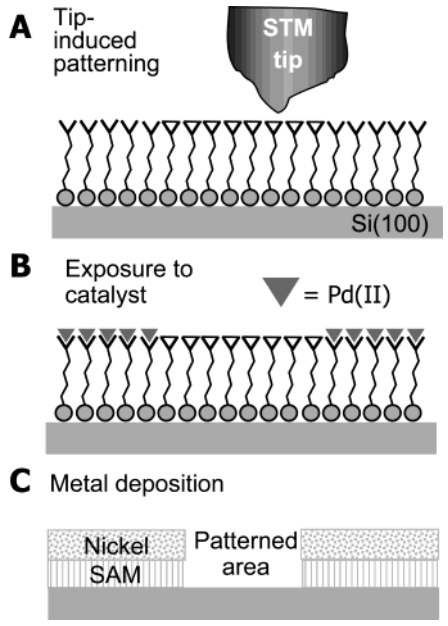

Figure 37. Schematic diagram of ligand-based substitution lithography. (A) The functional headgroup of the SAM was altered with a STM. (B) A Pd catalyst reacted with the nonexposed area of the sample. (C) The electroless Ni plating procedure led to metal growth outside of the STM pattern.

Clausen-Schaumann et al. functionalized an AFM tip with an enzyme and used this to locally hydrolyze a phospholipid in a bilayer. The AFM tip was functionalized with the enzyme phospholipase A_2 and was used to create patterns in a dipalmitylphosphatidylcholine (DPPC) bilayer supported on a gel. A line resolution of ca. 100 nm was achieved. It was suggested that the mechanical pressure of the AFM tip induced defects in the bilayer which allowed entry of the enzyme molecules.[229]

An AFM tip coated with a catalyst can also be employed to induce a localized chemical reaction at the terminal functional groups of a SAM. Müller et al. illustrated how the azide-terminal groups of a monolayer (N═N═NRSiO-) on glass could be locally reduced to amino groups using a Pt-coated AFM tip as a catalyst.[230] This reaction occurred without any applied potential between the tip and substrate. To facilitate the hydrogenation of the azide groups, the lithographic pattern was performed in hydrogen-saturated 2-propanol, and patterning was performed under a force of ca. 400 nN with a scan speed of 1 μm/s. By exploiting the reactivity between amino groups and aldehydes, fluorescently labeled latex microspheres functionalized with aldehydes were immobilized in the patterned areas of the SAM with little nonspecific binding (Figure 38A). In a second example, the modification of the amide groups with 3-(2-furoyl)quinoline-2-carboxaldehyde (ATTO-TAG) was illustrated. This compound was not fluorescent by itself, but after the binding to primary amines, the highly fluorescent isoindiol was formed (Figure 38B). This demonstration also illustrated that the surface was modified through the Pt-coated AFM tip. When the scanning was done with uncoated or Au-coated tips, no subsequent binding of the fluorescent labels occurred (Figure 38C).

Blasdel et al. reported the use of an AFM tip coated with a hydride reducing agent to selectively reduce in-situ a spatial region in a monolayer of imines

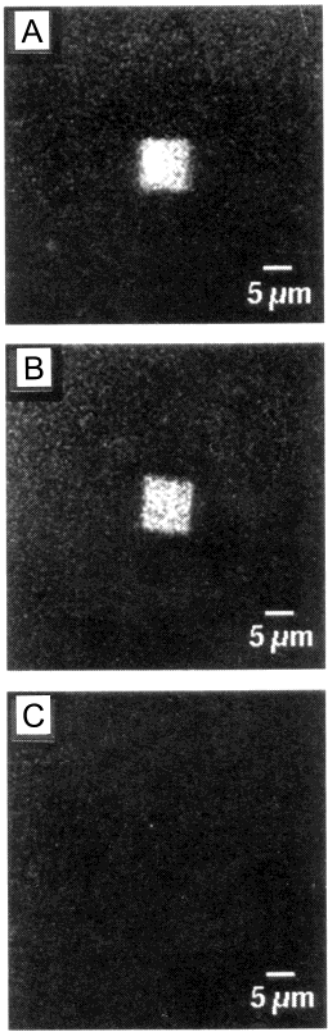

Figure 38. Fluorescence micrographs of a SAM with terminal azide groups after patterning under different parameters. (A) A nominally (10 μm × 10 μm) square area was written with a Pt-coated tip in hydrogen-saturated 2-propanol and subsequently modified with fluorescently modified latex beads. (B) A square fabricated as in A but modified with ATTO-TAG reagent. (C) A nominally (10 μm)^2 area scanned and modified under the same conditions as B but with a unmodified silicon tip. Reprinted with permission from *Science* (http://www.aaas.org), ref 230. Copyright 1995 American Association for the Advancement of Science.

(Table 4A).[231] A cystamine SAM (e.g., $H_2N-CH_2-CH_2S$-SAM) was reacted with cyclopentanone to form terminal imine. Micrometer-sized "chunks" of the reducing agent sodium triacetoxyborohydride ($Na(OAc)_3BH_4$) were attached to a gold-coated tip using a thin film of UV-curable glue. The tip was then scanned over the SAM to locally reduce the imine terminal groups to secondary amines. The scans were run in intermittent contact (tapping) mode in anhydrous methanol (under vigorous water exclusion) to avoid degradation of the reducing agent and the hydrolysis of the imine groups. After scanning, the wafers were washed with water and placed into a NaOH solution to hydrolyze the remaining imine terminal groups back to primary amines. A chloranil test was used to detect the secondary amines in the scanned region; this region appeared as a blue-colored area in bright field optical micrographs. The authors claimed that a (50 μm)^2 area had to be scanned for 1.5 h with a speed of 60.4 μm/s to achieve complete reduction. Thus, while this technique was slow and the spatial resolution was low, it did serve to illustrate how a tip could be used to selectively induce a chemical reaction.

Untreated AFM probes can also assist in the reaction of a functional headgroup. Porter and co-workers reported the tip-assisted base hydrolysis of an ester-terminated alkanethiol monolayer on gold (Table 4B).[232] The researchers self-assembled dithiobis(succinimido undecanoate) (DSU) on Au(111) and scanned the sample in 10 mM KOH solution with a force of 25 nN. The scanned area exhibited a higher friction than the surrounding regime, as observed in LFM images. The authors suggested that the tip induced a local disorder in the outer regime of the self-assembled layer, permitting better access of hydroxide ions to the acyl carbon of the DSU-SAM. A control experiment performed in deionized water showed no modification, but, after the addition of alkaline solution, the scanned area showed the expected contrast in friction mode images.

Blackledge and co-workers pursued an approach similar to that reported by Müller in which a Pd-coated AFM tip was used to alter the chemical functionality of the headgroups of self-assembled monolayers.[233] The Pd-tip-catalyzed hydrogenation was illustrated in which azide terminal groups of a SAM were reduced to form amines (Table 4C). The Pd-tip-catalyzed hydrogenation of *n*-benzyloxycarbonyl (CBZ) protected amino-terminal groups to free amines was also illustrated (Table 4D). The third approach showed the localized, tip-induced hydrosilation of aminobutyldimethylsilane (ASiH) from solution to the alkene headgroups of a SAM (Table 4E). This process resulted in a pattern terminated with amino groups. These amino groups were labeled by reaction with fluorescence probes (5- and 6-carboxytetramethylrhodamine succinimidyl ester or 6-((biotinoyl)amino)hexanoic acid succinimidyl ester). For the detection of the patterns on the substrate, the authors used confocal microscopy and various AFM techniques. The forces needed for these conversions were higher than the ones reported by Müller et al.[230] The authors concluded that the best results were obtained with the reduction of azide-terminated SAMs. The conversion of the azide groups into amines was specific, and nearly no nonspecific binding of the fluorescence labels occurred. The other two approaches were more problematic. The terminal CBZ groups appeared to spontaneously hydrolyze, and this process may have been enhanced by the deposition of palladium from the tip. The use of ASiH suffered from partial decomposition of this reagent in solution and unwanted adsorption of these products to the surface. The resulting species were postulated to chemisorb to the silanol groups present on the substrates.

Sagiv and co-workers developed a different type of substitution lithography, which they termed "constructive lithography". In this method, a conducting AFM tip was utilized to selectively induce nanoscale electrochemical oxidation to the terminal functional

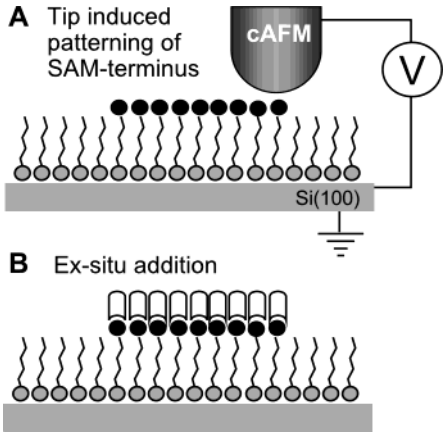

Figure 39. Schematic diagram of substitution lithography through the headgroup modification under an applied bias: (A) conductive AFM tip scanned under an applied bias voltage across a SAM and modified the headgroup without changing the structural integrity of the SAM; (B) altered functionality used for the subsequent binding of a second self-assembly molecule.

groups (methyl, (-CH_3) or vinyl, (-$CH{=}CH_2$)) of SAMs on silicon. Figure 39 illustrates the steps involved to fabricate a structure. The headgroup of a silane-based SAM is subject to a localized redox event initiated by a conducting AFM tip (Figure 39A). Subsequent in-situ chemistry was used to form organic bi- and multilayers or inorganic nanostructures (Figure 39B). The patterned nanostructures could be observed with AFM height and friction imaging modes. Line widths as low as 10 nm were illustrated; although the surface roughness of the silicon dictated that most clear demonstrations occur at larger length scales. Locally modified surfaces could then be used to induce site-selective self-assembly of a number of different materials (organic, metal, semiconducting).

The selective oxidation of terminal vinyl groups in a nonadecenyltrichlorosilane (NTS) SAM yielded patterns of terminal hydroxyl groups.[234] The modification occurred under an applied tip bias ca. 9 V with no measurable current (smaller than 0.5 nA) flowing in ambient conditions. Topography images showed no change in height; however, the friction images suggested a different functionality in the patterned area relative to surrounding unmodified NTS SAM. After in-situ addition of OTS, which reacted with the hydroxyl groups of the oxidized NTS, the topography data showed an area of higher apparent height relative to the surrounding SAM, consistent with the expected height of the bilayer structure fabricated. The friction data suggested that the patterned area and surrounding SAM were composed of similar low friction surfaces (hydrophobic functionality). The authors noted that disordered monolayers seemed to contribute to a lack of oxidation control, creating patches of SiO_2 in the defects of the SAM. To unambiguously correlate microscopic features, macroscopic structures were created through dipping procedures whose chemical identity and structural integrity was confirmed by IR spectroscopy.

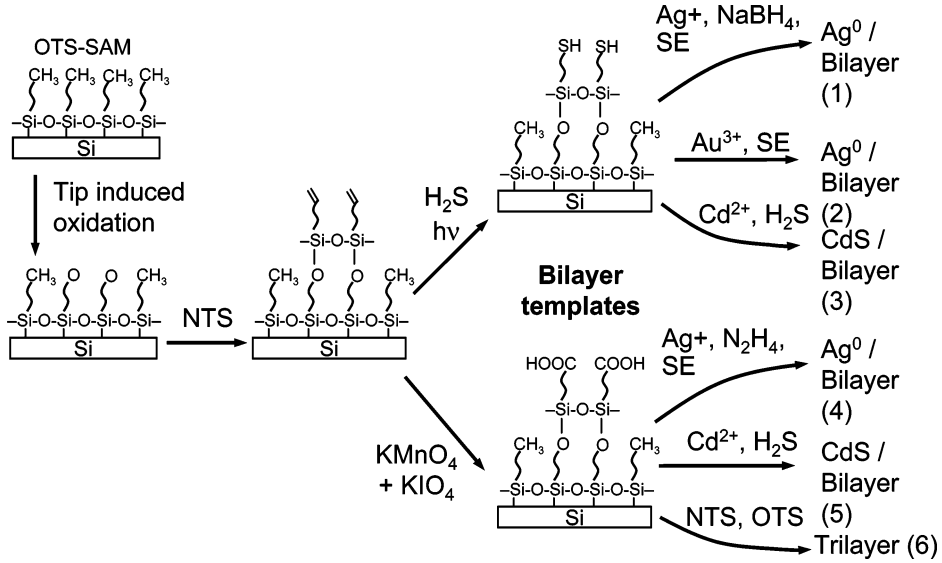

Figure 40. Schematic representation of constructive nanolithography as a generic approach to the planned surface self-assembly of diverse organic, metal, and semiconductor nanoentities. Six nanofabrication routes were indicated, starting with an "inert" silane monolayer (OTS/silicon) that was nondestructively patterned by an electrically biased AFM tip to locally form electrooxidized OTS (OTSeo), followed by the selective self-assembly of a vinyl-terminated silane overlayer (NTS) at the OTSeo polar sites defined by the tip. Subsequently, the terminal ethylenic functions of NTS were photoreacted with H_2S in the gas-phase or chemically oxidized with aqueous ($KMnO_2$ + KIO_4) to give the corresponding TFSM/OTSeo or NTSox/OTSeo bilayer template. Site-defined surface self-assembly of metallic silver, cadmium sulfide, or a third organic monolayer could be achieved using various template-controlled processes. The possibilities depicted here were (1, 4) binding of Ag^+ ions to the thiol or the carboxylic acid surface functions of the TFSM (1) and NTSox (4) template, followed by reduction with aqueous $NaBH_4$ or gaseous N_2H_4 and further development (if desired) of the silver nanoparticles obtained with a silver enhancer (SE) solution; (2) binding of gold species to the TFSM surface, followed by goal-catalyzed silver metal deposition from the SE solution; (3, 5) binding of Cd^{2+} ions to the TFMS (3) or the NTSox (5) surface, followed by the formation of CdS upon exposure of H_2S; and (6) exposure of NTSox to a solution of a self-assembling silane, resulting in the formation of an organic trilayer at the tip inscribed sites. Reprinted with permission from ref 238. Copyright 2000 Wiley-VCH.

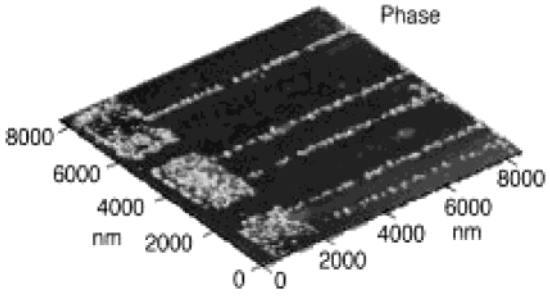

Figure 41. AFM phase image of controlled self-assembly of silver nano- and macrostructures on a template produced by AFM lithography. Reprinted with permission from ref 239. Copyright 2002 Wiley-VCH.

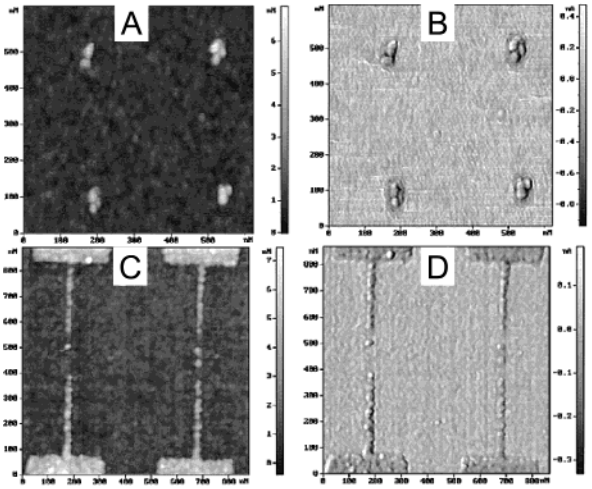

Figure 42. AFM images of an array of four Au_{55}/thiolated bilayer dots after annealing at 80 °C for 12 h ((A) topography, (B) phase image). Topography (C) and phase image (D) of a pattern combining dots, wires, and contact pads. Reprinted with permission from ref 241. Copyright 2002 American Chemical Society.

Starting with OTS-SAMs, the authors showed that it was possible to oxidize the $-CH_3$ terminal group with an AFM tip in a specific regime of applied bias. The researchers observed that, between 8.5 and 10 V, three different regimes were observed. Below a certain threshold voltage, nearly no conversion occurred, while, above a certain value, the underlying silicon surface was oxidized. The optimal values were dependent on the relative humidity and the required patterning bias increased with decreasing humidity. Using SAMs prepared by exposure of 1-octadecene to hydrogenated silicon surfaces, Pignataro et al. studied a similar, tip-induced nanoelectrochemical modification by TOF−SIMS and LFM.[235] The authors observed two different regimes dependent on the absolute value of the applied bias. It was suggested that, at low bias, a redox event at the headgroup occurred, while, at higher bias, the underlying silicon substrate was affected.

Recently, Pavlovic et al. described the local oxidation of thiol-derivatized SAMs (3-mercaptopropyltrimethoxysilanes (3-MPTMS) on p-doped silica) to thiolsulfinates or thiolsufonates with a cAFM tip (Table 4F). The patterns were used to (covalently) immobilize a thiol-rich protein (β-galactosidase) through disulfide bonds. Optimal potentials for patterning were reported to be between 2 and 4 V; higher voltages compromised the SAM. Partial release of the protein by treatment with dithiothreitol (DTT) was also observed.[236]

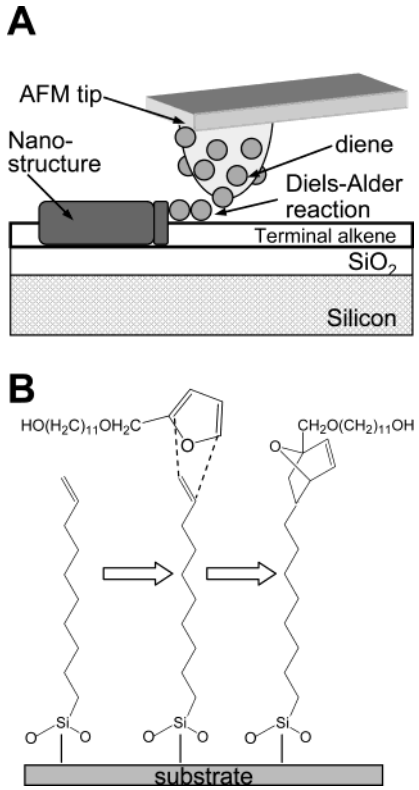

Figure 43. (A) Schematic diagram of the DPN procedure for the Diels−Alder reaction on a SAM. The tip, inked with a reactive molecule (diene), was scanned over a vinyl-terminated (alkene) SAM and a Diels−Alder reaction took place. (B) Sketch of the Diels−Alder reaction of 2-(13-hydroxy-2-oxatridecanyl)furan on the alkene terminal headgroup of a silane SAM.

The next demonstration of constructive lithography involved the site-selective reduction of chemisorbed silver ions generating surface-bound elemental silver nanoparticles atop a thiol-terminated SAM.[237] The vinyl headgroups of an NTS-SAM were photochemically converted by radical addition of H_2S to form thiol and/or disulfide functionalities. The addition of a silver acetate solution terminated the SAM with silver thiolate groups, which could be converted to metallic silver if the surface was scanned under a reductive applied bias. Upon the addition of a silver enhancer solution, silver nanoislands were further developed. A negative tip bias formed no site-selective Ag islands, nor did a positive tip bias followed by rewriting with a negative tip bias. Constructive nanolithography did not modify local surface sites at 0% RH regardless of tip bias, suggesting the water condensing from the atmosphere was essential in the faradaic process occurring at the tip. These observations were all consistent with the authors' proposal of a reduction process in which the sulfur−silver headgroup was converted into a thiol and silver under the influence of water. By applying locally well-defined drops of a $NaBH_4$ solution to a silver−thiolate-terminated SAM, macroscopic sized areas were converted into metallic silver as confirmed by AFM imaging, UV−vis spectroscopy, and XPS.

Table 3. Substitution Lithography

SPM and tip used	SAM	substrate	molecules inserted	line resolution	SIC	RC	comments	ref
STM; Pt/Ir	$C_{12}S$-	Au(111)/Cr/glass	2-ethyl-4:1-ethylphenyl-4:1-ethylphenyl-1,4-thioacetylbenzene	10 nm dots	1.5 V, ~15 pA	0.1 V, 0.5 nA, pulses: 1.8−3.6 V, 0.5 μs to 0.5 s, 1,4-dioxane + NH_4OH, ambient temp	first replacement expt	198
STM; Pt/Ir	$C_{12}S$-	Au(111)	$FcC_{11}SH$, $GalC_6SH$		0.1−1.5 V, 0.5−1 μm/s, 5−10 pA	2.1−3.7 V, 50 nm/s, 55−60% RH in N_2, dodecane, RT	$I-V$ measurements	200
STM; Pt/Ir	$C_{10}S$-, $C_{12}S$-	Au(111)	$C_{10}SH$, $C_{12}SH$	10 nm	1 V, 5−8 pA	3−4 V, 60−80% RH in N_2, dodecane, RT	apparent height contrast studies	199
STM; Pt/Ir	$C_{12}S$-	Au(111)	$FcC_{11}SH$	15 nm	1 V, 8−10 pA	2.6−3.7 V, 10−150 nm/s, 50−60% RH in N_2, dodecane, RT	gradients	201
STM; Pt/Ir	$C_{12}S$-	Au(111)	DAP thiol		0.05−2 V, 10 pA	2.8 V, 10 pA, 1 Hz, 55% RH in N_2, mesitylene, RT	hydrogen bond-mediated self-assembly	202
CSAFM; Pt coated, Si_3N_4, 0.12 N/m	$C_{18}S$-, $C_{10}S$-, C_8S-, C_6S-	Au(111) on mica	$C_{18}SH$, $C_{10}SH$, C_8SH, C_6SH	50 nm squares	same as RC but 0.5 V, ~0.9−3.4 μm/s	4−5 V, 0.245−0.68 μm/s, <4 nN, 20−30% RH, water-saturated toluene, 20 ± 2 °C	$I-V$ measurements	203
STM; Pt/Ir	$C_{16}S$-	Au(111)	Ag	25 nm squares	400 mV	bias steps for electrochemistry: 2.7−3 V with up to 2 μm/s, −0.6 to −1 V, ~1.5−2 μm/s for silver deposition in air or N_2, 50−66% RH	electrodeposition of Ag	197
AFM; Si_3N_4, 0.1 N/m	$C_{10}S$-, $C_{12}S$-	Au(111) on mica	$C_{18}SH$	3 × 5 nm^2	0.3 nN, butanol	>5.2 nN, 2-butanol	first nanografting paper	204
AFM; sharpened, Si_3N_4, 0.1 N/m	$C_{18}S$-, $C_{10}S$-, HOC_2S-, $C_{22}S$-	Au(111) on mica	$C_{18}SH$, $C_{22}SH$	2 nm	0.1 nN	250 nm/s to 10 μm/s, 1.2 nN	confinement effect	205
AFM; Si_3N_4, 0.1 N/m	$C_{10}S$-	Au(111) on mica	$C_{18}SH$, MHA, $C_{22}SH$	10 nm	0.2 nN (at least <1 nN), 0.05 N for molecular resolution	2−520 nN, 0.2−1 μm/s, 50 ms/line (~75 nm), 2-butanol	nanografting	245
AFM; Si_3N_4, 0.1 N/m	mixed C_6S-/$C_{18}S$-, or C_6S-	Au	MHA, $C_{18}SH$	~20 nm	LFM	0.78 or 1.6 μm/s	instrumental improvement	210
AFM; Si_3N_4	$C_{10}S$-	Au(111)	$C_{22}SH$, MHA		0.2−0.5 nN	10−100 nN	characterization of AFM tip shapes	211
AFM; Si_3N_4, sharpened, 0.1 N/m	C_6S-	Au(111)	thiolated ssDNA	15 nm	AFM	800 nm/s, 20 nN, 2-butanol/water/ethanol mixture	DNA pattern and enzyme cleavage of DNA	212
AFM; –	$C_{18}S$-	Au(111)	designed proteins, $C_{10}SH$	60 nm squares	1−10 nN	~15 nN water/triflouroethane	designed protein for the adsorption	213
AFM; Si_3N_4, sharpened, 0.1 N/m	$C_{10}S$-	Au(111)	-CHO, -COOH, -SH, -OH, $CF_{12}C_2SH$	10 nm	0.5−5 nN	5−10 nN	NPRW	214
AFM; Si_3N_4, sharpened, 0.1 N/m	$C_{10}S$-	template-stripped Au(111)	AuNP with mixed thiol/dithiol shell	150 nm wide rectangle	0.5 nN	hexadecane, 2-butanol	nanoparticles on surface	215
AFM; Au coated	thiol-modified 10-mer of thymine	Au	thiol-modified DNA	~20 nm	AFM topography, SEM	10−320 μm/s, 10−200 nN, 35−50% RH	hybridization of nanoparticles	216
AFM; sharpened, 0.1 N/m	$C_{10}S$-	Au(111)	$HS(CH_2)_2CO$ OH	40 nm squares			protein adsorption	217

Table 3. (Continued)

SPM and tip used	SAM	substrate	molecules inserted	line resolution	SIC	RC	comments	ref
AFM; Si_3N_4, sharpened, 0.1 or 0.5 N/m	C_8S-, PEG-thiolate	Au on mica and template-stripped Au	MUA, DSU disulfide, Fab-SH	0.5 μm × 1 μm rectangle	2−8 nN, 5−12 Hz, 35−144 μm/s	20−120 μm/s, 15−60 nN, 130−200 nN, buffer, water, ethanol	different parameters for different SAMs	218
AFM; Si_3N_4, sharpened, 0.5 N/m	$C_{18}S$-, MUA	annealed Au on mica	MUD, ODT	50 nm square		100 nm/s, 75 nN	adsorption of second layer	219
AFM; −	EOthiol	very smooth Au sphere	$HS(CH_2)_{11}(OCH_2CH_2)_6$-$OCH_2CO_2H$	30 nm	tapping mode		detection of enzyme product	220
AFM; −		hydrogen-terminated Si	heptafluorodecene, hexadecene, octanol	30 nm	AFM, SEM, TOF-SIMS	10−30 μm/s, 5−93 μN	DPN on Si	221
UHV-STM; −	PEDA, CMPTS	SiO_x		20 nm	SEM, STM	−4 to −35 V, 1 μm/s	Ni plating	226
UHV-STM; −	PEDA, CMPTS, OTS	SiO_x		20 nm	SEM	−4 to −40 V, 0.2−2 μm/s, 10−300 pA	etching into substrate	227
UHV-STM; −	PEDA	hydrogen-terminated Si		15 nm	SEM	−6 to −10 V, 0.21 μm/s, 200 pA, 9.6 μC/cm	Ni plating	228
AFM; −	phospholipid membrane (DPPC)	mica	hydrolysis of phospho-lipid membrane	∼11 nm	below 1 nN, ∼4.5−14 μm/s, buffer solution	9 ± 3 nN, repeated scanning ∼0.7−34 μm/s, buffer with PLA2 enzyme	hydrolysis of lipid under applied force	229
AFM; Pt-coated silicon	alkylalzides	glass	azides to amines	10 μm square	fluorescence micrographs	1 μm/s, 400 nN, 2-propanol saturated with H_2	Pt-coated tip, binding of	230
AFM; Si coated with Cr/Au, 1−5 N/m	cystamine treated with cyclopentanone	Au on silicon	primary amines to secondary amines	50 μm square	inverted optical microscope	60.4 μm/s for 1−4 h	fluorescence latex beads	231
AFM; Si_3N_4, 0.06 N/m	DSU	Au(111)		0.5 μm squares	∼30−275 μm/s, 25 nN	25 nN, 1 h, 10 mM KOH or water	tip-assisted hydrolysis	232
AFM; Pd coated, 0.305 and 0.176 N/m	*N*-benzyloxycarbonyl-protected aminobutyl-dimethylsiloxane, *N*-octenyl-siloxane, azide-terminated undecyltrimethoxysilane	SiO_x	conversion of functional groups into amines	33 nm	confocal microscopy, tapping mode AFM (etched silicon tips)	1−13.5 μm/s, 0.35−7.6 μN, mixture of formic acid, NaOH, water, and EtOH	Pd-coated tip	233
AFM; boron-doped, diamond-coated silicon, 2−5 N/m	NTS	SiO_x	oxidation of vinyl groups	∼9 nm	LFM, 50 nN or less	−8 to −10 V, 5 μm/s, multiple scans	binding of OTS to form bilayers	234
AFM; coated Pt/Ir, 1−3 N/m	1-octadecene	Si(100) p-type	change in headgroups, oxidation of Si	∼1 μm^2	AFM, LFM TOF-SIMS	±(2−9 V), 30−90 μm/s, >80% RH	modification of headgroups	235
AFM; ultrasharp, 0.03 N/m	3-MPTMS	p-doped SiO_x	oxidation of thiol into thiol-sulfinates/ thiol-sulfonates	∼70 nm	LFM	1−5 V (optimal range 2−4 V), 0.2 μm/s, 28−43% RH, ambient temp	binding of β-galactosidase	236
AFM; boron-doped, diamond-coated silicon, 2−5 N/m, or silver-coated Si_3N_4, W_2C-coated silicon, 0.5−2 N/m	NTS converted to thiols	SiO_x	conversion of Ag ions to Ag	∼30 nm	LFM 50 nN or less	5−10 V, 1−2 μm/s, 40−150 ms pulse duration, 50−60% RH, 23−25 °C	silver island growth	237
AFM; boron-doped, diamond-coated silicon, 2−5 N/m	OTS	SiO_x	adsorption of NTS and further building of metal or semiconductor structures	∼60 nm	contact or intermediate contact mode AFM, 50 nN or less	6−10 V, 1−4 μm/s, ambient conditions	multilayer systems	238

Table 3. (Continued)

SPM and tip used	SAM	substrate	molecules inserted	line resolution	SIC	RC	comments	ref
AFM; W_2C-coated silicon	OTS, NTS	SiO_x		~40 nm Ag wires	lateral conductivity intermediate contact mode AFM	9−10 V pulses, 3.5−3.7 ms/pixel, 65−70% RH in N_2	metal deposition	239
AFM; W_2C-coated silicon, 0.5−2 N/m	OTS	SiO_x	conversion of CH_3 into COOH	~10 nm	tapping mode AFM (phase, height images)	6−9 V, ~60% RH	AuNP adsorption on multilayer	241
AFM; Si_3N_4, 0.09 N/m	trimethoxy-undecanylsilane	SiO_x	diene (2-(13-hydroxy-2-oxatridecyl)furan)	12 nm	1 μm/s, 8 nN	0.1−0.2 μm/s, 8−64 nN	DPN with chemical reaction of headgroups	242

The novelty of constructive nanolithography is based upon the ability of the technique to create templating patterns atop inert, stable monolayers. Many different chemical strategies with the reactive sites could be employed.[238] This technique had the advantage that the surrounding nonpatterned SAMs were not reactive to many in-situ wet chemical treatments. From these templates, organic (insulator), metal, and semiconducting architectures could be created on highly ordered, inert monolayer scaffolds. An example of the schematic steps is shown in Figure 40.[238] CdS nanoparticles were fabricated on top of organic bilayer architectures, realized by two different chemical paths. Elemental silver structures were constructed by four different chemical pathways, while organic trilayers were fabricated with iterations (layer-by-layer hierarchical treatment) of NTS and subsequent oxidation treatments, followed by a final "capping" with OTS.

Constructive nanolithography was also employed to connect macroscopic with nanoscopic patterns.[239] Macroscopic electrodes were generated with a multistep process that involved the masking of headgroups with gallium metal and subsequent conversion of adjacent unmasked headgroups by UV irradiation followed by the guided self-assembly of new organic layers and ions. Between the millimeter-sized contact pads created, nanometer-wide connecting lines were drawn using constructive nanolithography that defined the sites for the silver ion reduction procedure described above. An AFM phase image (Figure 41) of a structure, created by this combined effort, revealed the successful combination of micro- and nanoscale patterns.

Recently, this group expanded constructive lithography to the micro- and millimeter range employing TEM grids as a rigid stamp. The conductive grids were used as anodes to oxidize the SAM headgroups under the stamp, provided there was a sufficient water bridge between stamp and SAM to facilate the electrochemical transformation. This new approach may be a practical means to parallel patterning at much larger length scales than the limited range inherent to SPL.[240]

Constructive nanolithography was also employed to fabricate an organic bilayer terminated with top thiol functionality to immobilize selectively triphenyl phosphine ligand-stabilized Au_{55} nanoparticles (1.4 nm core diameter) through a ligand exchange process.[241] The initial procedure was identical to the one described previously. After the fabrication of a thiol-terminated bilayer, the Au nanoparticles were adsorbed. The authors prepared metal−organic hybrid architectures with feature sizes from ca. 10 nm to 2000 nm, which were stable even after heating at 120 °C for an hour under vacuum. Parts A and B of Figure 42 present the topography and phase images of the patterned nanoparticle islands, while parts C and D of Figure 42 show Au particle wires connecting larger Au pads.

Matsubara et al. combined DPN with the type of substitution lithography approach discussed here to perform a Diels−Alder reaction at a vinyl-terminated SAM.[242] Triethoxy(10-undecenyl)silane was self-as-

Table 4

	Reaction Scheme	Reference
A	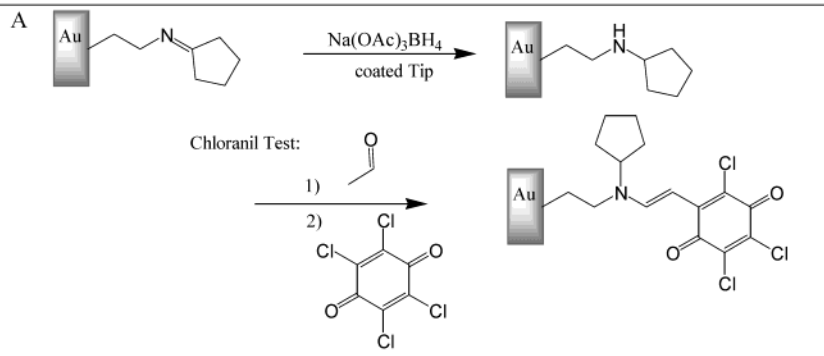	231
B	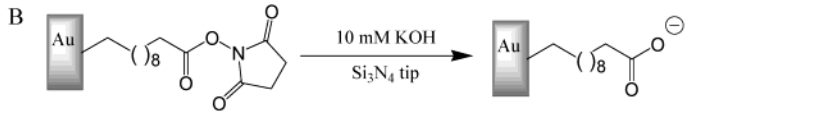	232
C	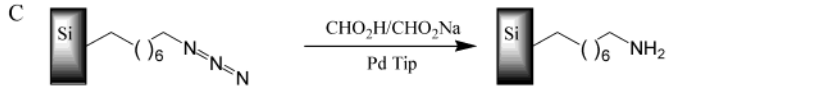	233
D	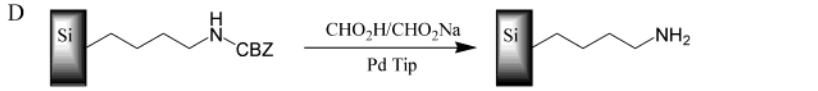	233
E	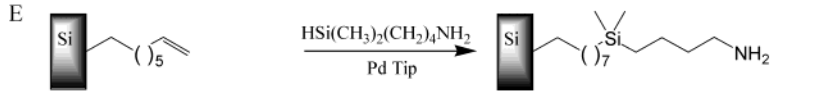	233
F	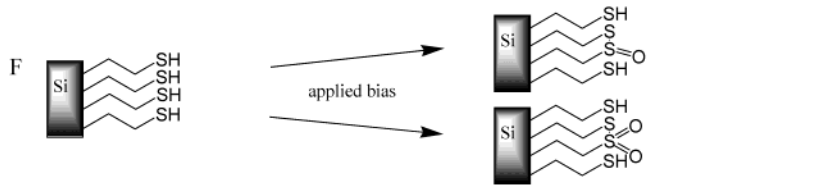	236

sembled onto thermally oxidized silicon, and the AFM tip was coated with a diene reactant (2-(13-hydroxy-2-oxatridecanyl)furan) (Figure 43A). As the tip was brought into contact with the surface, the 1-undecene underwent a reaction with the furan derivative (Figure 43B). The authors observed that initial contact of the tip with the surface produced larger structures than the following patterning attempts, and this result was ascribed to an initial excess of diene molecules on the coated tip. Once the excess was removed, the writing process was dependent on the applied pressure to the tip. With a force of 32 nN, the expected height (2.5 nm) was achieved. Higher forces resulted in very large structures, assumed to be oligomerized furan. Control experiments on methyl-terminated SAMs created no structures.

The mechanical action of an AFM tip can also induce structural changes within an adlayer. This process was recently suggested in the formation of nanodots of rotaxane-containing molecules.[35] This process did not involve a SAM, but rather thin films of 3−35 nm thickness. This structural reorganization is not well-characterized, but may suggest new opportunities for lithography on SAMs that involve larger-scale structural changes rather than functional group transformations.

5. Conclusions and Outlook

This review has shown that there is a diverse array of approaches to scanning probe lithography on SAMs. Each technique has been found to have some advantages and limitations over the others. These are summarized in Table 5. Scanning probe lithography emerges as one of the most expedient methods for making nanometer-scale patterns, at least in a laboratory setting. Other techniques do exist—for example, microcontact printing of SAMs has been extended to the ca. 50 nm scale.[137] Arguably, however, generation of stamps with features in this size regime requires some skill and has not been employed as routinely in the published literature.

SAMs are perhaps the ideal patterning elements as they offer the most convenient means to define the chemical functionality presented at a surface. Chemical definition is particularly important when the patterned regions have size features in the nanometer range, as these features display “countable” numbers of chemical functional groups. A wide

Table 5

technique	advantages	concerns
addition lithography: DPN	• operation with a variety of substrates (conductive and nonconductive) • deposition possible in both contact and tapping modes • writing with multiple inks on one substrate • operation with a variety of inks (insulating, semiconductive, conductive, biomolecules) • technique allows overwriting of a second component without destruction of the initial pattern • 15 nm resolution • offers the ability to write simultaneously with multiple tips with different inks • patterns have been shown to display molecular order within them	• sample contamination may be possible while imaging with modified tip • humidity dependent
substitution lithography: nanografting	• writing with multiple thiol inks on one substrate • patterns have been shown to display molecular order within them • erasing of prewritten patterns is possible • no tip modification is necessary	• few demonstrations aside from thiols on Au • requires a fluid to solvate and transport the molecules • resolution appears more limited than observed with other techniques
substitution lithography: replacement lithography	• 10 nm resolution • permits current−voltage measurements on patterned substrates • writing with multiple thiol inks on one substrate • erasing of prewritten patterns is possible	• operates on conductive substrates only • humidity dependent
substitution lithography: constructive nanolithography and terminal group modification	• nondestructive to SAM interior • use of both silanes/silica and thiols/Au demonstrated • demonstration of multilayer fabrication with inorganic molecules	• requires a "two-step process" • some techniques limited to functional groups that can be oxidized • more chemically specific to the nature of the headgroup, so the generalilty of this process is less well-defined

variety of different chemical structures have been patterned. The range of materials described here includes silicon, coinage metals, thiols, silanes, proteins, DNA, nanoparticles, and others.

Several basic issues are still unresolved with respect to these techniques. Mechanistically, many questions remain as to how these lithographic processes occur. For example, some of the details of the mechanism of ink transport and SAM formation in dip-pen nanolithography are still unclear. The ultimate resolution of these techniques is still ambiguous. Can other, sharper probes (e.g. carbon nanotubes) make smaller structures? Other issues that require clarification are reproducibility and the stability of the patterned nanostructures over time and in various environments.

There are opportunities in the further study and application of scanning probe lithography techniques. From an applications perspective, scanning probe lithography will always suffer from the problem that it is a serial and thus slow technique. Efforts have been made[152,243,244] to make parallel arrays of tips. These may obviate this concern. In any event, these techniques may serve to create functional patterns to make, for example, sensor element arrays and interconnects of macroscopic contact pads with nanoscopic metal lines. From the perspective of advancing basic scientific investigations, scanning probe lithography has much promise. Nanometer-scale patterns can facilitate the study of molecular recognition processes, electronic behaviors in small collections of molecules, and the manipulation and organization of biomolecules. Arguably, we have just begun to use this technique to prepare and to explore new functional architectures.

6. Acknowledgments

We thank the Office of Naval Research (Grant N00014-00-1-0633) and the National Science Foundation (Grant CHE-9905492) for support. We thank Tyson Chasse and Drew Wassel for a critical reading of this manuscript.

7. Glossary

AchE	acetylcholinesterase
AFM	atomic force microscope
APS	(aminopropyl)triethoxysilane
AR8	acid red 8
ASiH	aminobutyldimethylsilane
ATCh	acetylthiocholine
ATTO-TAG	3-(2-furoyl)quinoline-2-carboxaldehyde
Au(111)	crystal phase of gold with Miller indices 1,1,1
AuNP	gold nanoparticles
BOE	buffered oxide etch
C_6SH	hexanethiol ($CH_3(CH_2)_5SH$)
C_6S-SAM	hexanethiolate ($CH_3(CH_2)_5S$-) self-assembled monolayer
C_9SH	nonanethiol ($CH_3(CH_2)_8SH$)
C_9S-SAM	nonanethiolate ($CH_3(CH_2)_8S$-) self-assembled monolayer
$C_{10}SH$	decanethiol ($CH_3(CH_2)_9SH$)
$C_{10}S$-SAM	decanethiolate ($CH_3(CH_2)_9S$-) self-assembled monolayer

$C_{12}SH$	dodecanethiol ($CH_3(CH_2)_{11}SH$)
$C_{12}S$-SAM	dodecanethiolate ($CH_3(CH_2)_{11}S$-) self-assembled monolayer
C_{12}-uracil	dodecyl uracil
$C_{16}SH$	hexadecanethiol ($CH_3(CH_2)_{15}SH$)
$C_{16}S$-SAM	hexadecanethiolate ($CH_3(CH_2)_{15}S$-) self-assembled monolayer
$C_{18}SH$	octadecanethiol ($CH_3(CH_2)_{17}SH$)
$C_{18}S$-SAM	octadecanethiolate ($CH_3(CH_2)_{17}S$-) self-assembled monolayer
C6	coumarin 6
cAFM	conductive AFM
CBZ	*n*-benzyloxycarbonyl
CMPTS	(4-(chloromethyl)phenyl)trichlorosilane ($ClCH_2C_6H_4-SiCl_3$)
CSAFM	current sensing AFM
CV	cyclic voltammetry
CVD	chemical vapor deposition
DAD-2HCl	1,12-diaminododecane
DAP	diacyl 2,6-diaminopyridine decanethiol
DDA	1-dodecylamine
DPN	dip-pen nanolithography
dsDNA	double-stranded deoxyribonucleic acid
DSU	dithiobis(succinimido undecanoate)
DTT	dithiothreitol
EDC	1-ethyl-3-(3-(dimethylamino)propyl) carbodiimide hydrochloride
EDOT	3,4-ethylenedioxythiophene
E-DPN	electrochemical dip-pen nanolithography
FAS	heptadecafluoro-1,1,2,2-tetrahydrodecyl-1-trimethoxysilane
Fc	ferrocene
$FcC_{11}SAc$	ferrocenylundecanethioacetate
$Fc-C_{11}SH$	11-mercapto-1-undecylferrocene
$Fc-C_{11}S$-SAM	11-mercapto-1-undecylferrocenyl self-assembled monolayer
$FcCOC_{10}SH$	11-mercapto-1-oxoundecylferrocene
Fc-uracil	ferrocene-terminated uracil
FITC	fluorescein
GaAs	gallium arsenide
$GalC_6SAc$	galvinolphenoxyhexanethiolacetate
$GalC_6SH$	galvinolphenoxyhexanethiol
$GalC_6S$-SAM	galvinolphenoxyhexanethiolate self-assembled monolayer
HMDS	hexamethyldisilazane
HOC_6SH	mercaptohexanol
IgG	immunoglobulin gamma
I_t	tunneling current set point
KFM	Kelvin probe force microscopy
LB	Langmuir−Blodgett
LFM	lateral force microscopy
Li-EDA	lithium ethylenediamine
MHA	mercaptohexadecanoic acid ($HS(CH_2)_{15}COOH$)
MMEA	mercaptomethylethaneamide
MPTS	mercaptopropyltriethoxysilane
3-MPTMS	3-mercaptopropyltrimethoxysilane
MUA	mercaptoundecanoic acid ($HS(CH_2)_{10}COOH$)
NADH	reduced nicotinamide adenine dinucleotide
NHS	*N*-hydroxysuccinimide ester
Ni−NTA	nickel nitrilotriacetic acid
NPRW	nanopen reader and writer
NSOM	near-field scanning optical microscope
NTS	nonadecenyltrichlorosilane
ODS	octadecyltrimethoxysilane ($CH_3(CH_2)_{17}Si(CH_3)_3$)
ODS-SAM	octadecyltrimethoxysilane ($CH_3(CH_2)_{17}Si(CH_3)_3$) based self-assembled monolayer
OTS	octadecyltrichlorosilane ($CH_3(CH_2)_{17}SiCl_3$)
OTS-SAM	octadecyltrichlorosilane ($CH_3(CH_2)_{17}SiCl_3$) based self-assembled monolayer
PEDA	(aminoethylaminomethylphenethyl)trimethoxysilane ($NH_2(CH_2)_2NHCH_2C_6H_4(CH_2)_2Si(OCH_3)_3$)
PMMA	poly(methyl methacrylate)
R6G	rhodamine 6G
RC	replacement condition
RH	relative humidity
SAM	self-assembled monolayer
SECM	scanning electrochemical microscope
SEM	scanning electron microscope
SIC	standard imaging conditions
SPC	standard patterning conditions
SPL	scanning probe lithography
SPM	scanning probe microscope
ssDNA	single-stranded deoxyribonucleic acid
STM	scanning tunneling microscope
TDA-HCl	*n*-tridecylamine hydrochloride salt
TEM	transmission electron microscope
TFSM	thiol functionalized NTS
TMAH	tetramethylammonium hydroxide
TMS-SAM	trimethylsilyl ($(CH_3)_3Si$-) self-assembled monolayer
TOF-SIMS	time-of-flight secondary ion mass spectrometry
UHV	ultrahigh vacuum
V_b	bias voltage
XPS	X-ray photoelectron spectroscopy

8. References

(1) De Feyter, S.; Grim, P. C. M.; Rücker, M.; Vanoppen, P.; Meiners, C.; Sieffert, M.; Valiyaveettil, S.; Müllen, K.; Schryver, F. C. D. *Angew. Chem., Int. Ed.* **1998**, *37*, 1223.

(2) Lopinski, G. P.; Moffatt, D. J.; Wayner, D. D. M.; Wolkow, R. A. *Nature* **1998**, *392*, 909.

(3) Fang, H.; Giancarlo, L. C.; Flynn, G. W. *J. Phys. Chem. B* **1998**, *102*, 7311.

(4) De Feyter, S.; Gesquiere, A.; Grim, P. C. M.; DeSchryver, F. C.; Valiyaveettil, S.; Meiners, C.; Sieffert, M.; Mullen, K. *Langmuir* **1999**, *15*, 2817.

(5) Ohtani, B.; Shintani, A.; Uosaki, K. *J. Am. Chem. Soc.* **1999**, *121*, 6515.

(6) Giancarlo, L. C.; Flynn, G. W. *Acc. Chem. Res.* **2000**, *33*, 491.

(7) Lim, R.; Li, J.; Li, S. F. Y.; Feng, Z.; Valiyaveettil, S. *Langmuir* **2000**, *16*, 7023.

(8) Yablon, D. G.; Giancarlo, L. C.; Flynn, G. W. *J. Phys. Chem. B* **2000**, *104*, 7627.

(9) Böhringer, M.; Morgenstern, K.; Schneider, W.-D.; Berndt, R. *Angew. Chem., Int. Ed.* **1999**, *38*, 821.

(10) Stevens, F.; Dyer, D. J.; Walba, D. M. *Angew. Chem., Int. Ed. Engl.* **1996**, *35*, 900.

(11) Mena-Osteritz, E.; Meyer, A.; Langeveld-Voss, B. M. W.; Janssen, R. A. J.; Meijer, E. W.; Bäuerle, P. *Angew. Chem., Int. Ed.* **2000**, *39*, 2680.

(12) Lio, A.; Reichert, A.; Ahn, D. J.; Nagy, J. O.; Salmeron, M.; Charych, D. H. *Langmuir* **1997**, *13*, 6524.

(13) Grim, P. C. M.; De Feyter, S.; Gesquiére, A.; Vanoppen, P.; Rücker, M.; Valiyaveettil, S.; Moessner, G.; Müllen, K.; De Schryver, F. C. *Angew. Chem., Int. Ed. Engl.* **1997**, *36*, 2601.

(14) Takami, T.; Ozaki, H.; Kasuga, M.; Tsuchiya, T.; Mazaki, Y.; Fukushi, D.; Ogawa, A.; Uda, M.; Aono, M. *Angew. Chem., Int. Ed. Engl.* **1997**, *36*, 2755.

(15) Kumaki, J.; Hashimoto, T. *J. Am. Chem. Soc.* **1998**, *120*, 423.

(16) Karim, A.; Slawecki, T. M.; Kumar, S. K.; Douglas, J. F.; Satija, S. K.; Han, C. C.; Russell, T. P.; Liu, Y.; Overney, R.; Sokolov, J.; Rafailovich, M. H. *Macromolecules* **1998**, *31*, 857.

(17) Dziezok, P.; Sheiko, S. S.; Fischer, K.; Schmidt, M.; Möller, M. *Angew. Chem., Int. Ed. Engl.* **1997**, *36*, 2812.

(18) Kumaki, J.; Nishikawa, Y.; Hashimoto, T. *J. Am. Chem. Soc.* **1996**, *118*, 3321.

(19) Huisman, B. H.; Schonherr, H.; Huck, W. T. S.; Friggeri, A.; van Manen, H. J.; Menozzi, E.; Vancso, G. J.; van Veggel, F. C. J. M.; Reinhoudt, D. N. *Angew. Chem., Int. Ed.* **1999**, *38*, 2248.

(20) Takada, K.; Díaz, D. J.; Abruña, H. D.; Cuadrado, I.; Casado, C.; Alonso, B.; Morán, M.; Losada, J. *J. Am. Chem. Soc.* **1997**, *119*, 10763.

(21) Prokhorova, S. A.; Sheiko, S. S.; Mourran, A.; Azumi, R.; Beginn, U.; Zipp, G.; Ahn, C. H.; Holerca, M. N.; Percec, V.; Möller, M. *Langmuir* **2000**, *16*, 6862.

(22) Zhang, H.; Grim, P. C. M.; Foubert, P.; Vosch, T.; Vanoppen, P.; Wiesler, U. M.; Berresheim, A. J.; Müllen, K.; De Schryver, F. C. *Langmuir* **2000**, *16*, 9009.
(23) Barth, J. V.; Weckesser, J.; Cai, C. Z.; Günter, P.; Burgi, L.; Jeandupeux, O.; Kern, K. *Angew. Chem., Int. Ed.* **2000**, *39*, 1230.
(24) Semenov, A.; Spatz, J. P.; Moller, M.; Lehn, J. M.; Sell, B.; Schubert, D.; Weidl, C. H.; Schubert, U. S. *Angew. Chem., Int. Ed.* **1999**, *38*, 2547.
(25) Huisman, B. H.; van Veggel, F. C. J. M.; Reinhoudt, D. N. *Pure Appl. Chem.* **1998**, *70*, 1985.
(26) Böhringer, M.; Morgenstern, K.; Schneider, W. D.; Berndt, R.; Mauri, F.; De Vita, A.; Car, R. *Phys. Rev. Lett.* **1999**, *83*, 324.
(27) Eichhorst-Gerner, K.; Stabel, A.; Moessner, G.; Declerq, D.; Valiyaveettil, S.; Enkelmann, V.; Müllen, K.; Rabe, J. P. *Angew. Chem., Int. Ed. Engl.* **1996**, *35*, 1492.
(28) Manne, S.; Gaub, H. E. *Science* **1995**, *270*, 1480.
(29) Gimzewski, J. K.; Joachim, C.; Schlittler, R. R.; Langlais, V.; Tang, H.; Joahannsen, I. *Science* **1998**, *281*, 531.
(30) Jung, T. A.; Schlittler, R. R.; Gimzewski, J. K. *Nature* **1997**, *386*, 696.
(31) De Feyter, S.; Grim, P. C. M.; van Esch, J.; Kellogg, R. M.; Feringa, B. L.; De Schryver, F. C. *J. Phys. Chem. B* **1998**, *102*, 8981.
(32) Yamakoshi, Y.; Schlittler, R. R.; Gimzewski, J. K.; Diederich, F. *J. Mater. Chem.* **2001**, *11*, 2895.
(33) Stevens, F.; Beebe, T. P. *Langmuir* **1999**, *15*, 6884.
(34) Stipe, B. C.; Rezaei, M. A.; Ho, W. *Science* **1998**, *280*, 1732.
(35) Cavallini, M. *Science* **2003**, *299*, 662.
(36) Cavallini, M.; Biscarini, F.; Leon, S.; Zerbetto, F.; Bottari, G.; Leigh, D. A. *Science* **2003**, *299*, 531.
(37) Eigler, D. M.; Schweizer, E. K. *Nature* **1990**, *344*, 524.
(38) Shigekawa, H.; Miyake, K.; Sumaoka, J.; Harada, A.; Komiyama, M. *J. Am. Chem. Soc.* **2000**, *122*, 5411.
(39) Crommie, M. F.; Lutz, C. P.; Eigler, D. M. *Science* **1993**, *262*, 218.
(40) Stroscio, J. A.; Eigler, D. M. *Science* **1991**, *254*, 1319.
(41) Hecht, S. *Angew. Chem., Int. Ed.* **2003**, *42*, 24.
(42) McCarty, G. S.; Weiss, P. S. *Chem. Rev.* **1999**, *99*, 1983.
(43) Nyffenegger, R. M.; Penner, R. M. *Chem. Rev.* **1997**, *97*, 1195.
(44) Hla, S. W.; Meyer, G.; Rieder, K. H. *ChemPhysChem* **2001**, *2*, 361.
(45) Sullivan, T. P.; Huck, W. T. S. *Eur. J. Org. Chem.* **2003**, 17.
(46) Ulman, A. In *An Introduction to Ultrathin Organic Films from Langmuir−Blodgett to Self-Assembly*; Academic Press: New York, 1991; p 278.
(47) Schreiber, F. *Prog. Surf. Sci.* **2000**, *65*, 151.
(48) Dubois, L. H.; Nuzzo, R. G. *Annu. Rev. Phys. Chem.* **1992**, *43*, 437.
(49) Poirier, G. E. *Chem. Rev.* **1997**, *97*, 1117.
(50) Xia, Y. N.; Whitesides, G. M. *Angew. Chem., Int. Ed.* **1998**, *37*, 551.
(51) Xia, Y. N.; Rogers, J. A.; Paul, K. E.; Whitesides, G. M. *Chem. Rev.* **1999**, *99*, 1823.
(52) Chou, S. Y. *MRS Bull.* **2001**, *26*, 512.
(53) Torres, C. M. S.; Zankovych, S.; Seekamp, J.; Kam, A. P.; Cedeno, C. C.; Hoffmann, T.; Ahopelto, J.; Reuther, F.; Pfeiffer, K.; Bleidiessel, G.; Gruetzner, G.; Maximov, M. V.; Heidari, B. *Mater. Sci. Eng., C* **2003**, *23*, 23.
(54) Whitesides, G. M.; Grzybowski, B. *Science* **2002**, *295*, 2418.
(55) Whitesides, G. M.; Mathias, J. P.; Seto, C. T. *Science* **1991**, *254*, 1312.
(56) Kondo, S.; Heike, S.; Lutwyche, M.; Wada, Y. *J. Appl. Phys.* **1995**, *78*, 155.
(57) Majumdar, A.; Lindsay, S. M. In *Technology of Proximal Probe Lithography*; Marrian, C. R. K., Ed.; SPIE−The International Society for Optical Engineering: Bellingham, WA, 1993; Vol. IS 10, p 33.
(58) Marrian, C. R. K.; Dobisz, E. A.; Dagata, J. A. In *Technology of Proximal Probe Lithography*; Marrian, C. R. K., Ed.; SPIE−The International Society for Optical Engineering: Bellingham, WA, 1993; Vol. IS 10, p 58.
(59) Quate, C. F. *Surf. Sci.* **1997**, *386*, 259.
(60) Wiesendanger, R. In *Technology of Proximal Probe Lithography*; Marrian, C. R. K., Ed.; SPIE−The International Society for Optical Engineering: Bellingham, WA, 1993; Vol. IS 10, p 162.
(61) Lercel, M. J.; Craighead, H. G.; Parikh, A. N.; Seshadri, K.; Allara, D. L. *Appl. Phys. Lett.* **1996**, *68*, 1504.
(62) Gölzhäuser, A.; Eck, W.; Geyer, W.; Stadler, V.; Weimann, T.; Hinze, P.; Grunze, M. *Adv. Mater.* **2001**, *13*, 806.
(63) Inoue, A.; Ishida, T.; Choi, N.; Mizutani, W.; Tokumoto, H. *Appl. Phys. Lett.* **1998**, *73*, 1976.
(64) Hatzor, A.; Weiss, P. S. *Science* **2001**, *291*, 1019.
(65) Bumm, L. A.; Arnold, J. J.; Cygan, M. T.; Dunbar, T. D.; Burgin, T. P.; Jones, L., II.; Allara, D. L.; Tour, J. M.; Weiss, P. S. *Science* **1996**, *271*, 1705.
(66) Cygan, M. T.; Dunbar, T. D.; Arnold, J. J.; Bumm, L. A.; Shedlock, N. F.; Burgin, T. P.; II, L. J.; Allara, D. L.; Tour, J. M.; Weiss, P. S. *J. Am. Chem. Soc.* **1998**, *120*, 2721.
(67) Dunbar, T. D.; Cygan, M. T.; Bumm, L. A.; McCarty, G. S.; Burgin, T. P.; Reinerth, W. A.; Jones, L.; Jackiw, J. J.; Tour, J. M.; Weiss, P. S.; Allara, D. L. *J. Phys. Chem. B* **2000**, *104*, 4880.
(68) Weck, M.; Jackiw, J. J.; Rossi, R. R.; Weiss, P. S.; Grubbs, R. H. *J. Am. Chem. Soc.* **1999**, *121*, 4088.
(69) Jung, T. A.; Moser, A.; Hug, H. J.; Brodbeck, D.; Hofer, R.; Hidber, H. R.; Schwarz, U. D. *Ultramicroscopy* **1992**, *42−44*, 1446.
(70) Böhme, O.; Ziegler, C.; Göpel, W. *Adv. Mater.* **1994**, *6*, 587.
(71) Elkaakour, Z.; Aime, J. P.; Bouchacina, T.; Odin, C.; Masuda, T. *Phys. Rev. Lett.* **1994**, *73*, 3231.
(72) Rüetschi, M.; Grütter, P.; Fünfschilling, J.; Güntherodt, H.-J. *Science* **1994**, *265*, 512.
(73) Sumomogi, T.; Endo, T.; Kuwahara, K.; Kaneko, R. *J. Vac. Sci. Technol. B.* **1995**, *13*, 1257.
(74) Yamamoto, S.-i.; Yamada, H.; Tokumoto, H. *J. Appl. Phys.* **1995**, *34*, 3396.
(75) Green, J.-B. D.; McDermott, M. T.; Porter, M. D.; Siperko, L. M. *J. Phys. Chem.* **1995**, *99*, 10960.
(76) Sohn, L. L.; Willett, R. L. *Appl. Phys. Lett.* **1995**, *67*, 1552.
(77) Zhou, L.; Zhang, P. C.; Ho, P. K. H.; Xu, G. Q.; Li, S. F. Y.; Chan, L. *J. Mater. Sci. Lett.* **1996**, *15*, 2080.
(78) Kunze, U.; Klehn, B. *Adv. Mater.* **1999**, *11*, 1473.
(79) Kim, Y. T.; Bard, A. J. *Langmuir* **1992**, *8*, 1096.
(80) Schoenenberger, C.; Sondag-Huethorst, J. A. M.; Jorritsma, J.; Fokkink, L. G. J. *Langmuir* **1994**, *10*, 611.
(81) Touzov, I.; Gorman, C. B. *J. Phys. Chem. B* **1997**, *101*, 5263.
(82) Ross, C. B.; Sun, L.; Crooks, R. M. *Langmuir* **1993**, *9*, 632.
(83) Lercel, M. J.; Redinbo, G. F.; Craighead, H. G.; Sheen, C. W.; Allara, D. L. *Appl. Phys. Lett.* **1994**, *65*, 974.
(84) Xu, L. S.; Allee, D. R. *J. Vac. Sci. Technol., B* **1995**, *13*, 2837.
(85) Lercel, M. J.; Rooks, M.; Tiberio, R. C.; Craighead, H. G.; Sheen, C. W.; Parikh, A. N.; Allara, D. L. *J. Vac. Sci. Technol., B* **1995**, *13*, 1139.
(86) Sugimura, H.; Nakagiri, N. *Langmuir* **1995**, *11*, 3623.
(87) Schoer, J. K.; Ross, C. B.; Crooks, R. M.; Corbitt, T. S.; Hampden-Smith, M. J. *Langmuir* **1994**, *10*, 615.
(88) Schoer, J. K.; Zamborini, F. P.; Crooks, R. M. *J. Phys. Chem.* **1996**, *100*, 11086.
(89) Schoer, J. K.; Crooks, R. M. *Langmuir* **1997**, *13*, 2323.
(90) Weiss, P. S.; Bumm, L. A.; Dunbar, T. D.; Burgin, T. P.; Tour, J. M.; Allara, D. L. *Ann. N.Y. Acad. Sci.* **1998**, *852*, 145.
(91) Delamarche, E.; Hoole, A. C. F.; Michel, B.; Wilkes, S.; Despont, M.; Welland, M. E.; Biebuyck, H. *J. Phys. Chem. B* **1997**, *101*, 9263.
(92) Yang, W.; Chen, M.; Knoll, W.; Deng, H. L. *Langmuir* **2002**, *18*, 4124.
(93) Müller, H. U.; David, C.; Volkel, B.; Grunze, M. *J. Vac. Sci. Technol., B* **1995**, *13*, 2846.
(94) Mizutani, W.; Ishida, T.; Tokumoto, H. *Langmuir* **1998**, *14*, 7197.
(95) Hartwich, J.; Dreeskornfeld, L.; Heisig, V.; Rahn, S.; Wehmeyer, O.; Kleineberg, U.; Heinzmann, U. *Appl. Phys. A: Mater. Sci. Process.* **1998**, *66*, S685.
(96) Hartwich, J.; Sundermann, M.; Kleineberg, U.; Heinzmann, U. *Appl. Surf. Sci.* **1999**, *145*, 538.
(97) Sundermann, M.; Hartwich, J.; Rott, K.; Meyners, D.; Majkova, E.; Kleineberg, U.; Grunze, M.; Heinzmann, U. *Surf. Sci.* **2000**, *454*, 1104.
(98) Kleineberg, U.; Brechling, A.; Sundermann, M.; Heinzmann, U. *Adv. Funct. Mater.* **2001**, *11*, 208.
(99) Keel, J. M.; Yin, J.; Guo, Q.; Palmer, R. E. *J. Chem. Phys.* **2002**, *116*, 7151.
(100) Liu, G.-Y.; Salmeron, M. B. *Langmuir* **1994**, *10*, 367.
(101) Xiao, X. D.; Liu, G. Y.; Charych, D. H.; Salmeron, M. *Langmuir* **1995**, *11*, 1600.
(102) Kelley, S. O.; Barton, J. K.; Jackson, N. M.; McPherson, L. D.; Potter, A. B.; Spain, E. M.; Allen, M. J.; Hill, M. G. *Langmuir* **1998**, *14*, 6781.
(103) Zhou, D.; Sinniah, K.; Abell, C.; Rayment, T. *Langmuir* **2002**, *18*, 8278.
(104) Zhao, J. W.; Uosaki, K. *Langmuir* **2001**, *17*, 7784.
(105) Sugimura, H.; Okiguchi, K.; Nakagiri, N.; Miyashita, M. *J. Vac. Sci. Technol., B* **1996**, *14*, 4140.
(106) Sugimura, H.; Nakagiri, N. *J. Vac. Sci. Technol., B* **1997**, *15*, 1394.
(107) Sugimura, H.; Nakagiri, N. *Nanotechnology* **1997**, *8*, A15.
(108) Sugimura, H.; Nakagiri, N. *J. Am. Chem. Soc.* **1997**, *119*, 9226.
(109) Sugimura, H.; Hanji, T.; Hayashi, K.; Takai, O. *Adv. Mater.* **2002**, *14*, 524.
(110) Sugimura, H.; Takai, O.; Nakagiri, N. *J. Electroanal. Chem.* **1999**, *473*, 230.
(111) Sugimura, H.; Takai, O.; Nakagiri, N. *J. Vac. Sci. Technol., B* **1999**, *17*, 1605.
(112) Sugimura, H.; Hanji, T.; Hayashi, K.; Takai, O. *Ultramicroscopy* **2002**, *91*, 221.
(113) Zheng, J. W.; Zhu, Z. H.; Chen, H. F.; Liu, Z. F. *Langmuir* **2000**, *16*, 4409.
(114) Li, Q.; Zheng, J. W.; Liu, Z. F. *Langmuir* **2003**, *19*, 166.
(115) Zheng, J. W.; Chen, Z. C.; Liu, Z. F. *Langmuir* **2000**, *16*, 9673.

(116) Kim, J.; Oh, Y.; Lee, H.; Shin, Y.; Park, S. *Jpn. J. Appl. Phys., Part 1* **1998**, *37*, 7148.
(117) Oh, Y.; Kim, J.; Lee, H. *Mol. Cryst. Liq. Cryst.* **1999**, *337*, 7.
(118) Oh, Y.; Kim, J.; Lee, H. *J. Korean Phys. Soc.* **1999**, *35*, S1013.
(119) Kim, S. H.; Oh, Y.; Lee, H. *Mol. Cryst. Liq. Cryst.* **2000**, *349*, 175.
(120) Kim, S. M.; Ahn, S. J.; Lee, H.; Kim, E. R. *Ultramicroscopy* **2002**, *91*, 165.
(121) Lee, W. B.; Oh, Y.; Kim, E. R.; Lee, H. *Synth. Met.* **2001**, *117*, 305.
(122) Lee, W. B.; Kim, E. R.; Lee, H. *Langmuir* **2002**, *2002*, 8375.
(123) Lee, H.; Kim, S. A.; Ahn, S. J. *Appl. Phys. Lett.* **2002**, *81*, 138.
(124) She, J.; Song, J. Q.; Wang, Y. C.; Liu, Z. F. *Mol. Cryst. Liq. Cryst.* **1999**, *337*, 313.
(125) Ara, M.; Graaf, H.; Tada, H. *Appl. Phys. Lett.* **2002**, *80*, 2565.
(126) Tully, D. C.; Wilder, K.; Frechet, J. M. J.; Trimble, A. R.; Quate, C. F. *Adv. Mater.* **1999**, *11*, 314.
(127) Tully, D. C.; Trimble, A. R.; Frechet, J. M. J.; Wilder, K.; Quate, C. F. *Chem. Mater.* **1999**, *11*, 2892.
(128) Wittstock, G.; Hesse, R.; Schuhmann, W. *Electroanalysis* **1997**, *9*, 746.
(129) Wittstock, G.; Schuhmann, W. *Anal. Chem.* **1997**, *69*, 5059.
(130) Wilhelm, T.; Wittstock, G. *Angew. Chem., Int. Ed.* **2003**, *42*, 2247.
(131) Shiku, H.; Uchida, I.; Matsue, T. *Langmuir* **1997**, *13*, 7239.
(132) Turyan, I.; Matsue, T.; Mandler, D. *Anal. Chem.* **2000**, *72*, 3431.
(133) Sun, S. Q.; Chong, K. S. L.; Leggett, G. J. *J. Am. Chem. Soc.* **2002**, *124*, 2414.
(134) Sun, S. Q.; Leggett, G. J. *Nano Lett.* **2002**, *2*, 1223.
(135) Kolb, D. M.; Engelmann, G. E.; Ziegler, J. C. *Angew. Chem., Int. Ed.* **2000**, *39*, 1123.
(136) Kolb, D. M.; Ullmann, R.; Will, T. *Science* **1997**, *275*, 1097.
(137) Odom, T. W.; Thalladi, V. R.; Love, J. C.; Whitesides, G. M. *J. Am. Chem. Soc.* **2002**, *124*, 12112.
(138) Xia, Y. N.; Whitesides, G. M. *Annu. Rev. Mater. Sci.* **1998**, *28*, 153.
(139) Lopez, G. P.; Biebuyck, H. A.; Frisbie, C. D.; Whitesides, G. M. *Science* **1993**, *260*, 647.
(140) Hong, M. H.; Kim, K. H.; Bae, J.; Jhe, W. *Appl. Phys. Lett.* **2000**, *77*, 2604.
(141) Bruckbauer, A.; Ying, L. M.; Rothery, A. M.; Zhou, D. J.; Shevchuk, A. I.; Abell, C.; Korchev, Y. E.; Klenerman, D. *J. Am. Chem. Soc.* **2002**, *124*, 8810.
(142) Lewis, A.; Kheifetz, Y.; Shambrodt, E.; Radko, A.; Khatchatryan, E.; Sukenik, C. *Appl. Phys. Lett.* **1999**, *75*, 2689.
(143) Gaspar, S.; Mosbach, M.; Wallman, L.; Laurell, T.; Csoregi, E.; Schuhmann, W. *Anal. Chem.* **2001**, *73*, 4254.
(144) Voigt, J.; Shi, F.; Edinger, K.; Guthner, P.; Rangelow, I. W. *Microelectron. Eng.* **2001**, *57*−*8*, 1035.
(145) Jaschke, M.; Butt, H. J. *Langmuir* **1995**, *11*, 1061.
(146) Piner, R. D.; Mirkin, C. A. *Langmuir* **1997**, *13*, 6864.
(147) Mirkin, C. A. *MRS Bull.* **2001**, *26*, 535.
(148) Mirkin, C. A.; Hong, S. H.; Demers, L. *ChemPhysChem* **2001**, *2*, 37.
(149) Piner, R. D.; Zhu, J.; Xu, F.; Hong, S. H.; Mirkin, C. A. *Science* **1999**, *283*, 661.
(150) Hong, S. H.; Zhu, J.; Mirkin, C. A. *Science* **1999**, *286*, 523.
(151) Hong, S.; Mirkin, C. A. *Science* **2000**, *288*, 1808.
(152) Zhang, M.; Bullen, D.; Chung, S. W.; Hong, S.; Ryu, K. S.; Fan, Z. F.; Mirkin, C. A.; Liu, C. *Nanotechnology* **2002**, *13*, 212.
(153) Zou, J.; Bullen, D.; Wang, X.; Liu, C.; Mirkin, C. A. *Appl. Phys. Lett.* **2003**, *83*, 581.
(154) Belaubre, P.; Guirardel, M.; Garcia, G.; Pourciel, J. B.; Leberre, V.; Dagkessamanskaia, A.; Trevisiol, E.; Francois, J. M.; Bergaud, C. *Appl. Phys. Lett.* **2003**, *82*, 3122.
(155) Hong, S.; Zhu, J.; Mirkin, C. A. *Langmuir* **1999**, *15*, 7897.
(156) Ivanisevic, A.; McCumber, K. V.; Mirkin, C. A. *J. Am. Chem. Soc.* **2002**, *124*, 11997.
(157) Zhang, Y.; Salaita, K.; Lim, J. H.; Mirkin, C. A. *Nano Lett.* **2002**, *2*, 1389.
(158) Weinberger, D. A.; Hong, S. G.; Mirkin, C. A.; Wessels, B. W.; Higgins, T. B. *Adv. Mater.* **2000**, *12*, 1600.
(159) Zhang, H.; Chung, S. W.; Mirkin, C. A. *Nano Lett.* **2003**, *3*, 43.
(160) Ivanisevic, A.; Mirkin, C. A. *J. Am. Chem. Soc.* **2001**, *123*, 7887.
(161) Demers, L. M.; Ginger, D. S.; Park, S.-J.; Li, Z.; Chung, S.-W.; Mirkin, C. A. *Science* **2002**, *296*, 1836.
(162) Wilson, D. L.; Martin, R.; Hong, S.; Cronin-Golomb, M.; Mirkin, C. A.; Kaplan, D. L. *Proc. Natl. Acad. Sci. U.S.A.* **2001**, *98*, 13660.
(163) Agarwal, G.; Sowards, L. A.; Naik, R. R.; Stone, O. *J. Am. Chem. Soc.* **2003**, *125*, 580.
(164) Noy, A.; Miller, A. E.; Klare, J. E.; Weeks, B. L.; Woods, B. W.; DeYoreo, J. J. *Nano Lett.* **2002**, *2*, 109.
(165) Su, M.; Dravid, V. P. *Appl. Phys. Lett.* **2002**, *80*, 4434.
(166) McKendry, R.; Huck, W. T. S.; Weeks, B.; Florini, M.; Abell, C.; Rayment, T. *Nano Lett.* **2002**, *2*, 713.
(167) Lim, J. H.; Mirkin, C. A. *Adv. Mater.* **2002**, *14*, 1474.
(168) Lim, J. H.; Ginger, D. S.; Lee, K. B.; Heo, J.; Nam, J. M.; Mirkin, C. A. *Angew. Chem., Int. Ed.* **2003**, *42*, 2309.
(169) Lee, K. B.; Lim, J. H.; Mirkin, C. A. *J. Am. Chem. Soc.* **2003**, *125*, 5588.
(170) Manandhar, P.; Jang, J.; Schatz, G. C.; Ratner, M. A.; Hong, S. *Phys. Rev. Lett.* **2003**, *90*, art. no.
(171) Li, Y.; Maynor, B. W.; Liu, J. *J. Am. Chem. Soc.* **2001**, *123*, 2105.
(172) Li, Y.; Ben, M.; Liu, J. *Chin. J. Inorg. Chem.* **2002**, *18*, 75.
(173) Maynor, B. W.; Filocamo, S. F.; Grinstaff, M. W.; Liu, J. *J. Am. Chem. Soc.* **2002**, *124*, 522.
(174) Agarwal, G.; Naik, R. R.; Stone, M. O. *J. Am. Chem. Soc.* **2003**, *125*, 7408.
(175) Maynor, B. W.; Li, Y.; Liu, J. *Langmuir* **2001**, *17*, 2575.
(176) Porter, L. A.; Choi, H. C.; Schmeltzer, J. M.; Ribbe, A. E.; Elliott, L. C. C.; Buriak, J. M. *Nano Lett.* **2002**, *2*, 1369.
(177) Fu, L.; Liu, X. G.; Zhang, Y.; Dravid, V. P.; Mirkin, C. A. *Nano Lett.* **2003**, *3*, 757.
(178) Su, M.; Liu, X. G.; Li, S. Y.; Dravid, V. P.; Mirkin, C. A. *J. Am. Chem. Soc.* **2002**, *124*, 1560.
(179) Liao, J. H.; Huang, L.; Gu, N. *Chin. Phys. Lett.* **2002**, *19*, 134.
(180) Ben Ali, M.; Ondarcuhu, T.; Brust, M.; Joachim, C. *Langmuir* **2002**, *18*, 872.
(181) Lee, K. B.; Park, S. J.; Mirkin, C. A.; Smith, J. C.; Mrksich, M. *Science* **2002**, *295*, 1702.
(182) Hyun, J.; Ahn, S. J.; Lee, W. K.; Chilkoti, A.; Zauscher, S. *Nano Lett.* **2002**, *2*, 1203.
(183) Cheung, C. L.; Camarero, J. A.; Woods, B. W.; Lin, T. W.; Johnson, J. E.; De Yoreo, J. J. *J. Am. Chem. Soc.* **2003**, *125*, 6848.
(184) Smith, J. C.; Lee, K. B.; Wang, Q.; Finn, M. G.; Johnson, J. E.; Mrksich, M.; Mirkin, C. A. *Nano Lett.* **2003**, *3*, 883.
(185) Demers, L. M.; Mirkin, C. A. *Angew. Chem., Int. Ed.* **2001**, *40*, 3069.
(186) Liu, X. G.; Fu, L.; Hong, S. H.; Dravid, V. P.; Mirkin, C. A. *Adv. Mater.* **2002**, *14*, 231.
(187) Demers, L. M.; Park, S. J.; Taton, T. A.; Li, Z.; Mirkin, C. A. *Angew. Chem., Int. Ed.* **2001**, *40*, 3071.
(188) Ivanisevic, A.; Im, J. H.; Lee, K. B.; Park, S. J.; Demers, L. M.; Watson, K. J.; Mirkin, C. A. *J. Am. Chem. Soc.* **2001**, *123*, 12424.
(189) Zhang, H.; Li, Z.; Mirkin, C. A. *Adv. Mater.* **2002**, *14*, 1472.
(190) Jang, J. Y.; Hong, S. H.; Schatz, G. C.; Ratner, M. A. *J. Chem. Phys.* **2001**, *115*, 2721.
(191) Jang, J. Y.; Schatz, G. C.; Ratner, M. A. *J. Chem. Phys.* **2002**, *116*, 3875.
(192) Jang, J.; Schatz, G. C.; Ratner, M. A. *Phys. Rev. Lett.*, in press.
(193) Weeks, B. L.; Noy, A.; Miller, A. E.; De Yoreo, J. J. *Phys. Rev. Lett.* **2002**, *88*, 255505.
(194) Sheehan, P. E.; Whitman, L. J. *Phys. Rev. Lett.* **2002**, *88*, 156104.
(195) Schwartz, P. V. *Langmuir* **2002**, *18*, 4041.
(196) Rohzok, S.; Piner, R. D.; Mirkin, C. A. *J. Phys. Chem. B* **2003**, *107*, 751.
(197) Zamborini, F. P.; Crooks, R. M. *J. Am. Chem. Soc.* **1998**, *120*, 9700.
(198) Chen, J.; Reed, M. A.; Asplund, C. L.; Cassell, A. M.; Myrick, M. L.; Rawlett, A. M.; Tour, J. M.; Van Patten, P. G. *Appl. Phys. Lett.* **1999**, *75*, 624.
(199) Gorman, C. B.; Carroll, R. L.; He, Y. F.; Tian, F.; Fuierer, R. R. *Langmuir* **2000**, *16*, 6312.
(200) Gorman, C. B.; Carroll, R. L.; Fuierer, R. R. *Langmuir* **2001**, *17*, 6923.
(201) Fuierer, R. R.; Carroll, R. L.; Feldheim, D. L.; Gorman, C. B. *Adv. Mater.* **2002**, *14*, 154.
(202) Credo, G. M.; Boal, A. K.; Das, K.; Galow, T. H.; Rotello, V. M.; Feldheim, D. L.; Gorman, C. B. *J. Am. Chem. Soc.* **2002**, *124*, 9036.
(203) Zhao, J. W.; Uosaki, K. *Nano Lett.* **2002**, *2*, 137.
(204) Xu, S.; Liu, G. Y. *Langmuir* **1997**, *13*, 127.
(205) Xu, S.; Laibinis, P. E.; Liu, G. Y. *J. Am. Chem. Soc.* **1998**, *120*, 9356.
(206) Xu, S.; Miller, S.; Laibinis, P. E.; Liu, G. Y. *Langmuir* **1999**, *15*, 7244.
(207) Wadu-Mesthrige, K.; Amro, N. A.; Garno, J. C.; Xu, S.; Liu, G. Y. *Biophys. J.* **2001**, *80*, 1891.
(208) Liu, G. Y.; Xu, S.; Qian, Y. L. *Acc. Chem. Res.* **2000**, *33*, 457.
(209) Liu, G. Y.; Amro, N. A. *Proc. Natl. Acad. Sci. U.S.A.* **2002**, *99*, 5165.
(210) Cruchon-Dupeyrat, S.; Porthun, S.; Liu, G. Y. *Appl. Surf. Sci.* **2001**, *175*, 636.
(211) Xu, S.; Amro, N. A.; Liu, G.-Y. *Appl. Surf. Sci.* **2001**, *175*, 649.
(212) Liu, M. Z.; Amro, N. A.; Chow, C. S.; Liu, G. Y. *Nano Lett.* **2002**, *2*, 863.
(213) Case, M. A.; McLendon, G. L.; Hu, Y.; Vanderlick, T. K.; Scoles, G. *Nano Lett.* **2003**, *3*, 425−429.
(214) Amro, N. A.; Xu, S.; Liu, G. Y. *Langmuir* **2000**, *16*, 3006.
(215) Garno, J. C.; Yang, Y.; Amro, N. A.; Cruchon-Dupeyrat, S.; Chen, S.; Liu, G. Y. *Nano Lett.* **2003**, *3*, 389−395.
(216) Schwartz, P. V. *Langmuir* **2001**, *17*, 5971.
(217) Wadu-Mesthrige, K.; Xu, S.; Amro, N. A.; Liu, G. Y. *Langmuir* **1999**, *15*, 8580.
(218) Kenseth, J. R.; Harnisch, J. A.; Jones, V. W.; Porter, M. D. *Langmuir* **2001**, *17*, 4105.
(219) Liu, J. F.; Cruchon-Dupeyrat, S.; Garno, J. C.; Frommer, J.; Liu, G. Y. *Nano Lett.* **2002**, *2*, 937.

(220) Jang, C. H.; Stevens, B. D.; Carlier, P. R.; Calter, M. A.; Ducker, W. A. *J. Am. Chem. Soc.* **2002**, *124*, 12114.
(221) Wacaser, B. A.; Maughan, M. J.; Mowat, I. A.; Niederhauser, T. L.; Linford, M. R.; Davis, R. C. *Appl. Phys. Lett.* **2003**, *82*, 808.
(222) La, Y. H.; Jung, Y. J.; Kim, H. J.; Kang, T. H.; Ihm, K.; Kim, K. J.; Kim, B.; Park, J. W. *Langmuir* **2003**, *19*, 4390.
(223) Kim, C. O.; Jung, J. W.; Kim, M.; Kang, T. H.; Ihm, K.; Kim, K. J.; Kim, B.; Park, J. W.; Nam, H. W.; Hwang, K. J. *Langmuir* **2003**, *19*, 4504.
(224) Jung, Y. J.; La, Y. H.; Kim, H. J.; Kang, T. H.; Ihm, K.; Kim, K. J.; Kim, B.; Park, J. W. *Langmuir* **2003**, *19*, 4512.
(225) Maeng, I. S.; Park, J. W. *Langmuir* **2003**, *19*, 4519.
(226) Marrian, C. R. K.; Perkins, F. K.; Brandow, S. L.; Koloski, T. S.; Dobisz, E. A.; Calvert, J. M. *App. Phys. Lett.* **1994**, *64*, 390.
(227) Perkins, F. K.; Dobisz, E. A.; Brandow, S. L.; Koloski, T. S.; Calvert, J. M.; Rhee, K. W.; Kosakowski, J. E.; Marrian, C. R. K. *J. Vac. Sci. Technol., B* **1994**, *12*, 3725.
(228) Perkins, F. K.; Dobisz, E. A.; Brandow, S. L.; Calvert, J. M.; Kosakowski, J. E.; Marrian, C. R. K. *Appl. Phys. Lett.* **1996**, *68*, 550.
(229) Clausen-Schaumann, H.; Grandbois, M.; Gaub, H. E. *Adv. Mater.* **1998**, *10*, 949.
(230) Müller, W. T.; Klein, D. L.; Lee, T.; Clarke, J.; McEuen, P. L.; Schultz, P. G. *Science* **1995**, *268*, 272.
(231) Blasdel, L. K.; Banerjee, S.; Wong, S. S. *Langmuir* **2002**, *18*, 5055.
(232) Wang, J.; Kenseth, J. R.; Jones, V. W.; Green, J.-B. D.; McDermott, M. T.; Porter, M. D. *J. Am. Chem. Soc.* **1997**, *119*, 12796.
(233) Blackledge, C.; Engebretson, D. A.; McDonald, J. D. *Langmuir* **2000**, *16*, 8317.
(234) Maoz, R.; Cohen, S.; Sagiv, J. *Adv. Mater.* **1999**, *11*, 55.
(235) Pignataro, B.; Licciardello, A.; Cataldo, S.; Marletta, G. *Mater. Sci. Eng., C* **2003**, *23*, 7.
(236) Pavlovic, E.; Oscarsson, S.; Quist, A. P. *Nano Lett.* **2003**, *3*, 779.
(237) Maoz, R.; Frydman, E.; Cohen, S. R.; Sagiv, J. *Adv. Mater.* **2000**, *12*, 424.
(238) Maoz, R.; Frydman, E.; Cohen, S. R.; Sagiv, J. *Adv. Mater.* **2000**, *12*, 725.
(239) Hoeppener, S.; Maoz, R.; Cohen, S. R.; Chi, L. F.; Fuchs, H.; Sagiv, J. *Adv. Mater.* **2002**, *14*, 1036.
(240) Hoeppener, S.; Maoz, R.; Sagiv, J. *Nano Lett.* **2003**, *3*, 761.
(241) Liu, S.; Maoz, R.; Schmid, G.; Sagiv, J. *Nano Lett.* **2002**, *2*, 1055.
(242) Matsubara, S.; Yamamoto, H.; Oshima, K.; Mouri, E.; Matsuoka, H. *Chem. Lett.* **2002**, 886.
(243) Vettiger, P.; Despont, M.; Drechsler, U.; Durig, U.; Haberle, W.; Lutwyche, M. I.; Rothuizen, H. E.; Stutz, R.; Widmer, R.; Binnig, G. K. *IBM J. Res. Dev.* **2000**, *44*, 323.
(244) Wilder, K.; Soh, H. T.; Atalar, A.; Quate, C. F. *Rev. Sci. Instrum.* **1999**, *70*, 2822.
(245) Xu, S.; Liu, G. Y. *Scanning* **1999**, *21*, 71.

CR020704M